Neural Circuits Underlying Salt-Taste Valence

Thesis by

Yameng Zhang

In Partial Fulfillment of the Requirements for

the degree of

Doctor of Philosophy

CALIFORNIA INSTITUTE OF TECHNOLOGY

Pasadena, California

2026

Defended Oct 14th 2025

Yameng Zhang
ORCID: 0009-0005-7038-7049

ACKNOWLEDGEMENTS

If you imagine the whole volume of knowledge as a planet, what I contributed to science during my PhD journey is like a screw into the planet's surface, or even less. With my PhD completed, I'm proud of my humble progress and even more aware of the profound expanse of knowledge that remains.

The PhD journey is a personal Odyssey to find a better me. I spent a meaningful and challenging time to know more about nature and myself. There are love and tears along the way and I am glad that I did not give up in the middle. From my teenage years, I believed in carpe diem and valued beauty in ephemeral and serendipitous encounters. The short-lived enthusiasm led to nihilism in my undergrad time, during which I started to doubt the existence of life and truths. I wrote in my PhD application essay: "biological science provided me a sense of security that I can embrace this world with more concrete satisfaction." This was how I started the journey, and I feel luckily it even offered more than what I longed for. The fact that I was able to dedicate six years to performing experiments and studying one topic gave me the confidence that I can truly persist. I want to thank myself for making it through.

I want to thank equally between Prof. Yuki Oka and my parents. Prof. Yuki Oka taught me knowledge unreservedly, guided me how to do research patiently, and encouraged me like my family. I am happy that I chose him as my mentor. I will leave his lab soon, but he is my mentor all my lifetime. My parents, though far away in China, always supported me mentally and physically. I cannot make it through the process if my harbor is not as safe and sound as this. I am grateful that my parents offered me true freedom to let me control my own life and respected any choice I made. I hope I can take care of them more in the future.

I also want to thank all the researchers and scientists for cultivating such a professional and friendly environment at Caltech. I own a special thanks to Sangjun Lee who is my mentor during my rotation and guided me into my PhD life. His high quality of science amazed me, and I wish I did not fail his expectation. Tongtong Wang is my best friend in lab, and we endured all the six years together. Our friendship witnessed our progress. Haruka Ebisu and Zhe Yang both left the lab a few years ago, but their support meant a lot to me. I also want to thank Yuan Zhao, Mari Oka, Lu Liu, Allan-Hermann Pool, Elin Kang, Bochuan Teng, Avedis Tufenkjian, Wongyo Jung, Ukjin Choi, Daewon Lee, Takako Ichiki, Jacob Hauser, Ashil Koranne, and Brittany Ho as great colleagues in lab. Importantly, thanks to my committee members Prof. David J. Anderson, Prof. Carlos Lois and Prof. Matt Thomson, and my option representative Prof. Henry A. Lester. They are respectful scientists who selflessly shared their wisdom, and I really valued their insights.

My past experience during undergrad guided my journey to PhD, and I did not have any formal chance to express my gratefulness to my mentors along the way. Hwei-Ee Tan, Kyung-Ae Yang and Stevan Pecic were PhD student or postdocs who taught me hand by

hand how to do science. Over the years, they taught me more than science, and their kindness fueled me to lead my trainees. Prof. Charles Zuker, Prof. Milan N. Stojanovic and Prof. Paul Sajda are the first professors I met in the academia. Their profound knowledge and magnetic charisma intrigued me. Though I might not choose academia as my career, they are always my mentors and models.

At last, I cannot make the journal without the accompany of my dear friends who replaced the role of a partner. Though most of them relocated and scattered around the world, I cannot forget the nights we chatted, the wine we drank, and the places we went. I want to specifically mention Teona Chan, Jinrui Hou, Jiajing Mao, Naomi Xiao, Ali Wang, Jiawei Zhao, and Yutian Li. I met all of you when I just entered PhD, and I am happy that I did not lose any of you when I finished. At the same time, thanks to my old friends Shuiling Geng, Xueyao Wang, Jinfang Zhu, Bowen Zhou, Qiuyi Wang, Jingya Bi, Mingxin Jia, Ruiqi Zhong, and many others. Though I did not believe in forever, may our beautiful friendship last forever…

There are too many encounters, experience, and items that I want to acknowledge to. Thanks to the sacrifice of Mus musculus, Jaculus jaculus and many other animals whose contribution to science cannot be measured. Thanks to the pleasure and tranquil I got from wine, video games, and novels. I wish everyone a bright future and happy life. I hope my work in science can be a meaningful entry point to something bigger in the future.

O ever youthful, O ever weeping.
永远年轻，永远热泪盈眶。

ABSTRACT

Salt consumption is unique among the five basic tastes. The perception of salty taste revealed a concentration-dependent and internal-state-dependent valence pattern. Low concentrations of salt trigger sodium-specific taste receptors while high concentrations recruit bitter and sour pathways, which have been investigated by previous research and proven with daily experience. I focus on the dynamic nature of salt perception, in the perspective of physiological states.

In calorie restricted state, food cues become more appetitive, but in sodium depletion state, the hedonic value of salt fundamentally reversed. High concentrations of salt induce innate aversion under sated states, whereas such aversive stimuli transform into appetitive ones under sodium depletion. Neural mechanisms underlying this state-dependent salt valence switch are poorly understood. Using transcriptomics state-to-cell-type mapping and neural manipulations, we show that positive and negative valences of salt are controlled by anatomically distinct neural circuits in the mammalian brain. The hindbrain interoceptive circuit regulates sodium-specific appetitive drive, whereas behavioral tolerance of aversive salts is encoded by a dedicated class of neurons in the forebrain lamina terminalis (LT) expressing prostaglandin E2 (PGE2) receptor, Ptger3. We show that these LT neurons regulate salt tolerance by selectively modulating aversive taste sensitivity, partly through a PGE2-Ptger3 axis. These results reveal the bimodal regulation of appetitive and tolerance signals toward salt, which together dictate the amount of sodium consumption under different internal states.

Maintaining the fluid balance requires complex crosstalk within the neural circuits and endocrine systems through the brain-body axis. Despite the prevalence of fluid balance dysregulation and salt overconsumption in modern life, its health relevance remains underappreciated. I have been attracted to the global salt overconsumption crisis from the start of my Ph.D study. The current approaches to regulate salt intake rely heavily on imperfect salt substitutes. The PGE2-Ptger3 brain-body axis posed a new top-down approach to reduce salt intake. Interestingly, PGE2 is a critical biomarker in pro-inflammation state. It has been investigated that high salt intake induces chronic inflammation, desensitization of salty tastes, and intensified craving for consumption. I regard my research of the tolerance circuit as an entry point and hope future research into inflammation and its role in salt intake can be translated into concrete salt reduction solutions.

PUBLISHED CONTENT AND CONTRIBUTIONS

Zhang, Y., Pool, A. H., Wang, T., Liu, L., Kang, E., Zhang, B., Ding, L., Frieda, K., Palmiter, R., & Oka, Y. (2023). Parallel neural pathways control sodium consumption and taste valence. *Cell*, *186*(26), 5751–5765.e16. https://doi.org/10.1016/j.cell.2023.10.020

YZ. conceived the research program, designed experiments, performed genetic and behavioral experiments, analyzed the data, and wrote the paper.

Zhang, Y., & Oka, Y. (2025). Body fluid regulation. *Current opinion in neurobiology*, *92*, 103017. https://doi.org/10.1016/j.conb.2025.103017

YZ. wrote the paper.

TABLE OF CONTENTS

LIST OF ILLUSTRATIONS AND/OR TABLES

NOMENCLATURE

Acesulfame potassium (AceK): non-nutritive sweetener used in taste assays.
Aldosterone: mineralocorticoid that increases renal Na^+ reabsorption.
Amiloride : ENaC blocker that suppresses amiloride-sensitive salt taste.
Angiotensin II (AngII): vasoconstrictor that regulates thirst and sodium appetite.
Arginine vasopressin (AVP/ADH): antidiuretic hormone that modulates thirst.
Atrial natriuretic peptide (ANP): cardiac peptide promoting natriuresis and diuresis.
Bed nucleus of the stria terminalis (BNST): limbic relay integrating interoceptive and affective signals.
Capsaicin : TRPV1 agonist used as oral noxious stimulus control.
Channelrhodopsin-2 (ChR2): light-gated cation channel for optogenetic activation.
Chorda tympani nerve (CT): cranial nerve branch carrying anterior tongue taste afferents.
Chronic kidney disease (CKD): impaired renal function that perturbs fluid and sodium homeostasis.
Conditioned taste aversion (CTA): learned avoidance after pairing taste with malaise (e.g., LiCl).
Circumventricular organs (CVOs): brain areas with highly permeable blood brain barriers; important in fluid regulation.
Cyclooxygenase (COX): enzymes synthesize prostanoids including PGE2.
Diuresis/Antidiuresis: increase/decrease in urine flow.
DREADDs (hM3Dq/hM4Di): chemogenetic GPCRs enabling bidirectional neuronal control.
dLight: genetically encoded dopamine sensor for reward measurements (e.g., NAc).
Epithelial Sodium Channels (ENaC): epithelial Na^+ channel for amiloride-sensitive salt taste and collecting-duct Na^+ uptake.
Fiber photometry: bulk fluorescence recording of neural activity (e.g., GCaMP/dLight).
Furosemide: loop diuretic inhibiting NKCC2 to increase natriuresis.
GCaMP: genetically encoded Ca^{2+} indicator for neuronal activity.
Glomerular filtration rate (GFR): index of kidney filtration function.
Gustatory cortex/insula (InsCtx): cortical representation of taste quality and valence.
Gustometer/Lickometer: apparatus for controlled, lick-based taste assays.
Hedonic valence: pleasant–unpleasant value assigned to a stimulus.
HSD2 neurons: neurons expressing 11-beta-hydroxysteroid dehydrogenase type 2 (HSD2) at NTS neurons that regulate sodium appetite.
Hypovolemia: low circulating volume activating RAAS and thirst pathways.
Immunofluorescence: antibody-based protein labeling in tissue sections.
Insulin: metabolic hormone with central effects on taste/reward and ingestive drives.
Intracellular fluid (ICF): K^+-rich fluid compartment within cells.
Leptin: adipokine that suppresses appetite and modulates taste/reward circuits.
Lamina terminalis (LT): SFO/OVLT/MnPO macrostructure integrating osmolality and

hormone inputs.
Median preoptic nucleus (MnPO): a component of LT controlling fluid regulation.
Natriuresis: renal excretion of sodium.
Na(x) channel: glial sodium-level sensor implicated in LT osmosensing.
Nucleus accumbens (NAc): reward/palatability hub receiving dopamine.
Nucleus of the solitary tract (NTS): hindbrain interoceptive/taste hub receiving visceral inputs.
Nonsteroidal Anti-Inflammatory Drug (NSAIDs): COX inhibitors that reduce prostaglandin synthesis.
Osmolality: solute concentration per kg water.
Osmotic thirst: drive to drink water triggered by increased plasma osmolality.
Oxytocin (OT): hypothalamic neuropeptide modulating social/affective states and fluid intake.
Organum Vasculosum of the Lamina Terminalis (OVLT): a component of LT controlling fluid regulation.
Palatability : immediate affective liking during consumption.
Parabrachial nucleus (PBN): taste/visceral relay in the hindbrain.
Paraventricular nucleus (PVN): hypothalamic homeostatic center.
PDYN neurons: neurons expressing prodynorphin at pre-LC that drive sodium appetite.
Peri-locus coeruleus: hindbrain areas driving sodium appetite.
Prostaglandin E2 (PGE2): Eicosanoids synthesized from arachidonic acid by COX, enriched during inflammation.
PGE2 receptor 3 (PTGER3/EP3): PGE2 receptor.
Quinine: tastants deliver bitter taste.
Renin–angiotensin–aldosterone system (RAAS): endocrine axis for sodium retention, vasoconstriction, thirst and stress.
RNAscope: multiplex fluorescent in situ hybridization for RNA.
Satiation/Satiety: meal-ending processes and post-meal suppression of intake.
Subfornical organ (SFO): a component of LT controlling fluid regulation.
Sodium appetite: specific motivation to seek Na^+ when depleted.
Sodium-potassium-2-chloride cotransporter protein (NKCC2): thick-ascending limb Na^+-K^+-$2Cl^-$ cotransporter; loop diuretic target.
Transient Receptor Potential, Melastatin 5 (TRPM5): cation channel in type II taste cells required for sweet, bitter and umami transduction.
Two-bottle choice: preference assay presenting two solutions simultaneously.
Valence: hedonic value of a stimulus (appetitive vs aversive).
Valence switch (salt): sodium depletion converts high salt from aversive to appetitive.

Chapter 1

TASTE VALENCE

A stimulus can feel pleasant or unpleasant depending upon its usefulness as determined by internal signals. – Michel Cabanac[1]

Organisms maintain homeostasis while constantly exchanging energy and information with the external world. Sensation is the interface for this exchange. In classic work, Cabanac introduced *alliesthesia*, that the same stimulus can feel pleasant or unpleasant depending on the internal state.[1] He proposed the shifted perception of olfactory and gustatory cues in hunger and satiation states, along with the thermal sensation as examples of this dynamic process.[1,2] The perceived pleasantness represents its utility. If the stimulus helps the body retrieves internal homeostasis from deviation, then it is sensed as pleasant, and vice versa.[3] The pleasantness level determines the attraction or avoidance behavioral output. Cabanac later characterized sensation as tridimensional: qualitative, quantitative, and affective, which is defined with pleasure and displeasure.[4] In this perspective, the state-dependent pleasure serves as a common currency for weighing different motivations and making decisions.[5,6] The contemporary neuroeconomic view adopts the quantitative version of the utility theory that choices are made by a computation of values integrating internal state with expected outcomes.[7]

In contemporary affective science, the hedonic dimension of a stimuli is termed the *valence*. Valence is a critical concept in multiple theories. In the circumplex framework of affect, valence and the pleasant–unpleasant axis, together with the arousal and alert axis, organize emotion.[8] In reward theory, valence represents a spectrum of "liking," or hedonic value, whereas a separable concept is "wanting," characterizing the incentive salience of behavior.[9–11] In the perspective of constructionist, valence is a basic ingredient of affect built from interoceptive signals, echoing the *alliesthesia* concept.[12]

1.1 State-dependent change in taste valence

The phenomenon of state-dependent valence change spans multiple sensory modalities. In olfaction, food odors are sensitized in calorie deficiency.[13,14] In somatosensation, placebo analgesia has been reported in patients with less pain sensation of identical nociceptive stimuli and decreased fMRI responses in pain sensation brain areas.[15,16] In vision, the brightness and contrast of colors are biased with increased levels of stress and emotions.[17,18] Similar effects are demonstrated in audition with an altered amplitude and frequency sensation.[19,20] The thesis will focus on the state-dependent valence change in gustatory stimuli.

It has been well established that hunger or satiety states, or in other words, calorie deprivation or replenishment can alter taste valence.[21,22] Early human psychophysical studies show the hedonic value increase in hunger is specific to food cues rather than water.[23] Interestingly, in rodents with 48-hour food restriction, even the palatability of water is increased.[24] Food deprivation enhances sensitivity to certain tastes: for example, detection thresholds for sweet and salty tastes are significantly lowered during fasting compared to satiety.[21] The taste

sensitivity to bitter during hunger was not extensively studied, but some results indicated a significantly higher sensitivity during satiety and higher tolerance during hunger.[25–27] The taste sensitivity mentioned is implied from behavioral consumption assays rather than direct measurement of sensory input from taste cells. Instead, the activation of orexigenic Agouti-related peptide (AgRP)-expressing neurons did not alter sweet or bitter signals from chorda typamni.[28] Injection of leptin reduced the integrated responses of the chorda tympani and glossopharyngeal nerves selectively to sweet taste only during hunger.[29] Concluding from the behavioral data, hunger broadly enhances the appeal of palatable tastes and blunts the aversiveness of negative taste, an adaptive change that encourages food consumption when energy is needed. However, it is still unknown whether the internal state change will lead to any direct peripheral modification for taste sensation.[30]

1.2 Neural modulation in hunger-induced taste valence change

Early neurophysiology studies identified several brain areas where neural responses to taste stimuli depend on the internal state. Orbitofrontal cortex (OFC), lateral hypothalamus (LH), and amygdala respond strongly to palatable tastes like sucrose in hunger but the response is significantly reduced for the same taste after satiation.[21,31–34] Functional MRI studies in humans mirror these findings, showing that the signal in the OFC and anterior insular cortex to oral taste is higher when people are hungry and declines after they eat.[35–37]

In rodent models, direct stimulation on the hunger neurons in the arcuate nucleus (Arc) is sufficient to decrease the behavioral sensitivity to bitter.[28] AgRP expressing neurons and its downstream brain areas have been extensively studied in regards to its role in palatability and consumption.[38–45] Selective activation of glutamatergic Vglut2-expressing neurons in

the LHA is sufficient and necessary for the hunger-induced taste modification.[28] Separable neural populations from LHA projecting to lateral septum (LS) and lateral habenula (LHb) modulate sweet and bitter taste respectively.[28] Additionally, reward regions, for example insular cortex, receive indirect inputs from AgRP neurons and modulate responses towards the food cues in different internal states.[37,46–48] Though there is no evidence of how distinct neural populations are activated by internal states, there is topographically separable populations in the amygdala imposing positive and negative valence to taste stimuli.[49] Internal state shifts like hunger might tune the distinct projection from taste cortex to recalibrate taste.

In Drosophila, starvation reconfigures taste valence through parallel neuromodulatory cascades and modulates directly on primary gustatory channels.[50] The phenotype is similar to rodent models with a bidirectional, state-scalable shift in the hedonic value of the same tastants. Interestingly, the sweet and bitter sensitivity change demonstrates a different kinetics.[50] The sweet sensitivity enhancement occurs together with food seeking behaviors, allowing animals to consume as early as possible. During severe starvation, bitter desensitization takes over and amplifies food choices to recover as much energy as possible. Similar levels of onset time accuracy have not been studied in rodent or primate models.

1.3 Hormonal modulation in hunger-induced taste valence change

Taste valence is dynamically modulated by hormones that reflect internal physiological states. Interestingly, various research has demonstrated these hormones can act directly on primary sensory channels. Ghrelin is locally produced in taste cells, and mice lacking its cognate receptor (GHSR) show reduced salty and sour responsivity.[51] Endogenous leptin

acts on Ob-Rb receptors to hyper-polarize T1R sweet-sensitive taste cells and suppress sweet taste sensitivity, whereas injected leptin suppresses chorda tympani and glossopharyngeal responses to sweet without altering salty/sour/bitter.[52–54] By contract, glucagon and glucagon-like peptide-1 (glucagon-like peptide-1) are locally produced in the taste buds and enhance the sensitivity to sweet. [55–57] GLP-1 produced from the taste cells acts on adjacent intragemmal gustatory afferents whereas locally produced glucagon activates the glucagon receptor (GCGR) and enhances chorda tympani responses. Functionally, this mechanism provides a phasic, meal-time amplifier that sharpens detection of caloric sugars at the tongue, even though central GLP-1 pathways promote satiety over a longer time frame.

Recordings from taste cells showed insulin activates the epithelial sodium channel (ENaC) through phosphoinositide 3-kinase in taste receptor cells and systematic application of insulin induced avoidance in mice encountering low concentrations of sodium.[58] In humans, only intranasal experiments of insulin showed an increase in gustatory sensitivity to all tastes.[59] A long term high salt diet has been identified as a risk factor for type-2 diabetes. It will be interesting to investigate how excess salt interferes with insulin dynamics and leads to salt taste desensitization in the long term.

Beyond energy balance, cholecystokinin (CCK) is expressed in bitter-responsive taste cells and can enhance bitter signaling to gustatory nerves, reinforcing aversive feedback as meals progress.[60,61] Fluid-balance hormones, for example, angiotensin II, acting on AT1 receptors in taste buds, suppresses amiloride-sensitive salty signaling yet enhances sweet sensitivity, which matches the selective intake during dehydration.[62]Additionally, hormones for stress,

reproduction, and circadian timing can also shape taste. Acute stress and associated cortisol responses attenuate perceived sweet and reduce salt/sour intensity in humans.[63] While oxytocin has a mild reduction to sweet sensitivity, estrogen receptors are present in mouse taste cells and estradiol can bias sweet preference.[64,65] In pregnancy and menstrual cycles, many females have observed an altered taste profile. How hormones regulate the taste valence change remains unknown.

Chapter 2

TASTE VALENCE IN SODIUM DEPLETION

The same sensory stimuli often drive distinct behavioral responses depending on the internal nutrient state[66–70]. Such state-dependent changes in nutrient value represent a fundamental basis of energy and fluid homeostasis. As the most abundant extracellular cation, sodium has critical roles in many physiological functions, including osmoregulation and neural transduction[71,72]. While sufficient sodium ingestion is vital for animals, overconsumption can cause acute and chronic disorders, e.g., hypertension[73–75]. To achieve optimal ingestion, the brain modulates sodium saliency (palatability) based on internal state and salt concentration[76,77]. Under sodium-sated conditions, animals show modest attraction toward low concentrations of sodium (<100 mM) and strong aversion toward higher concentrations (>300 mM). This behavioral preference drastically switches when sodium is depleted in the body. Sodium-depleted animals vigorously ingest salt at higher concentrations that are normally aversive[68,78–81]. Thus, sodium depletion elevates both appetitive drive and behavioral tolerance toward salt. This internal-state- and concentration-dependent valence regulation allows animals to minimize sodium overconsumption under sated states while maximizing the chance of sodium ingestion under depletion. Such flexible ingestion requires the brain to precisely control both appetitive drive and aversion tolerance toward salt.

At the peripheral level, salts activate multiple taste pathways involved in appetitive and aversive behavioral responses. Low salt is detected by specific taste cells that express the epithelial sodium channel (ENaC)[82–84]. These signals mediate behavioral attraction under

depleted conditions. Moderate to high concentrations of salt generally trigger behavioral aversion in sated animals by recruiting additional aversive taste pathways (Figure S1A)[78,85]. Unlike the sodium-specific ENaC pathway, aversive salt pathways are promiscuous and activated by salts in general.

At the central level, sodium ingestion is controlled by at least two neural modules in the forebrain and hindbrain. First, specific neurons in the solitary nucleus tract (NTS) respond to internal sodium depletion through the action of aldosterone and angiotensin[86–89]. These signals are transmitted to their downstream brain areas, including the pre-locus coeruleus (pre-LC), to drive salt-ingestive behavior[90,91]. Second, sodium depletion activates neurons in the sensory organs of forebrain LT comprised of the subfornical organ (SFO) and organum vasculosum of the LT (OVLT)[72,92–94]. Although the genetic identity of the forebrain neurons is unknown, they were suggested to contribute to sodium preference[95,96]. Despite the accumulating evidence on interoceptive circuits, it is still unclear how the brain modulates positive and negative sensory valences in an internal-state-dependent manner.

2.1 Taste tolerance is functionally separable from salt appetite

Toward circuit-level understanding of sodium homeostasis, we examined whether appetitive drive and behavioral tolerance toward salt are independently regulated. Under sodium-depleted conditions, animals robustly consume both low (60 mM) and high (500 mM) salt solutions (Figure 1A and Figures S1B-C). Notably, these mice tolerate low salt containing aversive minerals such as KCl, $CaCl_2$ and $MgCl_2$ that frequently coexist with sodium in natural resources[97]. In sharp contrast, sated or thirsty animals only accepted pure water and

low salt with no tolerance toward aversive minerals (Figure 1A and Figures S1B-C). Similar results were obtained with a bitter compound: sodium-depleted animals consumed low salt supplemented with quinine, which was totally refused by sated or thirsty animals. These results show that sodium depletion regulates sensory valence of salt in two ways: 1) enhancing sodium-specific appetitive drive, and 2) suppressing behavioral aversion toward aversive compounds (Figures 1B-C).

We investigated if these two sensory modulations are controlled by independent neural circuits. Previously, we showed that specific excitatory neurons in the hindbrain pre-LC (pre-LC^{Pdyn}) neurons receive inputs from NTS interoceptive neurons and are causally linked to sodium ingestion[90,98]. We investigated whether pre-LC^{Pdyn} neurons mediate both appetitive drive and aversion tolerance or only one of the two aspects. Channelrhodopsin (ChR2) was expressed in pre-LC^{Pdyn} neurons using adeno-associated virus (AAV) carrying Cre-dependent ChR2, and animals were tested with different concentrations of salt with or without aversive taste (Figure 1D). As expected, both sodium-depleted and pre-LC^{Pdyn}–stimulated animals consumed to low and high salt (Figure 1D and Figure S1D, 60 and 500 mM NaCl). However, compared to sodium depletion, pre-LC^{Pdyn}–stimulated animals preferred low salt over high salt despite stronger appetitive signals through the ENaC pathway by high salt (Figure S1E). These results suggest that pre-LC^{Pdyn}–mediated sodium intake may lack the normal salt tolerance observed under sodium depletion. Indeed, only sodium-depleted, but not pre-LC^{Pdyn}-stimulated animals tolerated aversive KCl or quinine in low salt solutions (Figure 1D and Figure S1D, 60 mM NaCl with KCl or quinine). Furthermore, in the presence of a potent ENaC blocker, amiloride, photostimulation of pre-

LC^{Pdyn} neurons no longer induced sodium consumption (Figure S1F). These behavioral results demonstrate that the hindbrain circuit mainly controls sodium-specific appetitive drive, and that the attraction and aversion components toward salt are separable in the brain.

2.2 Distinct neural circuits encode taste tolerance

Where is aversive salt tolerance encoded in the brain? Besides the hindbrain interoceptive circuit, the forebrain LT has been suggested to regulate sodium intake[96,99]. Given sodium-specific appetite regulation by the hindbrain circuit, we hypothesized that forebrain LT neurons regulate aversive taste modulation and behavioral tolerance toward salt. In accordance with previous work[96,99], we found sparse but robust activation of LT neurons under sodium depletion based on an immediate early gene expression (Figure 2A and Figure S2A). To identify specific cell types activated under sodium depletion, we adapted stimulus-to-cell-type mapping[95,100] on the 10x Chromium platform. We compared transcriptomic data between sated and sodium-depleted conditions by collecting the SFO, enzymatically dissociating the tissue, and performing scRNA-seq experiments in the presence of a transcription blocker. Approximately 40,000 cells were collected from the SFO of sated and sodium-depleted animals, of which ~10,000 neurons were used for further analyses. The data from sodium-depleted animals were compared with those from sated animals (Figure 2B). Among all neurons, sodium depletion activated a single excitatory neuron type (Glut1) (Figure 2C). Gene expression comparison between neuron types (Figure 2D) identified that prostaglandin receptor type 3 mRNA (*Ptger3*) was selectively expressed in the sodium-depletion-activated Glut1 cluster (Figures 2E-F). Interestingly, Ptger3-positive neurons

(SFO^{Ptger3}) comprise a small population of neuron types activated under hypovolemic thirst, a condition where both water and salt are depleted (Figures S2B-C).

To test if the SFO^{Ptger3} population is anatomically distinct in the SFO, we performed spatial transcriptomic analyses using seq-FISH[101,102]. We selected 192 genes for mRNA hybridization based on transcriptomic data and annotated them in the anterior and posterior areas of the SFO (Figure 2G). By analyzing ~1700 neurons, we validated that Ptger3-expressing neurons are anatomically distinct from other neural populations (Figure 2H and Figure S2D). Moreover, SFO^{Ptger3} neurons were the only active population under sodium depletion (Figure 2I), in accordance with our scRNA-seq results.

2.3 LT^{Ptger3} neurons are sufficient and necessary for tolerance

To gain genetic access to *Ptger3*-positive neurons, we generated transgenic mice with IRES-Cre recombinase:GFP fusion protein targeted to the *Ptger3* locus (abbreviated as $Ptger3^{Cre}$, also see Figure S3A). Fluorescent *in situ* hybridization validated faithful Cre expression in endogenous *Ptger3*-expressing neurons (Figure 3A). To test the activation spectrum of these neurons, we exposed animals to different internal states and stimuli including various nutrient depletion, visceral malaise, pain, and inflammation (Figure 3B). Quantification of Fos immunofluorescence signals showed that SFO^{Ptger3} neurons are narrowly tuned to sodium-need states (Figure S3B). Interestingly, the only exception was inflammatory pain, which partially activated these neurons.

In $Ptger3^{Cre}$ transgenic line, gene-targeted Cre insertion results in premature *Ptger3* disruption. Thus, we used heterozygous $Ptger3^{Cre/wt}$ animals to test whether SFO^{Ptger3} neurons

mediate appetitive drive and/or aversion tolerance toward salt. To this end, we infected AAV-DIO-ChR2 in the SFO of *Ptger3*$^{Cre/wt}$ mice and implanted an optic fiber over the SFO (Figure S3C). Although photostimulation strongly activated SFO^{Ptger3} neurons, it did not induce ingestive behavior toward fluids with any stimulation parameters tested (Figure 3C). We next examined whether these neurons mediate behavioral tolerance. While thirsty mice showed dose-dependent aversion toward salt, SFO^{Ptger3}-stimulated animals exhibited greatly increased consumption of aversive high salt (Figure 3D, Figures S3D-E, and Videos S1-2). Importantly, photostimulation did not affect water or low-salt consumption, excluding the possibility that SFO^{Ptger3} neurons mediate general appetite modulation. The same photostimulation paradigm also enhanced behavioral tolerance toward aversive compounds presented with low salt (Figure 3E). Unlike pre-LC^{Pdyn} neurons, amiloride had no effect on SFO^{Ptger3}-mediated salt tolerance (Figure S3F). We note that the levels of SFO^{Ptger3}-induced tolerance were comparable to those under sodium depletion (Figure S3G).

We also investigated if LT^{Ptger3} neurons are functionally required for salt tolerance.

Because a subset of OVLT neurons also expressed *Ptger3* (Figure S3H), and were activated under sodium depletion, we expressed an inhibitory DREADD in Ptger3 neurons of these areas by transducing AAV-DIO-hM4Di. Inhibition of SFO/OVLT^{Ptger3} neurons by a synthetic DREADD ligand, CNO, drastically suppressed tolerance toward aversive salt under sodium-depleted or hypovolemic state (Figure 3F and Figure S3I). LT^{Ptger3}-inhibited mice no longer tolerated low salt with quinine or KCl, whereas the same inhibition had no effect on solute intake under osmotic thirst conditions where Ptger3 neurons are not activated (Figure 3F). The blunted tolerance was also observed when only SFO^{Ptger3} neurons were

inhibited (Figure S3J). Taken together, our neural perturbation experiments revealed an essential role of SFO^{Ptger3} neurons in regulating aversion tolerance, but not in appetitive drive toward salt.

2.4 Forebrain taste tolerance circuit is independent from hindbrain appetite circuit

Given the distinct functions of forebrain and hindbrain circuits for salt ingestion, we asked whether sodium depletion activates pre-LC^{Pdyn} and SFO^{Ptger3} neurons independently or in series (Figure 4A). To test this, we genetically probed pre-LC^{Pdyn} → SFO^{Ptger3} and SFO^{Ptger3} → pre-LC^{Pdyn} projections by expressing ChR2-EYFP/ChR2-mCherry in either neural population. While both populations send axonal projections to downstream areas, practically no anatomical interaction was observed between pre-LC^{Pdyn} and SFO^{Ptger3} neurons (Figures 4B-C, top). Optogenetic stimulation of each excitatory population did not activate neurons in the other nucleus, showing functional independence between these two neural populations (Figures 4B-C, bottom). Moreover, ablation of either pre-LC^{Pdyn} or LT^{Ptger3} by Cre-dependent expression of caspase did not affect Fos immunofluorescence signals in the remaining nucleus under sodium depletion (Figures 4D-E). Thus, forebrain and hindbrain circuits are independently activated under depleted states.

2.5 Taste tolerance is specific to bitter and sour taste

In the mammalian taste system, high salt activates aversive taste pathways, including bitter and sour[78,85]. Genetic silencing of aversive taste signals (e.g., *Trpm5*$^{-/-}$[103,104]) greatly reduced behavioral avoidance toward salt (Figure S4A). We suspected that the activity of Ptger3

neurons might control the sensitivity or saliency of aversive taste signals. If this was true, we anticipated that the stimulation of SFO^{Ptger3} neurons should reduce behavioral aversion toward bitter or sour taste stimuli. Indeed, while animals exhibited dose-dependent aversion toward bitter and sour tastes, acute stimulation of SFO^{Ptger3} neurons drastically blunted aversive responses to quinine and to a lesser degree, citric acid (Figures 5A-B). Because acids activate multiple oral sensory pathways[105–107], these multimodal signals may have masked the tolerance effects by SFO^{Ptger3} neurons. By contrast, such aversive taste tolerance was not induced by photostimulation of pre-LC^{Pdyn} neurons (Figure S4B). The behavioral responses to an attractive taste such as sweet was unaffected by the same neural manipulation (Figure 5C). Moreover, SFO^{Ptger3}-mediated behavioral tolerance was not generalized to conditioned taste aversion or capsaicin, a non-taste oral noxious stimulus[108] (Figure S4C and Figure 5D). Taken together, our data demonstrate that behavioral effects through SFO^{Ptger3} neurons are selective toward aversive taste stimuli (Figure 5E). Consistent with this model, the same neural manipulation had no effect on behavioral tolerance toward other aversive stimuli including heat, acute, and inflammatory pain (Figures S4D-G).

We reasoned that if SFO^{Ptger3} neurons encode aversive taste tolerance, artificial stimulation of this neural population should increase general taste palatability. To test this idea, food-deprived animals were given access to sugars (glucose and acesulfame K[109]) with or without an additional bitter component (Figure 5F). Because sugar and bitter taste mixture is less palatable than the pure sugar solution, mice show reduced preference toward the mix (Figure 5F and Figure 5G, left). However, stimulation of SFO^{Ptger3} neurons suppressed the aversiveness of the mixture, and animals showed increased preference toward the mixture

comparable to the pure sugar solution. Similar results were obtained for umami taste (Figure 5G, right).

2.6 Discussion

We demonstrated that two critical aspects of salt ingestion, sodium-specific appetitive drive and general salt tolerance are modulated by separate neural populations in an internal-state-specific manner. Our neural perturbation experiments showed that appetitive drive is regulated by the hindbrain neural pathway, while aversion tolerance is regulated by forebrain SFO^{Ptger3} neurons (Figure S5A). Such a bimodal neural architecture reveals a flexible regulatory mechanism of sodium ingestion by modulating the saliency of sodium taste depending on internal need.

Although sodium depletion suppresses the apparent sensitivity to aversive tastes, such sensory modulation may occur at the peripheral or/and central levels[110–113]. Our results favor the central modulation model, as peripheral taste signals were minimally unaffected by sodium deletion or SFO^{Ptger3} neuron activity. We stimulated the tongue with different concentrations of NaCl while recording peripheral taste nerves using *in vivo* electrophysiology[114,115] and observed that the response threshold and amplitude to NaCl were largely unchanged under sated, thirsty, sodium-depleted, or SFO^{Ptger3}-stimulated conditions (Figures S5B-D). Although the precise pathways of taste modulation remain to be investigated, these results suggest that regulation of behavioral sensitivity to aversive taste stimuli is likely mediated at the central levels.

While the LT is involved in water and sodium balance[81,84,96], how individual LT cell-types are involved in these regulations has been elusive[95]. Here we show that a genetically defined neuron class that expresses Ptger3 mediates a specific aspect (tolerance) of fluid ingestion. These findings provide key insights into central coding logic of internal water-sodium balance. Under sodium depletion or hypovolemia, SFO^{Ptger3} neurons are activated to promote salt ingestion[86,88,90]. Conversely, osmotic thirst activates non-SFO^{Ptger3} LT neurons to drive pure water intake[90,116]. Thus, each class of LT neurons are activated in an internal-state-dependent manner, yet encodes a specific physiological function (e.g., SFO^{Ptger3} for mineral tolerance). It is currently unclear how SFO^{Ptger3} and other LT neurons exert salt tolerance and fluid ingestion through downstream brain areas (Figure S5E). Future brain-wide downstream analyses will reveal how multiple neuron types regulate water and sodium balance under fluid imbalance.

Previous studies have observed elevated tolerance toward aversive stimuli under hunger states[70,117,118]. However, the underlying mechanisms appear distinct from salt tolerance. Stimulation of hunger neurons in the arcuate nucleus drives feeding and suppresses various noxious stimuli in parallel through their downstream projections[70,118]. By contrast, sodium appetite and tolerance are encoded by distinct neural circuits. Why do different interoceptive circuits employ distinct appetitive/tolerance mechanisms? It is well established that the valence of sodium switches in a concentration- and internal-state-dependent fashion. Thus, it is conceivable that the hindbrain pre-LC^{Pdyn} neurons mediate internal-state-specific regulation while forebrain SFO^{Ptger3} neurons encode concentration-dependent regulation toward sodium salts. Such neural architecture would allow interoceptive and exteroceptive signal integration to optimize sodium consumption.

Unlike non-caloric artificial sweeteners such as sugar substitutes, sodium is the only safe cation that exhibits salty taste[119]. Even though salt overconsumption is a significant health risk factor, modulation of salt consumption has been challenging due to the lack of sodium substitutes. Our findings shed light on a potential strategy to modulate salt taste by saliency control. We showed that activation and inhibition of SFO^{Ptger3} neurons bidirectionally regulated sodium tolerance and consumption (Figures 3D-F). The SFO lacks the normal blood-brain barrier, making it accessible to compounds in systemic blood circulation such as PGE2. Thus, identifying compounds that activate or inhibit LT^{Ptger3} neurons may provide a salt-taste-modifying strategy to control sodium consumption.

2.7 Limitations of the study

Our study employed a standard sodium depletion model by injecting a diuretic compound and testing behavior or histology at a fixed time (24 hr). In future studies, it will be important to test whether the development of sodium-specific appetite and general salt tolerance may have different time scales in the brain. Additionally, sodium depletion independent of salt furosemide should be tested.

2.8 Acknowledgements and Contributions

We thank the members of the Oka laboratory and Sangjun Lee for helpful discussion and feedback comments. We thank Ashil Koranne and Jacob Hauser for maintaining and genotyping animal lines, and the Single Cell Profiling and Engineering Center (SPEC) in the Beckman Institute at Caltech. R.D.P thanks Serina Tsang and Kathy Kafer for help

generating the *Ptger3*^{Cre} mice and Susan Phelps for mouse husbandry. We thank Tomomi Karigo for Caspase virus. This work was supported by Startup funds from the President and Provost of California Institute of Technology and the Biology and Biological Engineering Division of California Institute of Technology. Y.O. is supported by New York Stem Cell Foundation, NIH (R01NS109997, R01NS123918), Alfred P. Sloan Foundation, Edward Mallinckrodt Foundation, and Heritage Medical Research Institute. Y.Z. was supported by Chen Graduate Fellowship.

Y.Z. and Y.O. conceived the research program and designed experiments. Y.Z. performed genetic and behavioral experiments and analyzed the data. E.K. supported behavioral and histological analysis. R.D.P. generated and maintained *Ptger3*^{Cre} transgenic mice. Y.Z., T.W., and A.H.P. performed single-cell RNA sequencing experiments and analyzed the data. T.W., B.Z., L.D., and K.F. performed seqFISH experiments. Y.Z. and Y.O. wrote the paper. Y.O. supervised the entire work.

2.9 Method

Animals

All procedures followed the US NIH guidance for the care and use of laboratory animals and were approved by the California Institute of Technology Institutional Animal Care and Use Committee (protocol: 1694–14). Male and Female mice at least 8 weeks were used for behavioral tests and histology characterization. No sex difference is observed in this study. For scRNA-seq experiments, 7-8-week-old C57BL/6J mice were used. C57BL/6J were purchased (000664) from the Jackson Laboratory. *Pdyn*^{Cre} mice were a gift from B. Lowell

and M. Krashes (Jackson lab, 027958). Heterozygous *Pdyn*^{Cre} mice were used for all experiments. *Trpm5*$^{-/-}$ mice were generously provided by C. Zuker (Jackson lab, 013068). Mice were housed in temperature-controlled and humidity-controlled rooms with a 13:11 hr light:dark cycle. Mice are provided with ad libitum access to chow and water unless mentioned in the nutrient deprivation experiments.

Generation of the Ptger3^{Cre} *mouse line*

Ptger3^{Cre} animals were generated by inserting mnCre:GFP cassette just 5' of the initiation codon of *Ptger3* gene and deleting the first 40 amino acids. The cassette had a Myc-tag and nuclear localization signals at the N-terminus. The targeting construct was electroporated into G4 ES cells (C57Bl/6 × 129 Sv hybrid) and correct targeting was identified by Southern blot. The frt-flanked SV-Neo gene was removed via breeding with Gt(Rosa)26Sor-FLP recombinase mice and then backcrossing to C57BL/6J mice for >6 generations. Homozygous *Ptger3*$^{Cre/Cre}$ mice are equivalent to *Ptger3*$^{-/-}$ because of the amino acid deletion.

Viral constructs

We used the following viruses: AAV5-EF1a-DIO-ChR2-EYFP, 3.0×10^{13} viral genomes per ml. AAV2-EF1a-DIO-ChR2-mCherry, 5.1×10^{12} viral genome copies per ml. AAV2-EF1a-DIO-mCherry, 4.6×10^{12} genome copies per ml. AAV8-hSyn-DIO-hM4D(Gi)-mCherry, 1.9×10^{13} viral genomes per ml. AAV2-hSyn-DIO-hM3D(Gq)-mCherry, 6.5×10^{12} viral genomes per ml. AAV2-Flex-taCaso3-Tevp, 1.8×10^{12} viral genome copies per ml. AAV5-Flex-taCasp3-Tevp, 4.2×10^{12} viral genome copies per ml

Surgery

Surgery procedures were performed as described[90]. Briefly, ketamine (1 mg/ml) and xylazine (10 mg/ml) in saline were injected intraperitoneally at a dose of 10 ml per kg body weight (BW) for anaesthesia. Ketoprofen was injected subcutaneously at a dose of 5 ml per kg BW. Surgery was performed with a stereotaxic apparatus (Narishige, SR-5M-HT) on a heating pad at 37 °C. Virus was delivered with a microprocessor-controlled injection system (World Precision Instruments, Nanolitre 2000) at 100 nl/min. The following coordinates were used: for pre-LC: anterior–posterior (AP), 9,000, medial–lateral (ML), 1,000, ventral–dorsal (VD), 3,800; for SFO: AP, 4,000, ML, 0, VD, 2,500; for OVLT: AP, 2,475, ML, 0, VD, 4,750; for dorsal part of the NAc medial shell: AP, 2,100, ML, 700, VD, 4,000. For optogenetic experiments, virus was delivered unilaterally at a volume of 120-200 nl. Implants were made by gluing a 200-μm fibre bundle (Thorlabs, FT200EMT) to a ceramic ferrule (Thorlabs, CF230-10) with epoxy. The fibre implant was placed 200 μm above the virus injection site. For chemogenetic inhibition experiments, virus was delivered at 180-200 nl per region. For ablation experiments, virus was delivered at 200-250 nl per region.

Internal state induction

Sodium depletion: Mice were injected intraperitoneally with furosemide at a dose of 50 mg per kg BW and maintained with a low-sodium diet for 24 hr before behavioral assays or immunohistological staining[120].

Osmotic thirst: Mice were injected intraperitoneally with either 2 M NaCl (5 ml per kg BW) or mannitol solution (10 ml per kg BW) and maintained with no food or water for 10 min before the behavioral assay or 1 hr before immunohistological staining. Mannitol was used for long-term consumption assay and Fos immunostaining, and NaCl was used for

short-term consumption assay. We did not find significant differences between the results obtained with these two solutions.

Sodium depletion with osmotic thirst: Mice were sodium depleted via furosemide as mentioned above. Mice were injected intraperitoneally with 2M mannitol solution (10 mg per kg BW) and maintained with no food or water for 10 min before behavioral assay.

Hunger: Mice were food deprived for 24 hr before the behavior test or immunohistological staining.

Hypovolemic thirst: Mice were injected intraperitoneally with furosemide at a dose of 50 mg per kg BW and maintained with no food or water for 3 hr before behavior test or 4 hr immunohistological staining.

Visceral malaise: Mice were injected intraperitoneally with 0.15 M LiCl at a dose of 15 ml per kg BW and euthanized 1 hr after injection for immunohistological staining.

Solution preparation

Tastants: We chose the concentrations of taste/salt solutions based on previous literature[78,121]. In the mammalian taste system, aversive components of high salt and KCl share the same taste pathways[122]. Thus, we supplemented KCl in low-salt solutions to increase the aversiveness of salt solution without changing activity of the low-salt specific ENaC pathway.

Capsaicin[123]*:* Capsaicin was prepared as 3 mM stock in 30% ethanol. For brief access assay, the solution was further diluted to 1 or 0.3 μM with water. Water containing ethanol equal to 1 μM capsaicin was used for control.

Behavioral assays

All assays were performed in a custom gustometer (Dialog Instruments). All animals were at least trained with osmotic thirst and sodium depletion prior to the behavior trials. Animals were trained to drink at least 200 licks for 500 mM NaCl in 30 min under sodium depletion. Generally, two training sessions with sodium depletion are sufficient to achieve this criterion. Animals often show neophobia to a new solution even if it was an attractive stimulus. To prevent this, all tastants at lower concentrations were exposed to animals before experiment. For tolerance tests, we used one-bottle consumption assay in order to avoid preference development during the session.

For 30-min access assay, mice were presented with 1 bottle for 30 min and consumption was measured.

For 5-sec brief access assay, mice were presented with 1 bottle of solution for 30 sec per trial for maximum waiting time before the first lick, and 40 sec between trials. After an initial lick, animals were allowed to drink the solution for additional 5 sec before a shutter closed. To avoid taste conditioning effect, animals were tested with only one solution per day. After testing aversive solutions, bitter and high salt, animals sometimes refused to drink any solution. These animals were retrained with water and low salt until their behavioral level recovers to our criteria stated above.

Optogenetic and chemogenetic manipulation

For optogenetic activation, 473-nm laser-pulse sequences were delivered via an optic cable (Doric Lenses, MFP-FC-ZF) with pulse generators (World Precision Instruments, SYS-A310 or Quantum composers, Sapphire 9200). The laser intensity was maintained at 10 mW at the tip of the fiber. For 30-min access assay, the light stimulation was given at 20

Hz with a 1-sec on 3-sec off paradigm. For 5-sec brief access assay, the light stimulation was given at 20 Hz throughout the trial except the paradigm in Figure 3C.

For chemogenetic experiments, clozapine N-oxide (CNO) was administered intraperitoneally at doses of 10 mg per kg BW for inhibition or 1 mg per kg BW for activation 20 min before the consumption trial started. Pure water instead of saline was used as vehicle to avoid sodium repletion.

Long term consumption assay

Liquid consumption level was monitored in the Biodaq system (Research Diets)[124]. Mice were individually housed and acclimated in the cage at least for 24 hr before the data collection. We considered that animals were acclimated when they consumed more than 1 g of water and low salt overnight. Animals were offered only one type of liquid overnight and were provided with water during the daytime to replete. 60 mM NaCl, 60 mM NaCl with 440 mM KCl, 60 mM NaCl with 40 mM $CaCl_2$, 60 mM NaCl with 40 mM $MgCl_2$, 500 mM NaCl and water were applied. Data for consumption were analyzed from 6 to 9 pm. Prolonged measurement with aversive solutions often causes dehydration if animals refuse to drink. To avoid internal state transition over time, we measured consumption within a limited time window.

Pain induction

Acute Pain (foot shock): Animals were acclimatized in the operant conditioning chamber for 10 min (MedAssociates). A constant current of 0.25 mA was delivered to the metal grid floor. Animals moved freely in the setting. The shock was delivered for a continuous 5-sec window followed by a 10-sec rest. Each trial lasted 2 min. For immunohistological

staining, mice were euthanized 1 hr after exposure. The light stimulation was given at 20 Hz with a 1-sec on 3-sec off paradigm.

Thermal pain (heat shock): A hotplate (Columbus instruments, 93291) was maintained at 52°C. Animals were placed onto the hotplate and the latency for licking paws was recorded. To test the effect of optogenetic stimulation, animals were tested on the hotplate, and re-tested following stimulations of 15 and 45 min. The light stimulation was given at 20 Hz with a 1-sec on 3-sec off paradigm.

Mechanical threshold (von Frey Test): Mice were habituated on a metal grid floor, and were tested with von Frey filaments (Bioseb, BIO-VF-M) in ascending order. Each filament was tested 5 times. The withdrawal threshold was determined when the mice withdrew the paw for more than 3 times as the filament was applied until bent. To test the effect of optogenetic stimulation, mice were tested before stimulation and following a stimulation of 60 min. The light stimulation was given at 20 Hz with a 1-sec on 3-sec off paradigm.

Inflammatory pain (formalin test): Mice were injected with 2% formalin (20 μl) in the dorsal hindpaw and placed in behavior chamber. Videos were taken for 1 hr following the injection and analyzed for the time mice spent licking the dorsal hindpaw. Mice with more than 30-sec licking paw time in the first 5 min after injection were used for video analysis. Each mouse was subjected to formalin injection twice: in one hind paw under sated conditions, and another under either sodium depleted or photostimulated conditions. To test the effect of optogenetic stimulation, light stimulation was given at 20 Hz with a 1-sec on 3-sec off paradigm for 60 min. For ELISA assay, blood was collected 30 or 90 min after formalin injection.

Immunohistochemistry

Mice were euthanized with CO_2 and perfused with PBS and 4% paraformaldehyde. Extracted mouse brains were fixed overnight at 4 °C in 4% PFA and sectioned coronally to 100-μm slides via vibratome (Leica, VT-1000 S). The sections were blocked (10% donkey serum, 0.2% Triton X-100 in PBS) for 1 hr at room temperature and incubated with primary antibody at 4 °C overnight. The following primary antibodies were used: rabbit anti-FOS (1:500), sheep anti-Foxp2 (1:2,000), chicken anti-GFP (1:3,000), rat anti-mCherry (1:500), and goat anti-nNos (1:500). The sections were washed three times with PBS and incubated with the secondary antibody (1:500; Jackson Immunoresearch) and DAPI (2 μg/ml) for 4 hr under room temperature. After three times wash with PBS, the sections were mounted on the glass slide. All slides were imaged with confocal microscope (Leica, TCS SP8) or slide scanner (Olympus, BX61VS).

Taste nerve recording

Surgery and recording procedures were performed as described[78,125]. Briefly, mice were anesthetized with pentobarbital (100 mg per kg BW) and placed in a custom-made head-fixation setup, with body temperature maintained at 37 °C. Tracheotomy was performed. The right branch of the chorda tympani nerve was exposed, and recording was performed with a high-impedance tungsten electrode hooking the nerve bundle. Tastant stimuli were delivered with a pressurized perfusion system (AutoMate Scientific) for 20 sec, with a 40-sec wash with artificial saliva. The artificial saliva was made with 20x stock and on the day of experiment, was diluted with the addition of 6 mM $KHCO_3$ and 6 mM $NaHCO_3$. The pH was adjusted to 7.2-7.6. For recording, each mouse underwent two sets of experiments in a specific internal state. Two sets of experiments were in a randomized order and each

experiment was repeated with 2-3 trials according to the mice condition. For the NaCl experiment, 10/30/60/120/250/500 mM NaCl and 4 mM AceK were applied. For multiple tastant experiments, the following taste stimuli were used: 60 mM NaCl (salty), 10 mM citric acid (sour), 4 mM acesulfame potassium (sweet), 50 mM monopotassium glutamate plus 1 mM inosine monophosphate (umami), 500 mM KCl (bitter), and 1 mM quinine (bitter). Signals were recorded with Axon Digidata 1550B Low-Noise Data Acquisition System, and Grass RPS312 RM Power Supply with P511 AC Amplifier (Natus Neurology).

The data were processed using a custom Matlab code. Briefly, the original data (sampled at 10k Hz) were time-binned at 0.1 sec. The recording traces were visualized by processing time-binned data with a rolling-median of 3 sec. A 3-sec time window before each stimulus served as a baseline. A 30-sec response window was quantified, starting when the signals exceeded 3 standard deviations (SD) above baseline. The data were normalized to the average of two consecutive 4 mM AceK trials. For photostimulation trials, when the tastants washed through, light was delivered at 20 Hz, 10 mW for 30 sec.

Single cell RNA sequencing

Tissue processing into single-cell suspensions: For the sodium-depleted condition, 15-20 mice, 7-8 weeks old, were sodium depleted for 24 hr. For sated condition, 15 sated mice were used. The tissue processing procedure was performed as described. Briefly, upon isoflurane anaesthesia, the brains were exacted from the mice and kept in ice-cold carbogenated NMDG-HEPES-ACSF. Brains were sectioned to 2 mm, SFO was harvested into ice-cold NMDG-HEPES-ACSF by peeling the tissue (SFO)

microdissection under microscope. After tissue collection, NMDG-HEPES-ACSF was replaced with trehalose-HEPES-ACSF containing papain (80 U/ml; pre-activated with 2.5 mM cysteine and a 30-min incubation at 34 °C with 0.5 mM EDTA) and 15 μM actinomycin D. Extracted SFO tissue was incubated at 34 °C with gentle carbogenation for 60-90 min. The tissue was pipetted periodically every 10 min during this digestion. At the end of enzymatic digestion, the medium was replaced with 200 μl of trehalose-HEPES-ACSF with 3 mg/ml ovomucoid inhibitor 25 U/ml DNase I and 15 μM actinomycin D. The SFO tissue was gently triturated with 600, 300 and 150 μm-diameter fire-polished glass Pasteur pipettes in less than 10 mins. The tissue was processed into a uniform single-cell suspension and the total volume was brought up to 1 ml with trehalose-HEPES-ACSF with 3 mg/ml ovomucoid inhibitor. The suspension was filtered through a 40-μm cell strainer (Falcon, 352340) into a new microcentrifuge tube and was centrifuged with 300 g for 5 min at 4 °C. The supernatant was discarded, and the cell pellet was resuspended with fresh ice-cold resuspension buffer and kept on ice while cell densities were quantified with a hemocytometer. The final cell suspension volume estimated to retrieve ~10,000 single-cell transcriptomes were added to the 10x Genomics RT reaction mix and loaded to the 10X Single Cell G chip (10x Genomics, PN-1000127). The Chromium Single Cell 3′ GEM, Library and Gel Bead Kit v3.1 (PN-1000128) and the Single Index Kit T Set A (PN-1000213) were used. The cDNA and library amplification underwent 11 and 12 cycles respectively.

Sequencing data pre-processing and analysis

The scRNA-seq sequencing libraries were sequenced on an NovaSeq S4 lane. The sequencing reads were mapped to the custom-made pre-mRNA reference transcriptome,

and gene-cell matrices were generated via the 10x Genomics Cell Ranger pipeline as previously described[126]. Subsequent gene expression analyses were conducted in R (4.1.2) using Seurat (4.0.3) as previously described[95,127]. Cells were filtered if possessing fewer than 1,000 or more than 45,000 unique transcripts, or more than 15% of mitochondrial transcripts. Transcriptomic cell types were identified and cell clusters co-expressing two or more markers for canonical cell classes were excluded. Both sodium depletion and sated conditions included two trials collected from different time points for the consistency of the data. Four data sets were merged into a single-gene expression-matrix and canonical correlation analysis was applied. This yielded an SFO data set of 7819 neurons (four sets merged). Dimensionality reduction was performed with 25 principal components for major cell classes and 10 to 13 principal components for neural subtypes. The resolution of clustering was 0.8 for all cell classes and 0.6 - 2 for neural subtypes. Canonical correlation analysis was performed to adjust the misalignment of transcriptomic neuron types due to physiological-state-derived transcriptional changes. We normalized the gene expression with identified integration anchors based on the top 200 differentially expressed gene sets from the untreated neural data set. For Figure S2B, neuron matrix from sated- and sodium-depleted states were analyzed together with the previous hypovolemia neuron matrix.

Spatial transcriptomics

SeqFISH gene panel design: A custom seqFISH panel was designed to incorporate canonical cell-type-marker genes based on our scRNA-seq dataset analysis[101]. The panel contained 192 genes of which 174 were detected using barcoded seqFISH imaging and 18 were identified serially via single-molecule FISH. The panel was custom ordered by Spatial Genomics, Inc.

SeqFISH sample collection and preparation: Adult (8-12 weeks old) C57BL/6J male mice under sated or sodium depleted states were euthanized (n = 5 mice per state). Each brain was dissected, freshly embedded in Tissue-Tek O.C.T. Compound (Sakura, 4583), and then flash-frozen in liquid nitrogen. Cryosections of 10-µm thickness containing the SFO were cut and mounted onto treated coverslips. Immediately post-collection, sections were fixed in fresh 4% paraformaldehyde (Thermo Scientific, 28908) for 15 min at room temperature. After rinsing three times in 1X PBS for 5 min each, sections were dehydrated using 70% ethanol for 30 sec at room temperature. The sections were air-dried at room temperature for approximately 15 min and stored at -80C. SeqFISH experiments were performed using the seqFISH+ protocol with some modifications at Spatial Genomics, Inc. Briefly, the fixed tissue sections underwent permeabilization in 70% ethanol followed by clearing, rinsing, and air-drying steps. The coverslip containing each section was assembled into Spatial Genomics custom flow cells. The flow cells were then hybridized with the seqFISH primary probe panel and incubated in a humidified chamber at 37 °C for 24 hr. After hybridization, samples were washed with buffers for subsequent imaging.

seqFISH imaging via Gene Positioning System: Imaging was performed using the Gene Positioning System (GenePS, Spatial Genomics, Inc.), which enables automated image acquisition, reagent delivery, and data processing. The SFO was selected as a region of interest (ROI) for the experiment based on the brightfield and/or DAPI images. Automated experiment execution was initiated post-ROI selection. Each experiment proceeded through multiple rounds of decode probe hybridization, imaging, and signal removal until all the hybridization rounds were complete.

Image processing and analyses: Raw-image files were processed on-instrument to align images across multiple hybridization rounds and detect RNA fluorescent signals. The data were further analyzed using custom Spatial Genomics analysis software to decode the transcript identities and segment cells. Cell segmentation was performed using a machine learning algorithm based on the nuclear DAPI stain. The decoded RNA molecules were then assigned to individual cells, generating cell-by-gene count matrices and individual cell center coordinates for each ROI. For the downstream data analysis, cells that had unique gene counts of less than 10 were filtered. The images of the spatial distribution of the major cell types in the SFO with cell segmentation boundaries and color-coded cell type identities were directly generated by the Spatial Genomics analysis software. The spatial distribution of neurons was plotted according to cell center coordinates using Python (3.9.12). Individual neuron types were labeled with different colors based on raw transcripts of the neuronal subtype marker genes after manual curation. UMAP and violin plots were generated using Seurat (4.2.1) in R (4.1.1).

RNAscope-based multicolour in situ hybridization

In situ hybridization was performed with the RNAscope Multiplex Fluorescent Assay versions 1 or 2 (Advanced Cell Diagnostics, 320850). Fixed-frozen brains from C57BL/6J, *Ptger3*$^{Cre/wt}$ and *Ptger3*$^{Cre/Cre}$ (equivalent to knockout) were prepared following the manufacturer's protocols. Following probes were applied to the samples: *Cre* (312281), *Ptger3* (504481 and 501831), and *GFP* (409011). The samples were imaged with confocal microscopy and visualized via z-stacks.

Quantification and Statistical Analysis

No statistical methods were used to predetermine sample size. The experiments were not randomized, and investigators were not blinded to allocation during experiments and outcome assessment. Data are presented as means ± SEMs in figures. Wilcoxon test, Mann-Whitney test, and one- or two-way ANOVA with post hoc tests were applied to decide the significance level. Significant threshold was maintained at $\alpha = 0.05$ (ns $p > 0.05$, $*p < 0.05$, $**p < 0.01$, $***p < 0.001$).

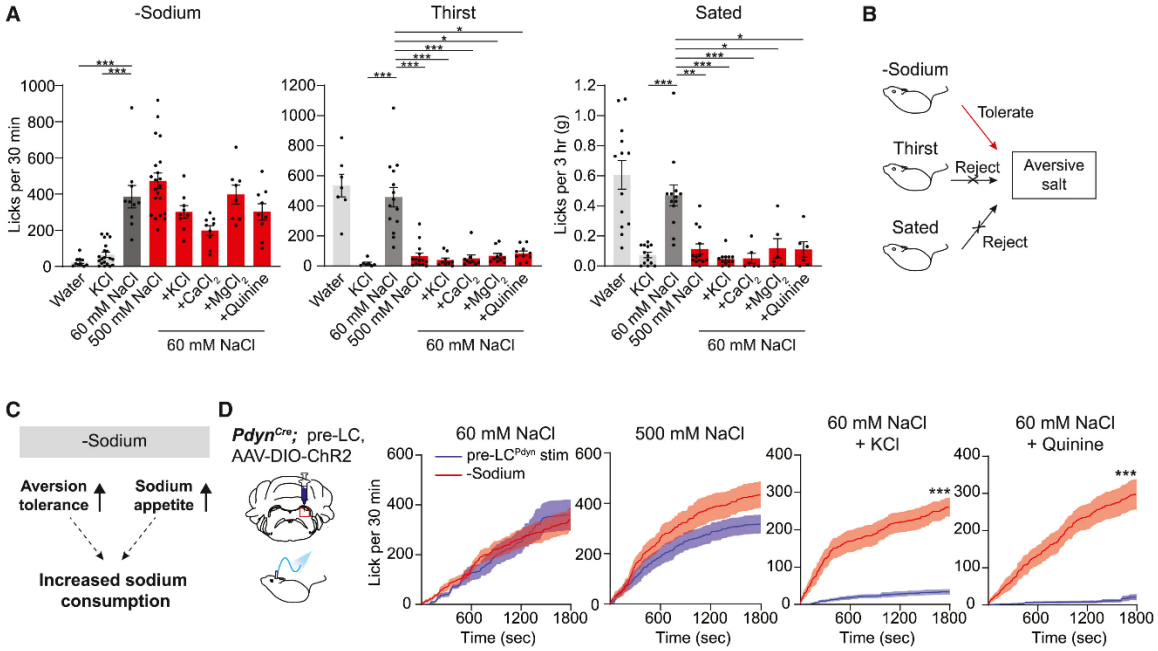
A
-Sodium
Thirst
Sated
Licks per 30 min
Licks per 3 hr (g)
Water
KCl
60 mM NaCl
500 mM NaCl
+KCl
+CaCl2
+MgCl2
+Quinine
60 mM NaCl
B
-Sodium
Tolerate
Thirst
Reject
Aversive salt
Sated
Reject
C
-Sodium
Aversion tolerance
Sodium appetite
Increased sodium consumption
D
Pdyn^Cre; pre-LC, AAV-DIO-ChR2
60 mM NaCl
500 mM NaCl
60 mM NaCl + KCl
60 mM NaCl + Quinine
pre-LC^Pdyn stim
-Sodium
Lick per 30 min
Time (sec)

Figure 1. Independent regulation of appetitive drive and tolerance toward salt.

(A) Consumption assay under sodium depleted (-Sodium, left), osmotic thirst (Thirst, middle), or sated (Sated, right) conditions. Animals were tested with pure water, KCl (500 mM), low salt (60 mM NaCl), high salt (500 mM NaCl), low salt + 440 mM KCl, low salt + 40 mM $CaCl_2$, and low salt + 40 mM $MgCl_2$, and low salt + 0.25 mM quinine (n = 6-21 mice).

(B) A diagram of state-dependent salt tolerance. Sodium-depleted animals accept aversive high salt or low salt with additional aversive stimuli. Conversely, sated or thirsty animals reject the same solutions.

(C) A bimodal regulation model of salt consumption under sodium depletion.

(D) Comparison of pre-LC^{Pdyn}-stimulated and sodium-depleted conditions. Left, a scheme of acute photostimulation of pre-LC^{Pdyn} neurons. Middle and right, Cumulative consumption curves of pre-LC^{Pdyn}-stimulated (blue) and sodium depleted (red) conditions during a 30-min session. Low and high salt (60 and 500 mM NaCl) was accepted by both pre-LC^{Pdyn}-stimulated and sodium-depleted animals. Only sodium-depleted animals tolerated low salt with KCl or quinine but not photostimulated animals (n = 9-15 mice).

Data are expressed as mean ± SEM, $*p < 0.05$, $**p < 0.01$, $***p < 0.001$.

See also Figure S1 and Table S1.

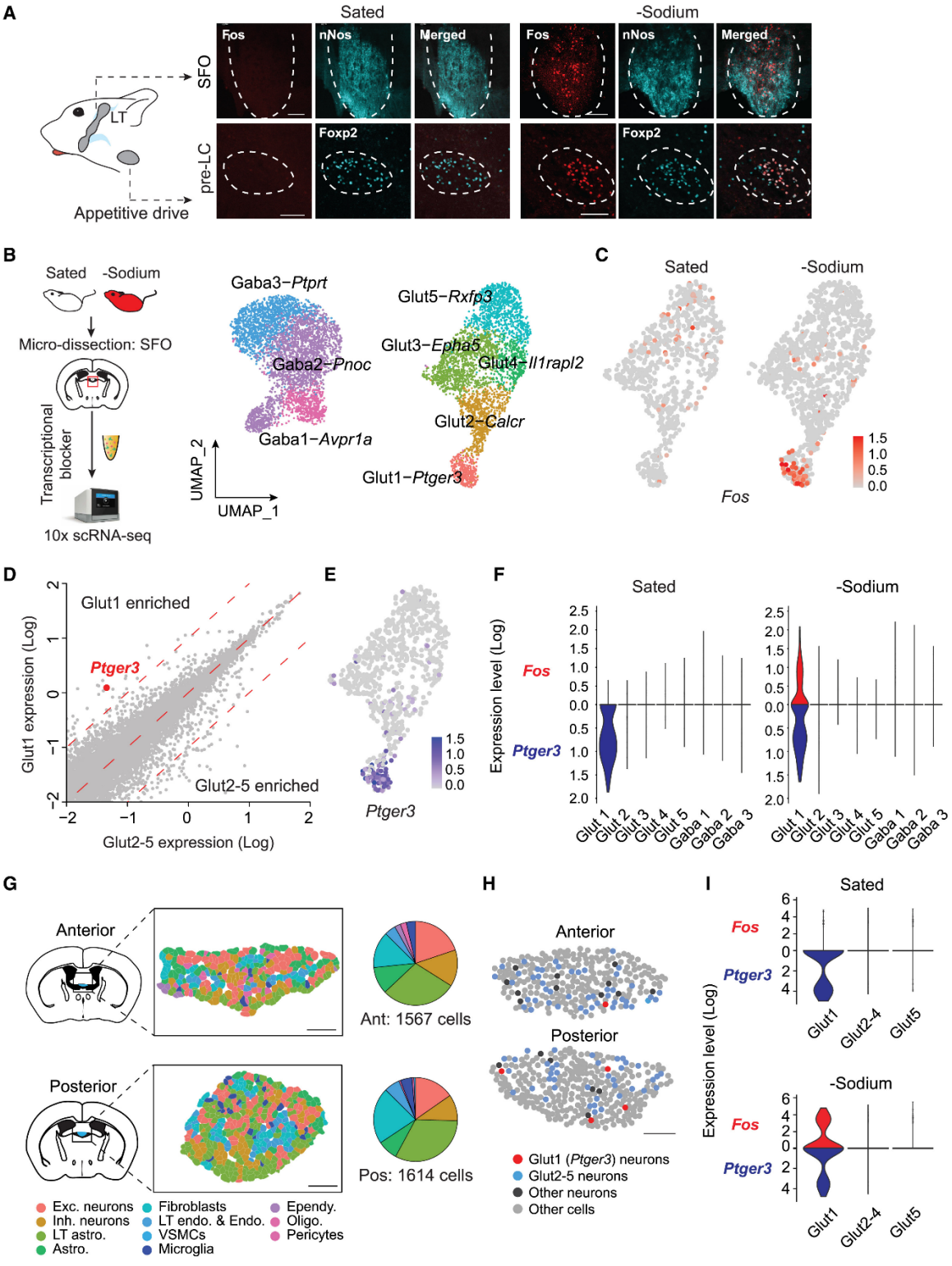
A
Sated
-Sodium
Fos
nNos
Merged
SFO
pre-LC
Foxp2
LT
Appetitive drive
B
Sated
-Sodium
Micro-dissection: SFO
Transcriptional blocker
10x scRNA-seq
Gaba3−Ptprt
Gaba2−Pnoc
Gaba1−Avpr1a
Glut5−Rxfp3
Glut3−Epha5
Glut4−Il1rapl2
Glut2−Calcr
Glut1−Ptger3
UMAP_2
UMAP_1
C
Sated
-Sodium
Fos
1.5
1.0
0.5
0.0
D
Glut1 enriched
Ptger3
Glut2-5 enriched
Glut1 expression (Log)
Glut2-5 expression (Log)
E
Ptger3
F
Sated
-Sodium
Fos
Ptger3
Expression level (Log)
Glut 1
Glut 2
Glut 3
Glut 4
Glut 5
Gaba 1
Gaba 2
Gaba 3
G
Anterior
Posterior
Ant: 1567 cells
Pos: 1614 cells
Exc. neurons
Inh. neurons
LT astro.
Astro.
Fibroblasts
LT endo. & Endo.
VSMCs
Microglia
Ependy.
Oligo.
Pericytes
H
Anterior
Posterior
Glut1 (Ptger3) neurons
Glut2-5 neurons
Other neurons
Other cells
I
Sated
-Sodium
Fos
Ptger3
Expression level (Log)
Glut1
Glut2-4
Glut5

Figure 2. Sodium depletion activates selective excitatory neuron types in the LT.

(A) Representative images of Fos (red) immunofluorescence signals in the forebrain SFO, and hindbrain pre-LC under sodium depletion and sated states. The SFO was counterstained by an excitatory marker nNos (blue) while the pre-LC was counterstained by Foxp2 (blue). The locations of the SFO and pre-LC are -5.52 and -0.7 mm relative to Bregma, respectively.

(B) Stimulus-to-cell-type scRNA-seq mapping of neurons activated under sodium depletion. Left, experimental diagram of scRNA-seq. Right, UMAP embedding of SFO neurons. Data from sodium-depleted and sated mice were integrated using CCA alignment (sated n = 3380 neurons, sodium depleted n = 4439 neurons).

(C) UMAP embedding for *Fos* log-normalized expression (red) in SFO excitatory neurons under sated (left) and sodium-depleted conditions (right).

(D) Identification of Glut1-enriched genes. Log-normalized average gene expression in Glut1 cluster was compared to other excitatory neural clusters. Glut1- and Glut2-5-enriched genes were shown outside the dotted lines (Table S2).

(E) UMAP embedding of *Ptger3* log-normalized expression demonstrates faithful expression of *Ptger3* in the Glut1 cluster.

(F) Violin plots of *Fos* (red) and *Ptger3* (blue) under sated (left) and sodium-depleted (right) conditions. *Ptger3* is selectively expressed in Glut1 (bottom) and Glut1 was specifically activated during sodium depletion in the SFO (top).

(G) SeqFish analysis of the SFO. Left, spatial distribution of all major cell types in representative anterior (top) and posterior (bottom) sections. After segmentation, cells were color-coded as indicated. Right, A total of 1,567 cells from five anterior sections and 1,614

cells from five posterior sections are quantified. Percentage of individual cell type is presented in the pie chart. Exc. Neurons, excitatory neurons; Inh. Neurons, inhibitory neurons; LT Astro, LT astrocytes; Astro, astrocytes; LT endo, LT endothelial cells; Endo, Endothelial cells; VSMCs, vascular smooth muscle cells; Ependy, Ependymal cells; Oligo, oligodendrocytes.

(H) Spatial distribution of all cells is plotted according to the original cell center coordinates. Excitatory neurons are highlighted in colors (red and blue). The Glut1/*Ptger3* cluster (red) is separate from other excitatory neuron clusters (blue). Neurons in gray represent excitatory neurons showing gene expression of multiple cluster markers.

(I) Violin plots showing the log-normalized expression of *Fos* (red) and *Ptger3* (blue) in SFO excitatory neurons. *Fos* expression was found specifically in the Glut1 cluster under sodium depletion.

Scale bar, 100 μm (A), 50 μm (G-H).

See also Figure S2 and Table S2.

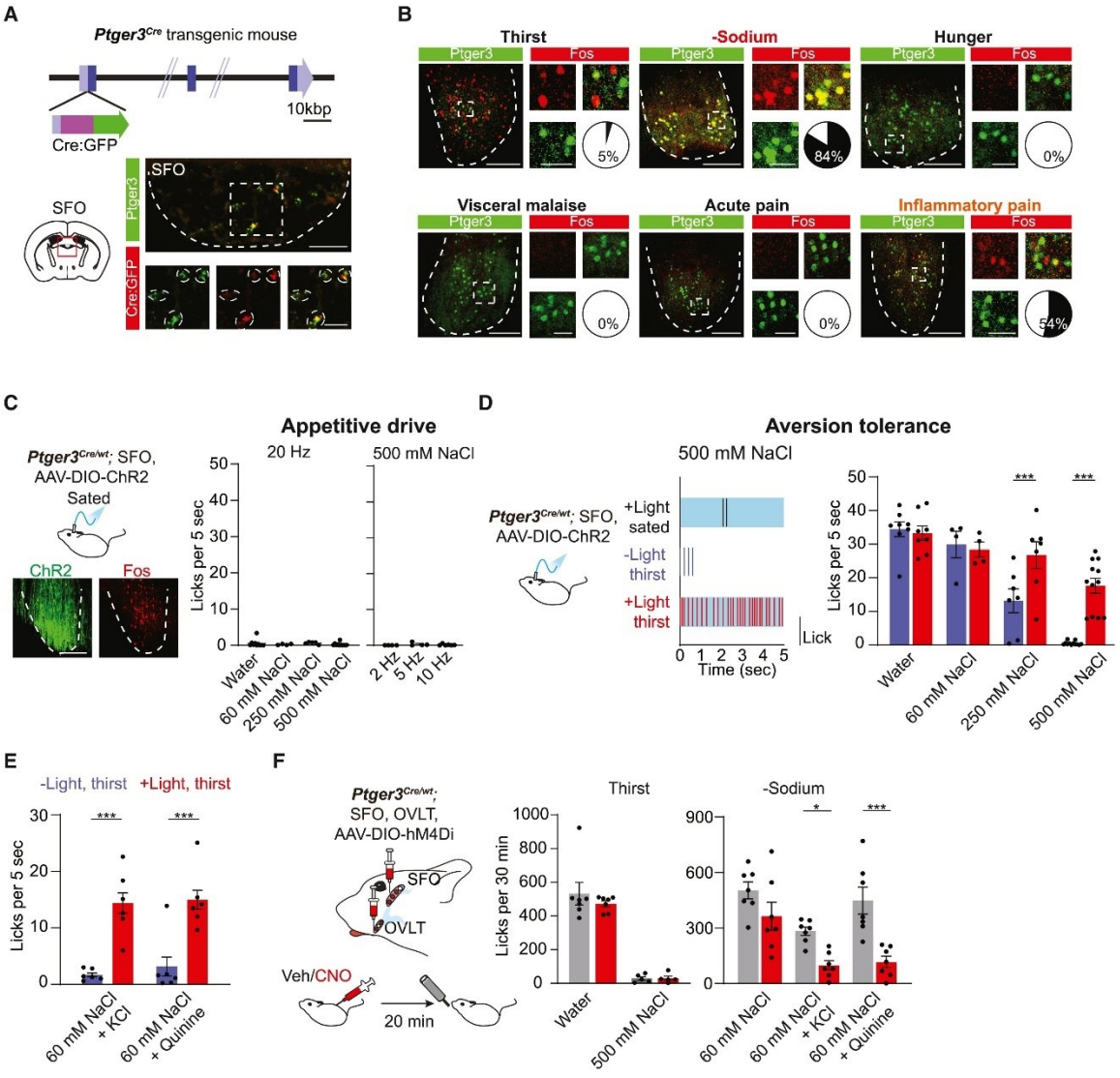
A
Ptger3Cre transgenic mouse
10kbp
Cre:GFP
SFO
Ptger3
Cre:GFP
B
Thirst
-Sodium
Hunger
Visceral malaise
Acute pain
Inflammatory pain
Ptger3
Fos
5%
84%
0%
0%
0%
54%
C
Ptger3Cre/wt; SFO, AAV-DIO-ChR2
Sated
ChR2
Fos
Appetitive drive
20 Hz
500 mM NaCl
Licks per 5 sec
Water
60 mM NaCl
250 mM NaCl
500 mM NaCl
2 Hz
5 Hz
10 Hz
D
Aversion tolerance
500 mM NaCl
Ptger3Cre/wt; SFO, AAV-DIO-ChR2
+Light sated
-Light thirst
+Light thirst
Time (sec)
Lick
Licks per 5 sec
***
***
Water
60 mM NaCl
250 mM NaCl
500 mM NaCl
E
-Light, thirst
+Light, thirst
Licks per 5 sec
***
***
60 mM NaCl + KCl
60 mM NaCl + Quinine
F
Ptger3Cre/wt; SFO, OVLT, AAV-DIO-hM4Di
SFO
OVLT
Veh/CNO
20 min
Thirst
-Sodium
Licks per 30 min
*
***
Water
500 mM NaCl
60 mM NaCl
60 mM NaCl + KCl
60 mM NaCl + Quinine

Figure 3. SFO^{Ptger3} neurons mediate salt tolerance.

(A) The genetic structure of the *Ptger3^{Cre}* mouse line (top). Light and dark blue shades indicate UTRs and exons of *Ptger3*. Cre is inserted into the first exon, resulting in *Ptger3* disruption. *In situ* hybridization showing co-expression of *Ptger3* (green) and *Cre:GFP* (red) expression (bottom); 86% of *Ptger3*+ cells expressed *Cre:GFP* and 83% of *Cre:GFP*+ neurons expressed *Ptger3* (n = 9 sections from 7 mice).

(B) Representative Fos immunofluorescence signals (red) under distinct internal states and noxious stimulus. SFO^{Ptger3} neurons are labeled green. Activation was highly selective under sodium depletion with a minor activation level induced by inflammation. Pie charts display the percentage of Fos+/Ptger3+ cells in all Fos+ cells.

(C) Appetitive-drive test. Photostimulation of SFO^{Ptger3} neurons did not induce salt consumption. Left, histological validation of Fos immunofluorescence signals (red) after photostimulation of ChR2-expressing SFO^{Ptger3} neurons (green). Middle, the averaged lick numbers of water, low (60 mM), medium (250 mM) and high (500 mM) concentrations of sodium at 20 Hz stimulation. Right, the averaged lick numbers of high salt with different stimulation frequency (n = 4-11 mice).

(D) High-salt tolerance test. Left, representative raster plots of licking behavior toward high salt during a 5-sec session from a sated + photostimulated (black), thirsty (blue), or thirsty + photostimulated (red) animal. Right, quantified lick numbers without (blue) or with (red) photostimulation across different concentrations of sodium: water, 60 mM, 250 mM, 500 mM (n = 4-12 mice).

(E) Aversive-taste-tolerance test. The number of licks without (blue) or with (red) photostimulation for low salt supplemented with KCl or quinine (n = 6 mice).

(F) LT^{Ptger3} neurons are required for normal salt tolerance. Left, a diagram of chemogenetic loss-of-function experiments. Middle, the number of licks for water or high salt during a 30-min session with vehicle (grey) or CNO (red) injection under osmotic thirst (n = 5-7 mice). Right, the same behavioral analyses under sodium depletion for low salt, low salt with KCl, or quinine (n = 7 mice).

Data are expressed as mean ± SEM, $*p < 0.05$, $***p < 0.001$. Scale bar, 25 μm (magnified images), 50 μm (A), 100 μm (B-C).

See also Figure S3, Videos S1-2 and Table S1.

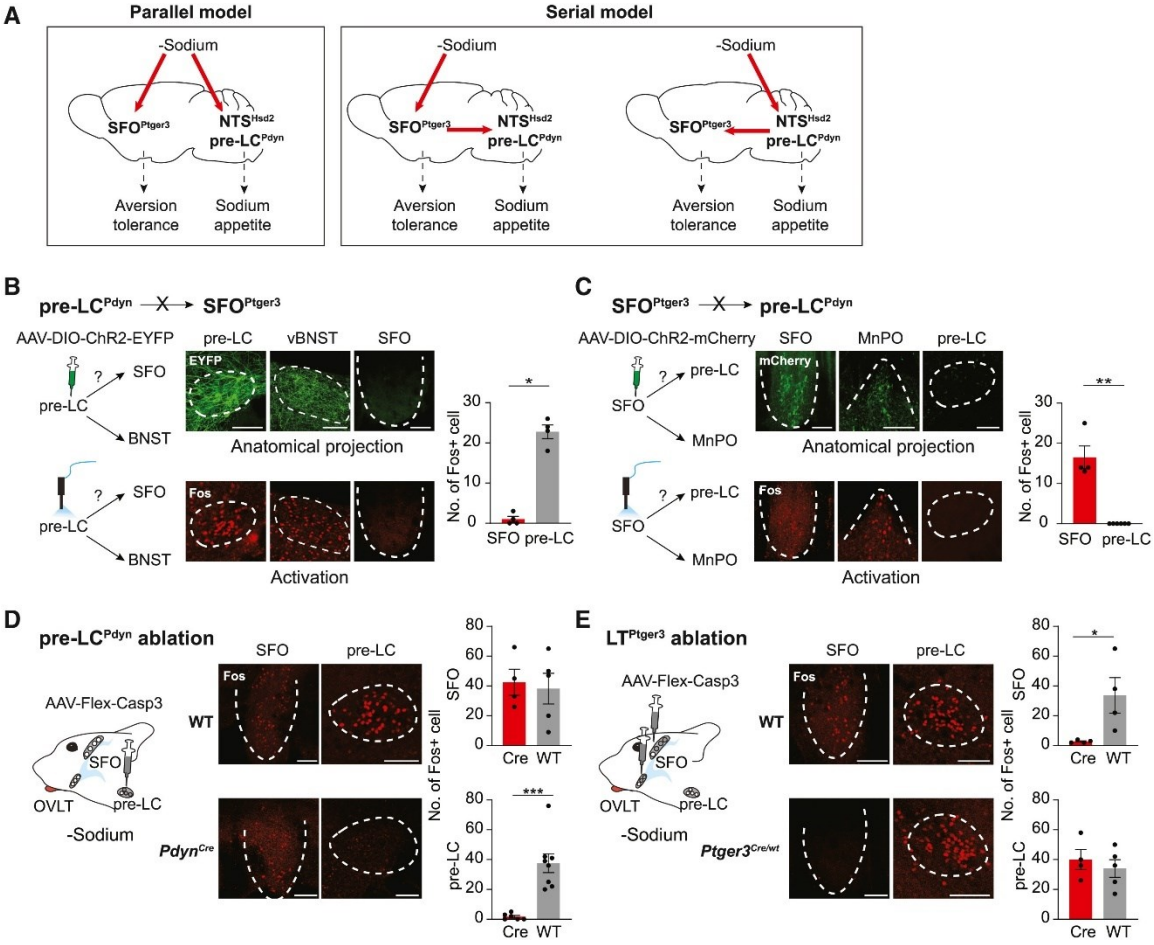
A
Parallel model
Serial model
-Sodium
SFO Ptger3
NTS Hsd2
pre-LC Pdyn
Aversion tolerance
Sodium appetite
B
pre-LC Pdyn → SFO Ptger3
AAV-DIO-ChR2-EYFP
pre-LC
vBNST
SFO
EYFP
Anatomical projection
Fos
Activation
No. of Fos+ cell
C
SFO Ptger3 → pre-LC Pdyn
AAV-DIO-ChR2-mCherry
MnPO
mCherry
D
pre-LC Pdyn ablation
AAV-Flex-Casp3
WT
Pdyn Cre
OVLT
E
LT Ptger3 ablation
Ptger3 Cre/wt
Cre
WT

Figure 4. Parallel and independent activation of fore- and hindbrain circuits under sodium depletion

(A) Two distinct circuit models between fore- and hindbrain neurons related to sodium ingestion. Left, a parallel model where sodium depletion independently activates SFO^{Ptger3} and pre-LC^{Pdyn} neurons. Right, a serial-activation model depicting the hierarchical relationship between the two neural circuits.

(B) Testing pre-LC^{Pdyn} → SFO^{Ptger3} projections. AAV-DIO-ChR2-EYFP was transduced in pre-LC^{Pdyn} neurons. Top, representative images showing axonal projections to the ventral bed nucleus of stria terminalis (vBNST) and SFO. Note that the vBNST is a known downstream area of pre-LC^{Pdyn} neurons. Bottom, similarly, photostimulation-induced Fos immunofluorescence signals were observed in the BNST but not SFO. Right, the number of Fos+ cells was compared between SFO (red) and pre-LC (grey, n = 4 sections from 4 mice).

(C) Testing SFO^{Ptger3} → pre-LC^{Pdyn} projections. Top, SFO^{Ptger3} neurons showed no projection to the pre-LC when compared to the MnPO, a known downstream target of the SFO. Bottom, no activation was found in pre-LC^{Pdyn} neurons after photostimulating SFO^{Ptger3} neurons. Right, the number of Fos+ cells by photostimulation (n = 4-6 sections from 3 mice).

(D) Activation of SFO^{Ptger3} neurons under sodium depletion did not rely on functioning pre-LC^{Pdyn} neurons. AAV-FLEX-taCasp3-TEVP was injected into the pre-LC bilaterally in $Pdyn^{Cre}$ or wild-type mice. Middle, representative images of sodium-depletion-induced Fos in the SFO and pre-LC. Right, the numbers of Fos+ cells in the SFO and pre-LC were

quantified in transgenic (Cre, red, n = 4-6 sections from 3 mice) and wild-type mice (WT, grey, n = 5-8 sections from 4 mice).

(E) Pre-LC activation with ablated LT^{Ptger3} neurons. AAV-FLEX-taCasp3-TEVP was injected to the SFO and OVLT in *Ptger3*$^{Cre/wt}$ or wild-type mice. Middle, representative images of sodium-depletion-induced Fos. Right, quantified Fos+ cells in the SFO and pre-LC. Ablation of LT^{Ptger3} neurons had no effect on the pre-LC activity (red, n = 4 sections from 2 mice; grey, n = 4 sections from 3 mice for SFO, and red, 4 sections from 2 mice and 5 sections from 3 mice for pre-LC).

Data are shown as mean ± SEM, $*p < 0.05$, $**p < 0.01$, $***p < 0.001$. Scale bar, 100 μm. See also Table S1.

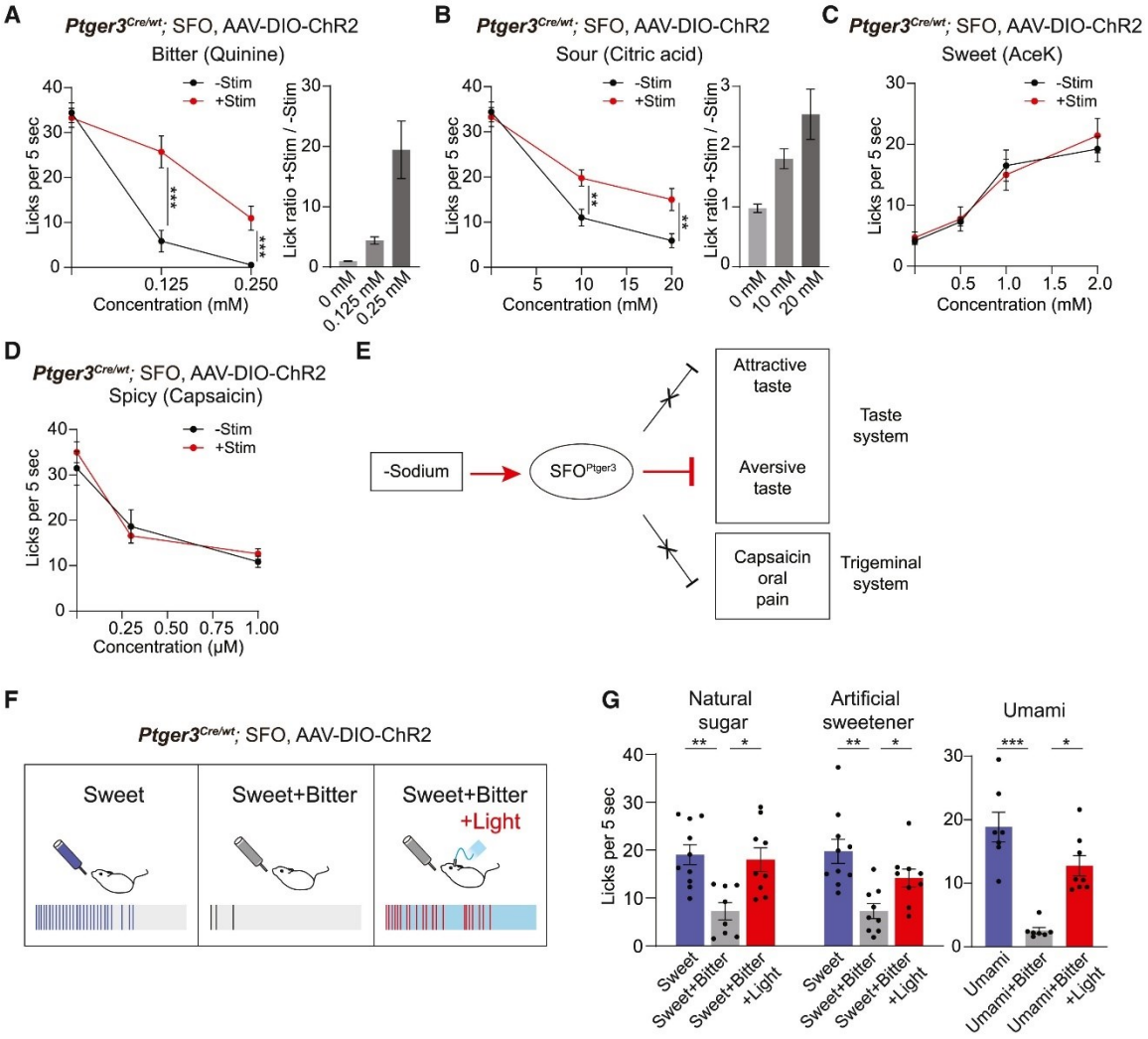
A
Ptger3Cre/wt; SFO, AAV-DIO-ChR2
Bitter (Quinine)
-Stim
+Stim
Licks per 5 sec
Concentration (mM)
Lick ratio +Stim / -Stim
0 mM
0.125 mM
0.25 mM
B
Ptger3Cre/wt; SFO, AAV-DIO-ChR2
Sour (Citric acid)
Concentration (mM)
0 mM
10 mM
20 mM
C
Ptger3Cre/wt; SFO, AAV-DIO-ChR2
Sweet (AceK)
Concentration (mM)
D
Ptger3Cre/wt; SFO, AAV-DIO-ChR2
Spicy (Capsaicin)
Concentration (μM)
E
-Sodium
SFOPtger3
Attractive taste
Aversive taste
Taste system
Capsaicin oral pain
Trigeminal system
F
Ptger3Cre/wt; SFO, AAV-DIO-ChR2
Sweet
Sweet+Bitter
Sweet+Bitter +Light
G
Natural sugar
Artificial sweetener
Umami
Licks per 5 sec
Sweet
Sweet+Bitter
Sweet+Bitter +Light
Umami
Umami+Bitter
Umami+Bitter +Light

Figure 5. Selective modulation of aversive taste saliency by SFO^{Ptger3} neurons

(A) Dose-dependent behavioral aversion toward bitter tastes. Left, the number of licks was quantified for water, 0.125, and 0.25 mM quinine under osmotic thirst conditions in the absence (black) or presence (red) of photostimulation to SFO^{Ptger3} neurons. Right, preference changes are shown as a ratio by calculating the lick numbers with photostimulation divided by those without photostimulation (n = 5-8 mice). Lick number of water was reanalyzed from Figure 3D.

(B) Similar analyses as (A) using sour taste. Water, 10, and 20 mM citric acid were used to quantify taste preference (n = 8-11 mice). Lick number of water was reanalyzed from Figure 3D.

(C) Acute stimulation of SFO^{Ptger3} neurons did not change preference toward attractive tastant under food deprivation. Average lick numbers for water, 0.5, 1, and 2 mM AceK are shown without (black) or with (red) photostimulation (n= 4-7 mice).

(D) Dose-dependent behavioral aversion toward capsaicin, a non-taste oral aversive compound. 0, 0.3, and 1 μM capsaicin were used to calculate avoidance curve (n = 4-5 mice).

(E) Saliency modulation by SFO^{Ptger3} neurons was specific toward aversive stimuli through the taste system. The effect was not generalized to non-oral aversive stimuli.

(F) Stimulation of Ptger3 neurons alleviate aversive taste response under hunger. Shown are raster plots from representative food-deprived mice to sweet (2 mM AceK), sweet with bitter (2 mM AceK with 0.125 mM quinine), and the same mixture with photostimulation. With the photostimulation of SFO^{Ptger3} neurons, the bitter taste was tolerated.

(G) The effect of photostimulation of SFO^{Ptger3} neurons on glucose (500 mM), AceK (2 mM) and monopotassium glutamate + inosine monophosphate (30 mM + 0.6 mM) supplemented with bitter. The average lick numbers toward pure attractive tastants (blue), mixture with 0.125 mM quinine (grey), and together with photostimulation (red) are shown (n = 7-10 mice).

Data are shown as mean ± SEM, $*p < 0.05$, $**p < 0.01$, $***p < 0.001$.

See also Figure S4 and Table S1.

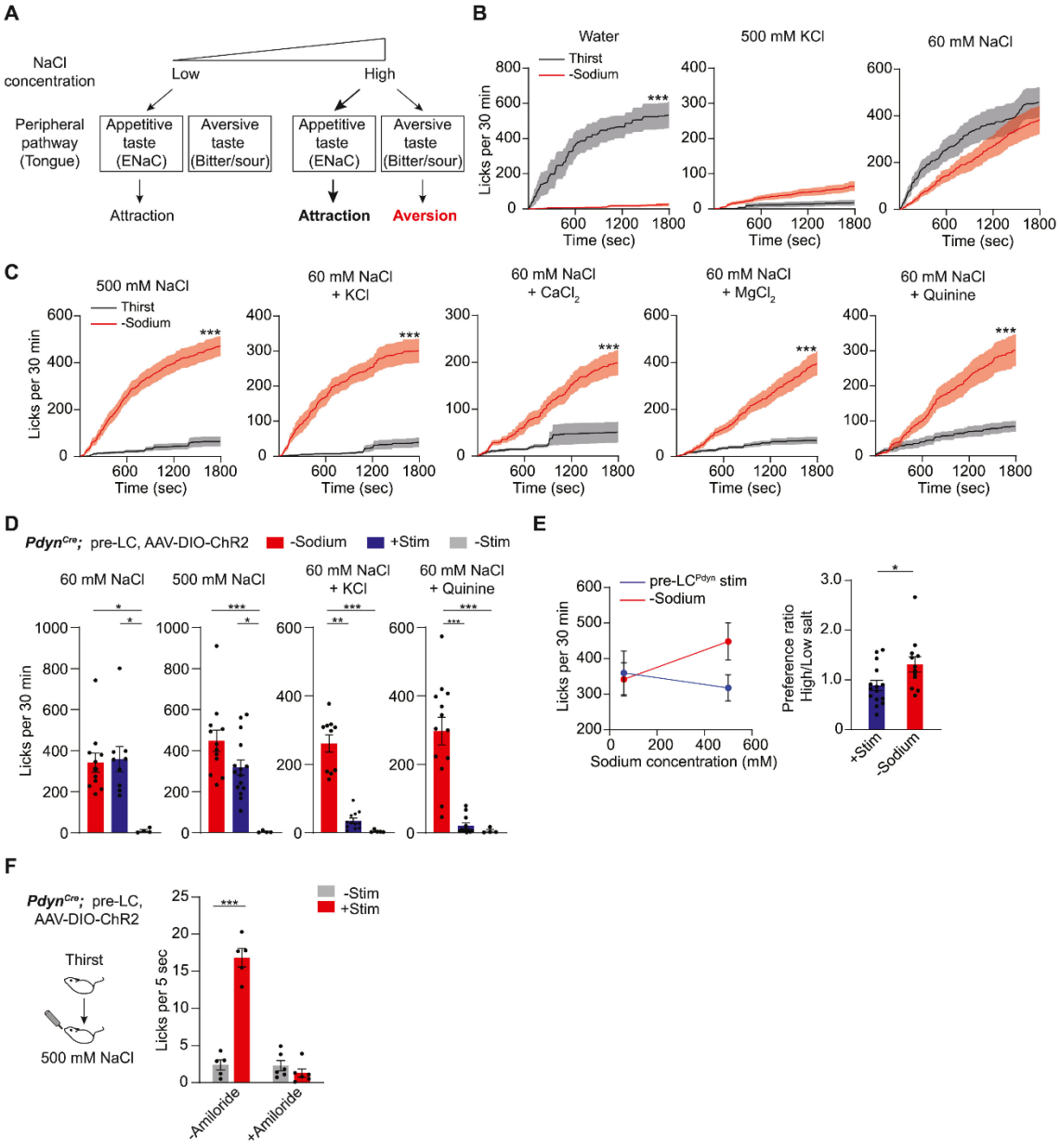
A
NaCl concentration
Low
High
Peripheral pathway (Tongue)
Appetitive taste (ENaC)
Aversive taste (Bitter/sour)
Appetitive taste (ENaC)
Aversive taste (Bitter/sour)
Attraction
Attraction
Aversion
B
Water
Thirst
-Sodium
500 mM KCl
60 mM NaCl
Licks per 30 min
Time (sec)
C
500 mM NaCl
60 mM NaCl + KCl
60 mM NaCl + CaCl2
60 mM NaCl + MgCl2
60 mM NaCl + Quinine
D
Pdyn^Cre; pre-LC, AAV-DIO-ChR2
-Sodium
+Stim
-Stim
60 mM NaCl
500 mM NaCl
60 mM NaCl + KCl
60 mM NaCl + Quinine
Licks per 30 min
E
pre-LC^Pdyn stim
-Sodium
Licks per 30 min
Sodium concentration (mM)
Preference ratio High/Low salt
+Stim
-Sodium
F
Pdyn^Cre; pre-LC, AAV-DIO-ChR2
Thirst
500 mM NaCl
-Stim
+Stim
Licks per 5 sec
-Amiloride
+Amiloride

Figure S1. Salt tolerance is enhanced under sodium depletion but not under thirst or pre-LC^{Pdyn}-induced appetite, related to Figure 1.

(A) A diagram of appetitive and aversive salt taste pathways. Low concentrations of salt only activate the appetitive ENaC pathway, and animals exhibit a behavioral attraction. Higher concentrations of salt recruit additional aversive taste pathways (bitter and sour), driving strong behavioral aversion despite the activation of appetitive ENaC pathway.

(B-C) Cumulative consumption curves under osmotic thirst and sodium-depleted conditions from the data in Figure 1A.

(D) The total lick numbers were quantified from the data in Figure 1D. Unstimulated control data (grey) were shown together.

(E) Left, Comparison of low- and high-salt consumption in pre-LC^{Pdyn}-stimulated animals (blue) and sodium-depleted animals (red). Right, consumption ratio between low salt and high salt. pre-LC^{Pdyn}-stimulated animals preferred low salt while sodium-depleted animals consumed significantly more high salt (n = 12-15 mice). The data were reanalyzed from Figure 1D.

(F) Sodium-selective, behavioral attraction is mediated by pre-LC^{Pdyn} neurons. The number of licks toward high salt (500 mM NaCl) was quantified during pre-LC^{Pdyn} photostimulation with or without 30 mM amiloride. High salt consumption induced by pre-LC^{Pdyn} neurons was ENaC dependent (n = 5-6 mice).

Data are expressed as mean ± SEM, $*p < 0.05$, $**p < 0.01$, $***p < 0.001$. See also Table S1.

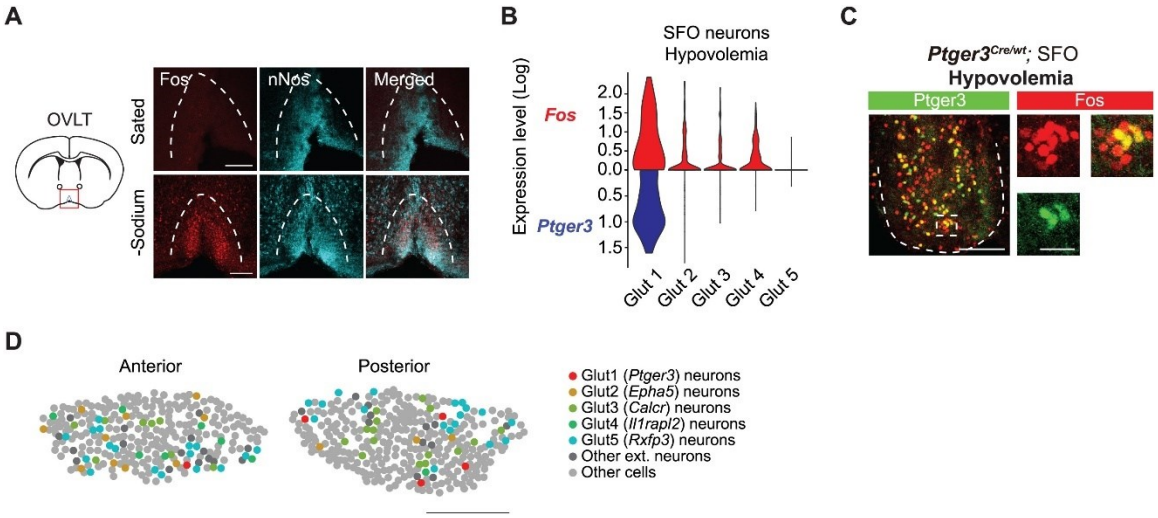
A
OVLT
Sated
-Sodium
Fos
nNos
Merged
B
SFO neurons
Hypovolemia
Expression level (Log)
Fos
Ptger3
2.0
1.5
1.0
0.5
0.0
0.5
1.0
1.5
Glut 1
Glut 2
Glut 3
Glut 4
Glut 5
C
Ptger3Cre/wt; SFO
Hypovolemia
Ptger3
Fos
D
Anterior
Posterior
Glut1 (Ptger3) neurons
Glut2 (Epha5) neurons
Glut3 (Calcr) neurons
Glut4 (Il1rapl2) neurons
Glut5 (Rxfp3) neurons
Other ext. neurons
Other cells

Figure S2. Neural activation of SFO and OVLT under sodium depletion and hypovolemia, related to Figure 2.

(A) Representative images of OVLT activation in sated (top) and sodium-depleted (bottom) conditions. The OVLT was visualized with nNos (blue) and Fos (red) activation was compared between conditions.

(B) Violin plots of *Fos* (red) and *Ptger3* (blue) in the SFO under hypovolemia conditions. *Ptger3*-expressed neurons were a partial population active in hypovolemia.

(C) Representative Fos immunofluorescence signals (red) under hypovolemia in the SFO. Ptger3 neurons are labeled in green.

(D) Spatial distribution of all cells according to the original cell center coordinates. Individual excitatory neuron types are highlighted in colors (as indicated).

Scale bar, 25 μm (C, magnified images), 100 μm (A, C, and D). See also Table S1.

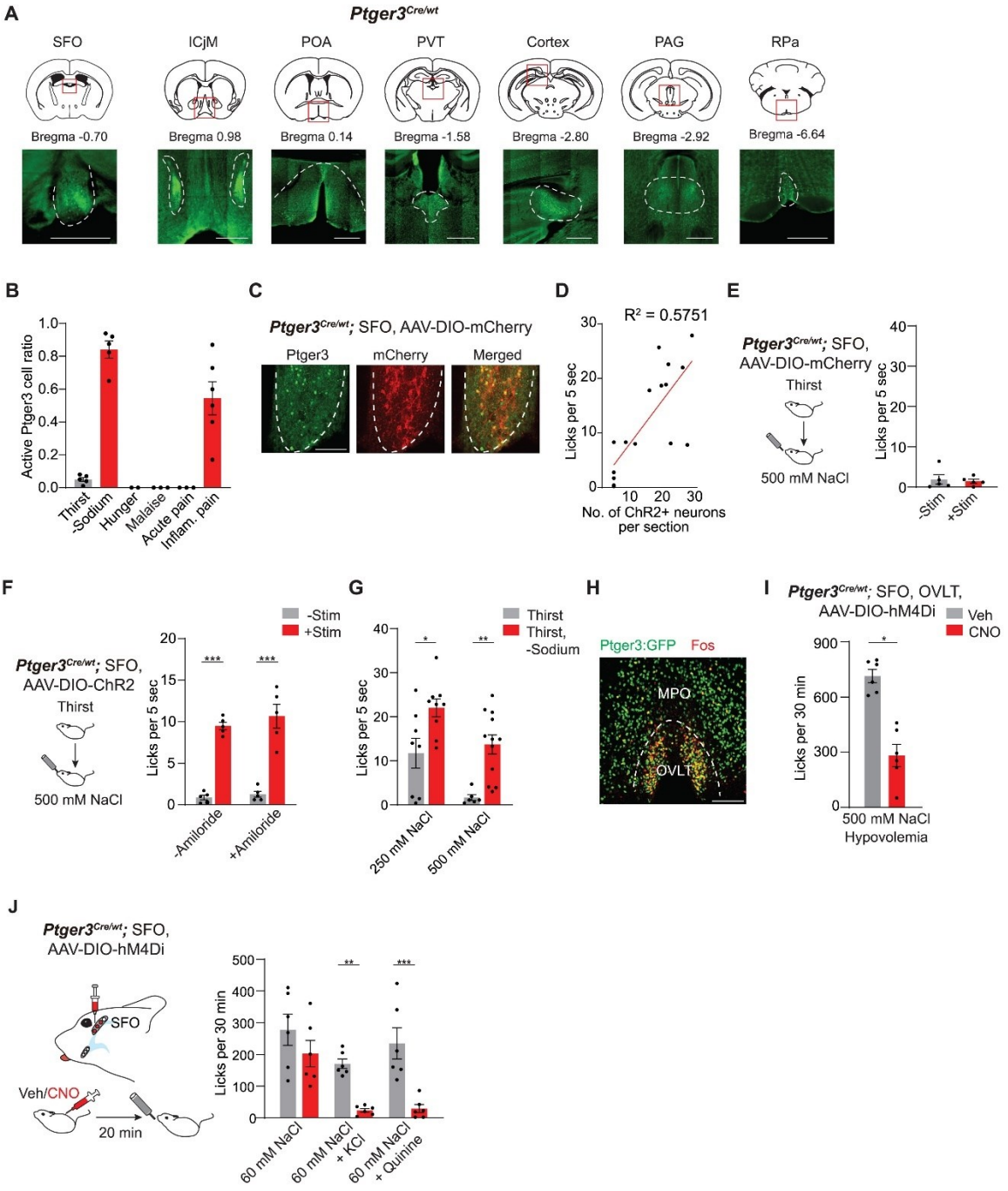
A
Ptger3Cre/wt
SFO
ICjM
POA
PVT
Cortex
PAG
RPa
Bregma -0.70
Bregma 0.98
Bregma 0.14
Bregma -1.58
Bregma -2.80
Bregma -2.92
Bregma -6.64
B
Active Ptger3 cell ratio
Thirst
-Sodium
Hunger
Malaise
Acute pain
Inflam. pain
C
Ptger3Cre/wt; SFO, AAV-DIO-mCherry
Ptger3
mCherry
Merged
D
R² = 0.5751
Licks per 5 sec
No. of ChR2+ neurons per section
E
Ptger3Cre/wt; SFO, AAV-DIO-mCherry
Thirst
500 mM NaCl
Licks per 5 sec
-Stim
+Stim
F
Ptger3Cre/wt; SFO, AAV-DIO-ChR2
Thirst
500 mM NaCl
-Stim
+Stim
Licks per 5 sec
-Amiloride
+Amiloride
G
Thirst
Thirst, -Sodium
Licks per 5 sec
250 mM NaCl
500 mM NaCl
H
Ptger3:GFP Fos
MPO
OVLT
I
Ptger3Cre/wt; SFO, OVLT, AAV-DIO-hM4Di
Veh
CNO
Licks per 30 min
500 mM NaCl
Hypovolemia
J
Ptger3Cre/wt; SFO, AAV-DIO-hM4Di
SFO
Veh/CNO
20 min
Licks per 30 min
60 mM NaCl
60 mM NaCl + KCl
60 mM NaCl + Quinine

Figure S3. Functional characterization of SFO^{Ptger3} neurons, related to Figure 3.

(A) Characterization of Ptger3^{Cre} transgenic line in the whole brain. Shown are representative GFP signals from a Ptger3$^{Cre/wt}$ animal. Strong GFP signals were found in the SFO, island of Calleja major (ICjM), preoptic area (POA), paraventricular thalamus (PVT), cortex, periaqueductal gray (PAG), and raphe pallidus (RPa).

(B) Quantified Fos+ cells in the SFO that overlapped with Ptger3-GFP signals. Shown are the ratio of activated Ptger3+ neurons divided by total Fos+ cells (n = 2-6 sections from 2-5 mice).

(C) Representative images of Ptger3-Cre:GFP (green) overlap with AAV-DIO-ChR2-mCherry (red). 88% of mCherry+ neurons expressed Ptger3-Cre:GFP, and 72% of Cre:GFP+ neurons were mCherry+ (n = 7 sections from 6 mice).

(D) Relationship between virus expression level and salt tolerance. The number of ChR2+ neurons per section and lick numbers toward high salt are shown for individual animals tested. Note that salt tolerance and the number of ChR2+ neurons have a high correlation coefficient (n = 16 mice).

(E) Control experiments for ChR2 photostimulation using mCherry (n = 5 mice).

(F) Amiloride did not affect salt tolerance induced by SFO^{Ptger3}. Unlike pre-LC^{Pdyn} neurons, SFO^{Ptger3} -induced tolerance is independent of the ENaC pathway (n = 5 mice).

(G) Sodium-depletion-induced tolerance in thirsty mice. Mice were subjected to osmotic thirst (grey) and osmotic thirst + sodium depletion (red), and the number of licks toward 250 and 500 mM NaCl were quantified (n = 6-12 mice). The thirst data for 250 mM NaCl included the data from Figure 3D.

(H) A representative image of Ptger3 (green) and Fos (red) immunofluorescence signals in the OVLT.

(I) LT^{Ptger3} neurons are required for normal salt tolerance under hypovolemia. The number of licks toward 500 mM NaCl during a 30-min trial with vehicle (grey) or CNO (red) injection under hypovolemia (n = 6 mice).

(J) SFO^{Ptger3} neurons are required for normal salt tolerance. Left, a diagram of chemogenetic loss-of-function experiments. AAV-DIO-hM4Di was injected into the SFO. Right, the number of licks for low salt, low salt with KCl or quinine was quantified during a 30-min session under sodium depletion. Before behavioral experiments, animals received intraperitoneal injection of either vehicle (grey) or CNO (red) (n = 6 mice).

Data are expressed as mean ± SEM, $*p < 0.05$, $**p < 0.01$, $***p < 0.001$. Scale bar, 500 μm (A), 100 μm (C and H). See also Table S1.

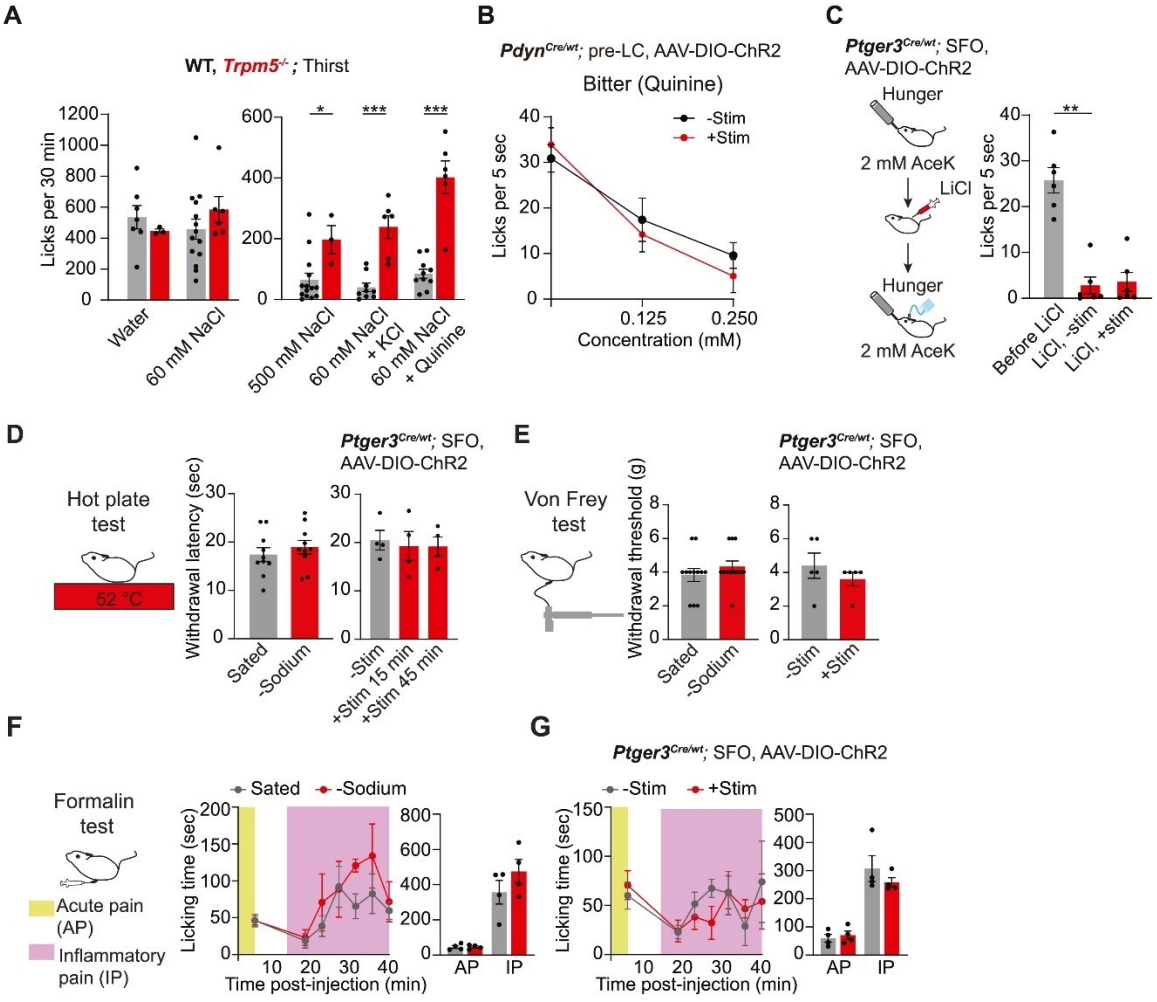
A
WT, Trpm5-/-; Thirst
Licks per 30 min
Water
60 mM NaCl
500 mM NaCl
60 mM NaCl + KCl
60 mM NaCl + Quinine
B
Pdyn Cre/wt; pre-LC, AAV-DIO-ChR2
Bitter (Quinine)
-Stim
+Stim
Licks per 5 sec
Concentration (mM)
C
Ptger3 Cre/wt; SFO, AAV-DIO-ChR2
Hunger
2 mM AceK
LiCl
Licks per 5 sec
Before LiCl
LiCl, -stim
LiCl, +stim
D
Hot plate test
52 °C
Withdrawal latency (sec)
Sated
-Sodium
-Stim
+Stim 15 min
+Stim 45 min
E
Von Frey test
Withdrawal threshold (g)
F
Formalin test
Acute pain (AP)
Inflammatory pain (IP)
Licking time (sec)
Time post-injection (min)
AP
IP
G

Figure S4. Specificity of sensory modulation by SFO^{Ptger3} neurons, related to Figure 5.

(A) *Trpm5*$^{-/-}$ animals that lack bitter, sweet, and umami tastes showed elevated tolerance toward aversive tastes. Left, consumption of water and 60 mM NaCl during a 30-min session under osmotic thirst in wild-type (grey) and *Trpm5*$^{-/-}$ mice (red, n = 3-14). Right, consumption of 500 mM NaCl, 60 mM NaCl with 440 mM KCl, and 60 mM NaCl with 0.25 mM quinine during a 30-min session under osmotic thirst in wild-type (grey) and *Trmp5*$^{-/-}$ mice (red) (n = 3-14). For wild-type control, the data were reanalyzed from Figure 1A.

(B) Stimulation of pre-LC^{Pdyn} neurons did not affect behavioral aversion toward bitter tastes. The number of licks was quantified for water, 0.125 and 0.25 mM quinine under osmotic thirst conditions in the absence (black) or presence (red) of photostimulation to pre-LC^{Pdyn} neurons (n = 4-6 mice).

(C) Learned taste aversion was not alleviated by the activity of SFO^{Ptger3} neurons. Left, a conditioned-taste-avoidance paradigm toward AceK (2 mM) by LiCl injection. Right, consumption of AceK before (grey) and after (-stim, blue; +stim, red) conditioning (n = 6).

(D-E) Various aversive stimuli were presented to animals under sated, sodium-depleted, and SFO^{Ptger3}-stimulated conditions. Animals were subjected to noxious heat on a hot plate (D), and von Frey test (E). Neither sodium depletion nor SFO^{Ptger3}-stimulation blunted general aversive or tactile responses (n = 4-12 mice).

(F) Acute and inflammatory pain test. Left, a histogram showing the time spent paw-licking after formalin injection plotted in 5-min bins in sated and sodium-depleted conditions. Right, a cumulative time of paw-licking during the acute pain period (0-5 min after formalin injection) and the inflammatory pain period (15-45 min after formalin injection).

The data were compared between sated (grey) and sodium-depleted (red) groups (n = 4 mice).

(G) Photostimulation of SFO^{Ptger3} neurons had no effects on pain responses. Left, a histogram showing the time spent paw-licking after formalin injection without (grey) or with (red) photostimulation. Right, quantified cumulative time of paw-licking (n = 4 mice). Data are expressed as mean ± SEM, $*p < 0.05$, $**p < 0.01$, $***p < 0.001$. Scale bar, 100 μm. See also Table S1.

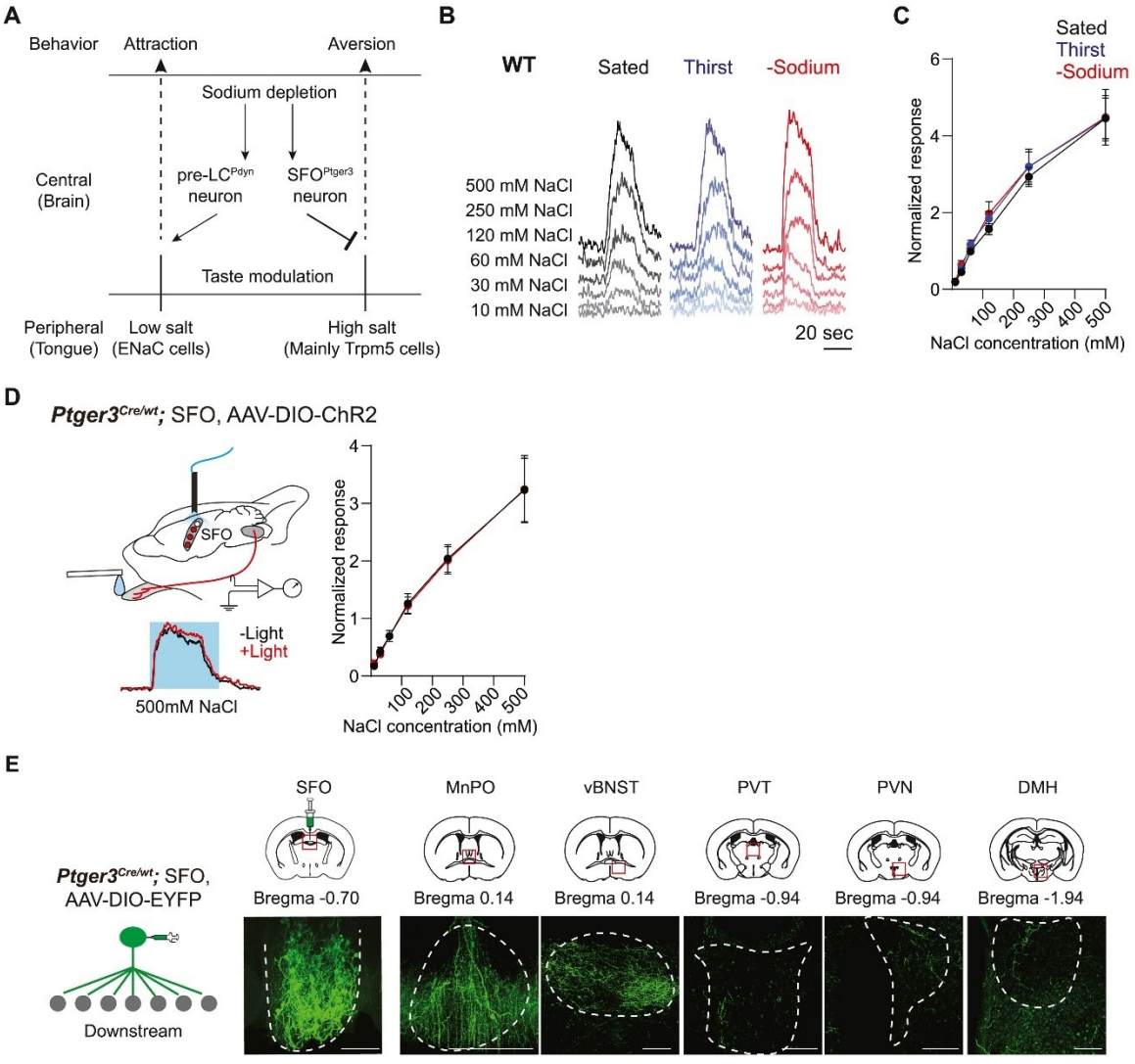
A
Behavior
Attraction
Aversion
Sodium depletion
Central (Brain)
pre-LC^Pdyn neuron
SFO^Ptger3 neuron
Taste modulation
Peripheral (Tongue)
Low salt (ENaC cells)
High salt (Mainly Trpm5 cells)
B
WT
Sated
Thirst
-Sodium
500 mM NaCl
250 mM NaCl
120 mM NaCl
60 mM NaCl
30 mM NaCl
10 mM NaCl
20 sec
C
Sated
Thirst
-Sodium
Normalized response
NaCl concentration (mM)
D
Ptger3Cre/wt; SFO, AAV-DIO-ChR2
SFO
-Light
+Light
500mM NaCl
Normalized response
NaCl concentration (mM)
E
Ptger3Cre/wt; SFO, AAV-DIO-EYFP
Downstream
SFO
MnPO
vBNST
PVT
PVN
DMH
Bregma -0.70
Bregma 0.14
Bregma 0.14
Bregma -0.94
Bregma -0.94
Bregma -1.94

Figure S5. Bimodal modulations of attractive and aversive taste signals by the brain, related to Discussion.

(A) A diagram of bimodal salt taste modulation. Low salt through the ENaC pathway and aversive high salt through bitter/sour pathways are modulated by two separate interoceptive circuits in the forebrain (SFO) and hindbrain (pre-LC) circuits. These circuits sense internal sodium balance and trigger bimodal modulation signals that affect the hedonic value of salt in a concentration- and internal-state-dependent manner.

(B-C) B. Representative taste responses from chorda tympani nerve under distinct internal states. C. 10, 30, 60, 120, 250, and 500 mM NaCl were applied to the tongue, and integrated nerve responses were quantified for each concentration (n = 5 mice).

(D) Taste nerve recording with SFO^{Ptger3} photostimulation. Left, a diagram of chorda tympani nerve recording combined with optogenetics. Right, quantification of normalized responses to NaCl without (black), or with photostimulation (red) state (n = 3 mice). ChR2 expression was validated by immunohistology and behavioral tolerance induction.

(E) AAV-DIO-ChR2-EYFP was injected into SFO^{Ptger3} and the downstream projections were visualized. Strong projections were found in the following brain areas: MnPO, vBNST, paraventricular nucleus of the thalamus (PVT), paraventricular nucleus of the hypothalamus (PVN), and dorsomedial hypothalamus (DMH).

Scale bar, 100 μm.

Videos S1. SFO^{Ptger3} induced salt tolerance, related to Figure 3.

Representative drinking behavior toward high salt under osmotic thirst with photostimulation of SFO^{Ptger3} neurons.

Videos S2. Control experiment for Video S1 without light, related to Figure 3.

Representative drinking behavior toward high salt under osmotic thirst without photostimulation of SFO^{Ptger3} neurons.

Chapter 3

PROSTAGLANDIN IN TASTE VALENCE AND SALT IMBALANCE

3.1 Ptger3 is necessary in sodium depletion induced taste valence change

Ptger3 is a receptor for prostaglandins (mainly PGE2), and is involved in various physiological responses[128–131]. Since Ptger3 is a dominant PGE2 receptor subtype expressed in the SFO (Figure S1A), we speculated that PGE2-Ptger3 signaling may be involved in salt taste modulation and ingestion. To test this hypothesis, we examined the role of Ptger3 using a global receptor knockout animal model, *Ptger3*$^{-/-}$ (or *Ptger3*$^{Cre/Cre}$ Figures 1A-C) and local *Ptger3* knockdown in the SFO (*Ptger3* KD, Figures 1D-F). *Ptger3*$^{-/-}$ mice were obtained as homozygous *Ptger3*$^{Cre/Cre}$ animals due to premature gene disruption. Deletion of *Ptger3* expression was confirmed by *in situ* hybridization in both cases (Figures 1A and 1D). Compared to control animals, *Ptger3*$^{Cre/Cre}$ and *Ptger3* KD significantly reduced Fos immunofluorescence signals under sodium depletion (Figures 1B and 1E, SFO), whereas neural activation in the pre-LC was unchanged (Figures 1B and 1E, pre-LC). To test the behavioral consequences, we examined salt preference in *Ptger3*$^{Cre/Cre}$ and *Ptger3* KD mice. Consistent with histological results, animals lacking Ptger3 no longer tolerated aversive stimuli including high salt, KCl, and quinine (Figure 1C, Figure 1F and Figure S1B). While Ptger3 is required for salt tolerance, *Ptger3* KD in the background of *Trpm5*$^{-/-}$ did not abolish salt tolerance (Figure S1C), indicating that behavioral tolerance through Ptger3 requires intact taste signals. Collectively, these data demonstrate that the function of Ptger3 is required

for activation of SFO^{Ptger3} neurons and normal salt tolerance under sodium-depleted conditions.

3.2 PGE2 is necessary in sodium depletion induced taste valence change

We next asked whether PGE2 plays a role in salt taste modulation and tolerance. Considering that SFO^{Ptger3} neurons are activated under sodium depletion and inflammation, we tested if sodium depletion elevates PGE2 levels. Our ELISA measurement confirmed that circulating PGE2 is significantly increased under sodium depletion, but we did not observe such elevation for other inflammation-related molecules such as progesterone or serotonin (Figure 2A and Figure S2A). We synthesized PGE2 conjugated with a small fluorescent dye (PGE2-AMCA) to test whether peripheral PGE2 have access to the SFO. Our acute SFO preparation confirmed that fluorescent levels of PGE2-AMCA increased selectively in the SFO within 5 min of peripheral injection (Figure 2B). This rapid PGE2 penetration is presumably due to the lack of the normal blood brain barrier in the SFO. Moreover, photometry recording from SFO^{Ptger3} neurons that express GCaMP7s (AAV-Flex-GCaMP7s) demonstrated time-locked calcium increases by peripheral PGE2 injections (Figure 2C). These calcium responses were not observed under osmotic thirst, hunger, or visceral malaise (Figure S2B). Consistently, we found strong Fos immunofluorescence signals in the SFO by peripheral PGE2 injection in a Ptger3-dependent fashion (Figures S2C-D).

To directly test tolerance regulation, we examined the effects of PGE2 injection on taste preference. Indeed, like SFO^{Ptger3} neuron stimulation, PGE2-injected wild-type or *Ptger3*$^{Cre/wt}$ animals exhibited increased salt tolerance under osmotic thirst (Figure 2D and Figures S2E)

and food-deprived conditions (Figure S2F), but PGE2 itself did not induce any appetite under sated conditions. Importantly, PGE2-mediated tolerance was largely abolished in *Ptger3*$^{Cre/Cre}$ animals and *Ptger3* KD animals, showing that PGE2-induced high-salt tolerance is mediated through Ptger3 (Figures 2D-E and Figures S2G-H). Furthermore, we tested whether prostaglandin production is required for the induced salt tolerance using anti-inflammatory drugs (NSAIDs: ibuprofen and aspirin), a commonly used method to reduce prostaglandin production[132–134]. We found that NSAID treatments significantly reduced salt tolerance under sodium depletion (Figure 2F). Conversely, formalin-induced inflammation increased the PGE2 levels (Figure 2A) and partially induced high salt tolerance (Figure S2I). While these studies highlighted the contribution of the PGE2-Ptger3 axis to salt taste modulation, Ptger3 is also activated by other prostaglandin-related molecules[135]. It is feasible that these molecules may play additional roles in sensory modulation under physiological conditions.

Ingestive behavior is intimately linked to the activity of reward circuits[136–139]. We tested whether sodium depletion and SFO^{Ptger3} neuron activity alter the activity of dopamine release in the nucleus accumbens (NAc) using genetically encoded biosensor, dLight[140,141]. We injected AAV-syn-dLight1.3b and an optic fiber into the Nac for real-time optical imaging of dopamine release. We found that dLight signals rapidly increased when sodium-depleted animals consumed high salt while the same animals under osmotic thirst exhibited minimal activation (Figure 2G). After subcutaneous PGE2 injection, thirsty mice showed increased high-salt consumption and enhanced dopamine release (Figure 2G). To test if this effect is recapitulated by the stimulation of SFO^{Ptger3} neurons, we expressed an activation DREADD,

hM3Dq, into SFO^{Ptger3} neurons. We then tested dLight signals from the Nac while activating SFO^{Ptger3} neurons by CNO. Compared to vehicle-injected control animals, dopamine signals in the Nac were greatly enhanced during high-salt ingestion only when SFO^{Ptger3} neurons are chemogenetically activated (Figure 2H). These results further extend our results by showing that the perceived quality of high salt is altered in the presence of salt tolerance signals from the SFO.

3.3 Discussion

Brain interoceptive circuits monitor internal states through various molecules. Angiotensin and aldosterone are well-characterized molecules that regulate water and sodium ingestion. This study identified PGE2 as an additional candidate molecular mediator underlying salt tolerance. However, the origin and pathway of PGE2 production awaits further studies. Moreover, since Ptger3 is activated by various ligands besides PGE2[142], other molecules may also be involved in salt taste modulation. Brain-derived PGE2 is known to regulate core body temperature[143,144], while peripheral-derived PGE2 modulates sensory sensitivity, including nociception[145–147]. Since sodium depletion has no obvious thermoregulatory effects[148], we speculate that the source of PGE2 is from peripheral organs such as the kidney[149–151], which leads to activation of SFO^{Ptger3} neurons through Ptger3. Future research will be required to clarify if PGE2 is the only molecule that regulates salt tolerance, and whether other brain areas contribute to this sensory modulation process.

3.4 Limitations of the study

The effects of PGE2 on salt ingestion were analyzed using homozygous Ptger3$^{Cre/Cre}$ mice, where Cre:GFP-polyA was inserted right before the initiation codon of Ptger3. Although this transgene insertion should prevent Ptger3 expression, there may be low levels of residual expression of the downstream reading frame. Ptger3 binds various ligands other than PGE2, and we cannot exclude the contribution of other molecules to salt taste modulation *in vivo*. Further studies are needed to test if other Ptger3 ligands are involved in salt ingestion. PGE2 is produced both in the brain and body. While our study used formalin injection as an inflammation model, our data do not directly show that PGE2 released during sodium depletion endogenously stimulates Ptger3 to suppress aversion. Thus, a more thorough investigation will be required to test the function of PGE2 from different sources during sodium depletion. GCaMP7s fluorescence is a proxy for neuronal firing, and *in vivo* voltage recordings during salt depletion or inflammation will be important to reveal the activation patterns of SFO^{Ptger3} neurons.

3.5 Acknowledgements and Contributions

We thank the members of the Oka laboratory and Sangjun Lee for helpful discussion and feedback comments. We thank Ashil Koranne and Jacob Hauser for maintaining and genotyping animal lines, and the Single Cell Profiling and Engineering Center (SPEC) in the Beckman Institute at Caltech. R.D.P thanks Serina Tsang and Kathy Kafer for help generating the *Ptger3^{Cre}* mice and Susan Phelps for mouse husbandry. We thank Henry Lester and Anand k. Muthusamy for support for photometry recording setup. This work was supported by Startup funds from the President and Provost of California Institute of

Technology and the Biology and Biological Engineering Division of California Institute of Technology. Y.O. is supported by New York Stem Cell Foundation, NIH (R01NS109997, R01NS123918), Alfred P. Sloan Foundation, Edward Mallinckrodt Foundation, and Heritage Medical Research Institute. Y.Z. was supported by Chen Graduate Fellowship.

Y.Z. and Y.O. conceived the research program and designed experiments. R.D.P. generated and maintained *Ptger3*^{Cre} transgenic mice. Y.Z. and L.L. performed and analyzed fiber photometry experiments. Y.Z. and Y.O. wrote the paper. Y.O. supervised the entire work.

3.6 Method

Animals

All procedures followed the US NIH guidance for the care and use of laboratory animals and were approved by the California Institute of Technology Institutional Animal Care and Use Committee (protocol: 1694–14). Male and Female mice at least 8 weeks were used for behavioral tests and histology characterization. No sex difference is observed in this study. For scRNA-seq experiments, 7-8-week-old C57BL/6J mice were used. C57BL/6J were purchased (000664) from the Jackson Laboratory. *Pdyn*^{Cre} mice were a gift from B. Lowell and M. Krashes (Jackson lab, 027958). Heterozygous *Pdyn*^{Cre} mice were used for all experiments. *Trpm5*$^{-/-}$ mice were generously provided by C. Zuker (Jackson lab, 013068). Mice were housed in temperature-controlled and humidity-controlled rooms with a 13:11 hr light:dark cycle. Mice are provided with ad libitum access to chow and water unless mentioned in the nutrient deprivation experiments.

Generation of the Ptger3^{Cre} *mouse line*

Ptger3^{Cre} animals were generated by inserting mnCre:GFP cassette just 5' of the initiation codon of *Ptger3* gene and deleting the first 40 amino acids. The cassette had a Myc-tag and nuclear localization signals at the N-terminus. The targeting construct was electroporated into G4 ES cells (C57Bl/6 × 129 Sv hybrid) and correct targeting was identified by Southern blot. The frt-flanked SV-Neo gene was removed via breeding with Gt(Rosa)26Sor-FLP recombinase mice and then backcrossing to C57BL/6J mice for >6 generations. Homozygous *Ptger3*$^{Cre/Cre}$ mice are equivalent to *Ptger3*$^{-/-}$ because of the amino acid deletion.

Viral constructs

We used the following viruses: AAV9-syn-dLight1.3b, 2.6 × 10^{13} viral genomes per ml. AAV1-syn-FLEX-jGCaMP7s-WPRE, 1.9 x 10^{13} viral genomes per ml. AAV9-GFP-U6-scrmb-shRNA, 3 × 10^{13} viral genomes per ml. AAV9-GFP-U6-m-Ptger3-shRNA (shAAV-269740), 1.5 × 10^{13} viral genomes per ml.

Surgery

Surgery procedures were performed as described[90]. Briefly, ketamine (1 mg/ml) and xylazine (10 mg/ml) in saline were injected intraperitoneally at a dose of 10 ml per kg body weight (BW) for anaesthesia. Ketoprofen was injected subcutaneously at a dose of 5 ml per kg BW. Surgery was performed with a stereotaxic apparatus (Narishige, SR-5M-HT) on a heating pad at 37 °C. Virus was delivered with a microprocessor-controlled injection system (World Precision Instruments, Nanolitre 2000) at 100 nl/min. The following coordinates were used: for pre-LC: anterior–posterior (AP), 9,000, medial–lateral (ML), 1,000, ventral–dorsal (VD), 3,800; for SFO: AP, 4,000, ML, 0, VD, 2,500; for OVLT: AP, 2,475, ML, 0, VD, 4,750; for dorsal part of the NAc medial shell: AP, 2,100, ML, 700,

VD, 4,000For fiber photometry experiments, virus was delivered at a volume of 150-200 nl (calcium measurement) or 500 nl (dopamine measurement) per region. A 400-μm fiber bundle (Thorlabs, FT400UMT) was used instead. For local knockdown experiments, virus was delivered at 150-200 nl per region. At the end of experiments, all animals were euthanized for histological examination.

Internal state induction

Sodium depletion: Mice were injected intraperitoneally with furosemide at a dose of 50 mg per kg BW and maintained with a low-sodium diet for 24 hr before behavioral assays or immunohistological staining[120].

Sodium repletion: Mice were injected intraperitoneally with furosemide at a dose of 50 mg per kg BW 24 hr before the experiment and maintained on a normal diet.

Osmotic thirst: Mice were injected intraperitoneally with either 2 M NaCl (5 ml per kg BW) or mannitol solution (10 ml per kg BW) and maintained with no food or water for 10 min before the behavioral assay or 1 hr before immunohistological staining. Mannitol was used for long-term consumption assay and Fos immunostaining, and NaCl was used for short-term consumption assay. We did not find significant differences between the results obtained with these two solutions.

Hunger: Mice were food deprived for 24 hr before the behavior test or immunohistological staining.

PGE2-induced behavior: PGE2 was injected subcutaneously at a dose of 1 mg per kg BW. Animals had no food or water for 15-90 min before behavioral experiments. For immunohistochemistry, PGE2 was injected at a dose of 3 mg per kg BW and maintained with no food or water for 60 min before euthanasia.

Prostaglandin: PGE2 powder was diluted in DMSO at 50 mg/ml as stock. For behavioral assay, we used the final concentration of 1 mg per kg BW in PBS containing 1.7% DMSO (v/v). The same vehicle with DMSO was used as control.

Behavioral assays

All assays were performed in a custom gustometer (Dialog Instruments). All animals were at least trained with osmotic thirst and sodium depletion prior to the behavior trials. Animals were trained to drink at least 200 licks for 500 mM NaCl in 30 min under sodium depletion. Generally, two training sessions with sodium depletion are sufficient to achieve this criterion. Animals often show neophobia to a new solution even if it was an attractive stimulus. To prevent this, all tastants at lower concentrations were exposed to animals before experiment. For tolerance tests, we used one-bottle consumption assay in order to avoid preference development during the session.

For 30-min access assay, mice were presented with 1 bottle for 30 min and consumption was measured.

For 5-sec brief access assay, mice were presented with 1 bottle of solution for 30 sec per trial for maximum waiting time before the first lick, and 40 sec between trials. After an initial lick, animals were allowed to drink the solution for additional 5 sec before a shutter closed. To avoid taste conditioning effect, animals were tested with only one solution per day. After testing aversive solutions, bitter and high salt, animals sometimes refused to drink any solution. These animals were retrained with water and low salt until their behavioral level recovers to our criteria stated above.

Taste aversion

Animals accessed 2 mM AceK in the gustometer after 24 hr food deprivation. Within 5 min after the trials finished, animals were given 0.15 M LiCl intraperitoneally, at a dose of 15 ml per kg BW. After one day rest, animals were food deprived again for 24 hr, and exposed to 2mM AceK in the gustometer. Photostimulation was given alternatively in 10 trials. Lick number was quantified respectively for the light stimulation on and off sessions.

Inflammation and consumption

Formalin-induced tolerance: Mice were injected with formalin or PBS in the dorsal hindpaw 45-60 min prior to the lick access. Osmotic thirst was induced 10-15 min prior to the lick access. Lick number was recorded for 30 min.

NSAIDs-induced loss-of-tolerance: NSAIDs were used to suppress PGE2 production[152,153]. Mice were given water supplemented with ibuprofen (1 mg per ml) for three days. On the second day, mice were injected with furosemide to induce sodium depletion. On the third day, aspirin (40 mg per kg BW) was injected intraperitoneally 1-2 hr prior to the lick access. Lick number was recorded for 30 min.

Fiber photometry

Calcium measurement from SFO^{Ptger3} neurons: Mice were headfixed to eliminate the interference from movement. Photometry recording was performed using a commercial photometry system (Neurophotometrics, FP3002). Two LED of different wavelength (470nm and 415nm) were bandpass filtered and a patch cord (0.48NA, Doric lenses) was attached to the photometry system via a 20x objective. The sampling rate was fixed at 40Hz. Data were acquired with Bonsai (Neurophotometrics) by drawing a region of interest and calculating the mean pixel value, and then were exported to MATLAB for further analysis. The isosbestic signal (415 nm) was fit with a biexponential model and was then

linearly scaled to the calcium signal (470 nm). The ΔF/F was calculated as (raw 470-nm signal – fitted 415-nm signal)/ (fitted 415-nm signal). For all sessions, stimulus time was recorded through a customized TTL button. During PGE2 activation experiment (Figure 7C), mice were given PGE2 at a dose of 1 mg per kg BW or DMSO in 100 μl PBS subcutaneously. During other internal-state treatments, mice were exposed to the following stimuli via intraperitoneal injection: 2M mannitol (10 ml per kg BW); 10 μg of ghrelin (in 100 μl PBS), and 0.15M LiCl (15 ml per kg BW). All analysis used the average of 5 min prior to the stimulus as a baseline mean. Normalized ΔF/F was calculated by subtracting the baseline ΔF/F from the mean ΔF/F between 100 and 1500 sec after the stimulus.

Dopamine measurement: Mice were freely moving in the chamber with gustometer. Bulk fluorescence signals were collected with a fiber photometry setting as described[139] with the light of 405 nm and 490 nm. The ΔF/F was calculated as (raw 490-nm signal – fitted 405-nm signal)/ (fitted 405-nm signal). Mice were induced with osmotic thirst 10-15 min, or sodium depletion 24 hr before the access of 500 mM NaCl. For wild-type mice, under PGE2 activation condition, mice were injected PGE2 at a dose of 1 mg per kg BW subcutaneously 1 hr before the shutter open. For *Ptger3*^{Cre} mice, mice were injected with either CNO or vehicle 20 min before the shutter opened. Lick number was recorded simultaneously with the fluorescence signal collection. The first lick bout was identified with the lick rate more than 3.5 and lick number more than 5, with less than 1-sec interval to the subsequent lick. If no lick bout was detectable (observed with osmotic thirst), any first lick event was included into the data. All baseline signals were calculated by averaging signals between 10-20 sec prior to the first lick. Response amplitude (normalized ΔF/F)

was calculated by subtracting the baseline ΔF/F from the mean ΔF/F between 0 and 10 sec after the lick initiated.

PGE2-AMCA dye infusion

PGE2 was conjugated to AMCA as a synthesized dye. Mice were anaesthetized with ketamine (1 mg/ml) and xylazine (10 mg/ml) at a dose of 10 ml per kg BW. Mice were administrated with the dye or vehicle via tail vein at a dose of 1 mg per kg BW. Five minutes post-injection, fresh brain was extracted, and SFO was dissected under a microscope, Several drops of PBS was added onto the slice to prevent tissue dryness. Slices were imaged under LSM 880 with Fast Airyscan using 20x z-stack (Airyscan SR Mode, detector-1.25 AU). SFO was identifiable between two paralleled blood vessels. For analysis in ImageJ, the image was rotated to an angle that the two blood vessels were vertical. Fluorescence was extraced by an arbitrary horizontal line at the dorsal side. The ΔF/F was calculated as (fluorescence from 100-μm in SFO – average of fluorescence from dorsal and ventral 100-μm outside of SFO) / (average of fluorescence from dorsal and ventral 100-μm outside of SFO).

Immunohistochemistry

Mice were euthanized with CO_2 and perfused with PBS and 4% paraformaldehyde. Extracted mouse brains were fixed overnight at 4 °C in 4% PFA and sectioned coronally to 100-μm slides via vibratome (Leica, VT-1000 S). The sections were blocked (10% donkey serum, 0.2% Triton X-100 in PBS) for 1 hr at room temperature and incubated with primary antibody at 4 °C overnight. The following primary antibodies were used: rabbit anti-FOS (1:500), sheep anti-Foxp2 (1:2,000), chicken anti-GFP (1:3,000), rat anti-mCherry (1:500), and goat anti-nNos (1:500). The sections were washed three times with

PBS and incubated with the secondary antibody (1:500; Jackson Immunoresearch) and DAPI (2 μg/ml) for 4 hr under room temperature. After three times wash with PBS, the sections were mounted on the glass slide. All slides were imaged with confocal microscope (Leica, TCS SP8) or slide scanner (Olympus, BX61VS).

Plasma PGE2, progesterone, and serotonin concentration measurement

Mice were anaesthetized with isoflurane. Blood was collected via heart puncture into EDTA-coated tubes (BD Microtainer, 365974) and kept on ice. Plasma was then separated by centrifugation at 1,500 g for 20 min. ELISA assays were performed following the protocols of PGE2 ELISA kit (Cayman Chemical, 514531), serotonin ELISA kit (Eagle Bio, SER39-K01), and progesterone ELISA kit (Cayman Chemical, 582601).

RNAscope-based multicolour in situ hybridization

In situ hybridization was performed with the RNAscope Multiplex Fluorescent Assay versions 1 or 2 (Advanced Cell Diagnostics, 320850). Fixed-frozen brains from C57BL/6J, *Ptger3*$^{Cre/wt}$ and *Ptger3*$^{Cre/Cre}$ (equivalent to knockout) were prepared following the manufacturer's protocols. Following probes were applied to the samples: *Ptger3* (504481 and 501831), *GFP* (409011), and *Pdyn* (318771). The samples were imaged with confocal microscopy and visualized via z-stacks.

Quantification and Statistical Analysis

No statistical methods were used to predetermine sample size. The experiments were not randomized, and investigators were not blinded to allocation during experiments and outcome assessment. Data are presented as means ± SEMs in figures. Wilcoxon test, Mann-Whitney test, and one- or two-way ANOVA with post hoc tests were applied to decide the

significance level. Significant threshold was maintained at $\alpha = 0.05$ (ns $p > 0.05$, $*p < 0.05$, $**p < 0.01$, $***p < 0.001$).

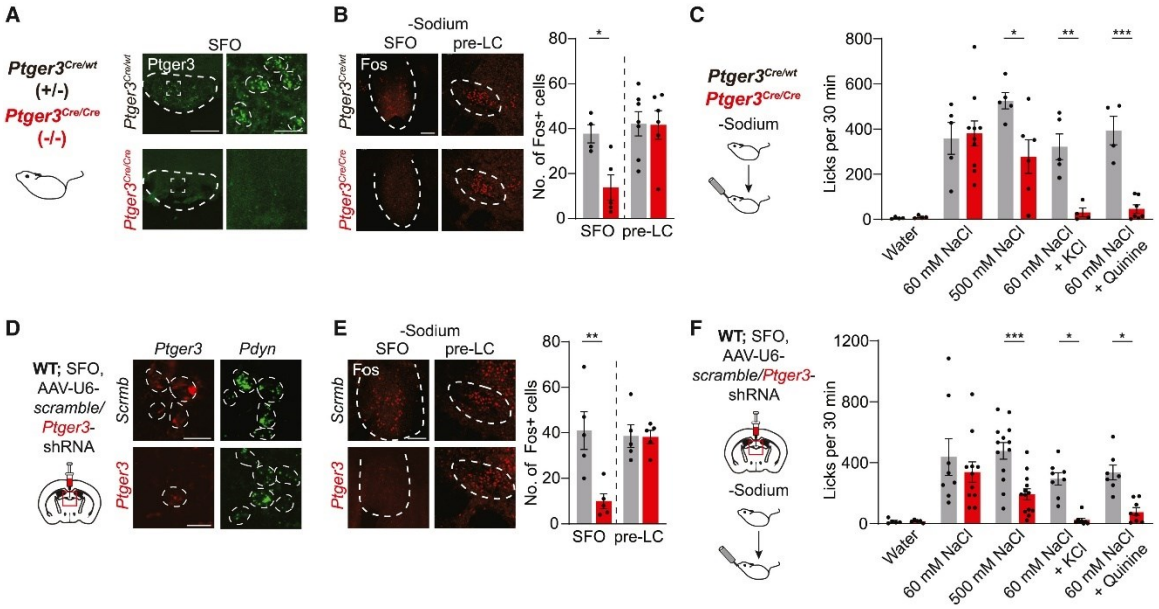
A
Ptger3Cre/wt (+/-)
Ptger3Cre/Cre (-/-)
SFO
Ptger3
B
-Sodium
SFO
pre-LC
Fos
No. of Fos+ cells
SFO
pre-LC
C
Ptger3Cre/wt
Ptger3Cre/Cre
-Sodium
Licks per 30 min
Water
60 mM NaCl
500 mM NaCl
60 mM NaCl + KCl
60 mM NaCl + Quinine
D
WT; SFO, AAV-U6-scramble/Ptger3-shRNA
Ptger3
Pdyn
Scrmb
E
-Sodium
SFO
pre-LC
Fos
No. of Fos+ cells
F
WT; SFO, AAV-U6-scramble/Ptger3-shRNA
-Sodium
Licks per 30 min

Figure 1. Ptger3 in the SFO is required for salt tolerance.

(A) Fluorescence in situ hybridization validates the lack of *Ptger3* transcripts in the SFO in homozygous *Ptger3*$^{Cre/Cre}$ (*Ptger3*$^{-/-}$) animals compared to heterozygous *Ptger3*$^{Cre/wt}$ (*Ptger3*$^{+/-}$) animals. 89% of *Ptger3* signals were abolished in *Ptger3*$^{Cre/Cre}$ mice (n = 4 sections from 3 mice) compared to *Ptger3*$^{Cre/wt}$ mice (n = 5 sections from 3 mice).

(B) Left, Representative images of the SFO and pre-LC under sodium depletion in *Ptger3*$^{Cre/wt}$ (grey) and *Ptger3*$^{Cre/Cre}$ (red) animals. Sodium depletion activated the SFO in a Ptger3-dependent manner but Fos immunofluorescence signals in pre-LC were unaffected. Right, quantification of the cell activation (grey, n = 4 sections from 4 mice; red, n = 5 sections from 5 mice for SFO, and grey, n = 7 sections from 4 mice; red, n = 6 sections from 3 mice for pre-LC).

(C) Aversion tolerance is abolished in *Ptger3*$^{Cre/Cre}$ mice. Left, the number of licks toward water, low salt (60 mM NaCl), high salt (500 mM NaCl), and low salt with KCl or quinine in *Ptger3*$^{Cre/wt}$ (grey) and *Ptger3*$^{Cre/Cre}$ (red) mice under sodium depletion (n = 4-10 mice).

(D) Fluorescence *in situ* hybridization validates the lack of *Ptger3* transcripts in the *Ptger3*-shRNA-injected animals. Compared to *scramble*-shRNA-injected animals, 87% of *Ptger3* signals were abolished in *Ptger3*-shRNA-injected mice (n = 4 sections from 2 mice) compared to *scramble*-shRNA-injected mice (n = 4 sections from 2 mice).

(E) Left, representative images of the SFO and pre-LC under sodium depletion in *scramble*- (grey) and *Ptger3*- (red) shRNA-injected mice. Right, quantification of the cell activation (grey, n = 5 sections from 5 mice; red, n = 5 sections from 5 mice).

(F) Aversion tolerance is abolished in *Ptger3* KD mice. Left, a diagram of gene knockdown and behavioral paradigm. Right, consumption of the same solutions as Figure 6C was tested in *scramble*- (grey) and *Ptger3*- (red) shRNA-injected mice (n = 5-13 mice). Data are expressed as mean ± SEM, $*p < 0.05$, $**p < 0.01$, $***p < 0.001$. Scale bar, 25 μm (A right, and D), 100 μm (A left, B, and E).

See also Figure S1 and Table S1.

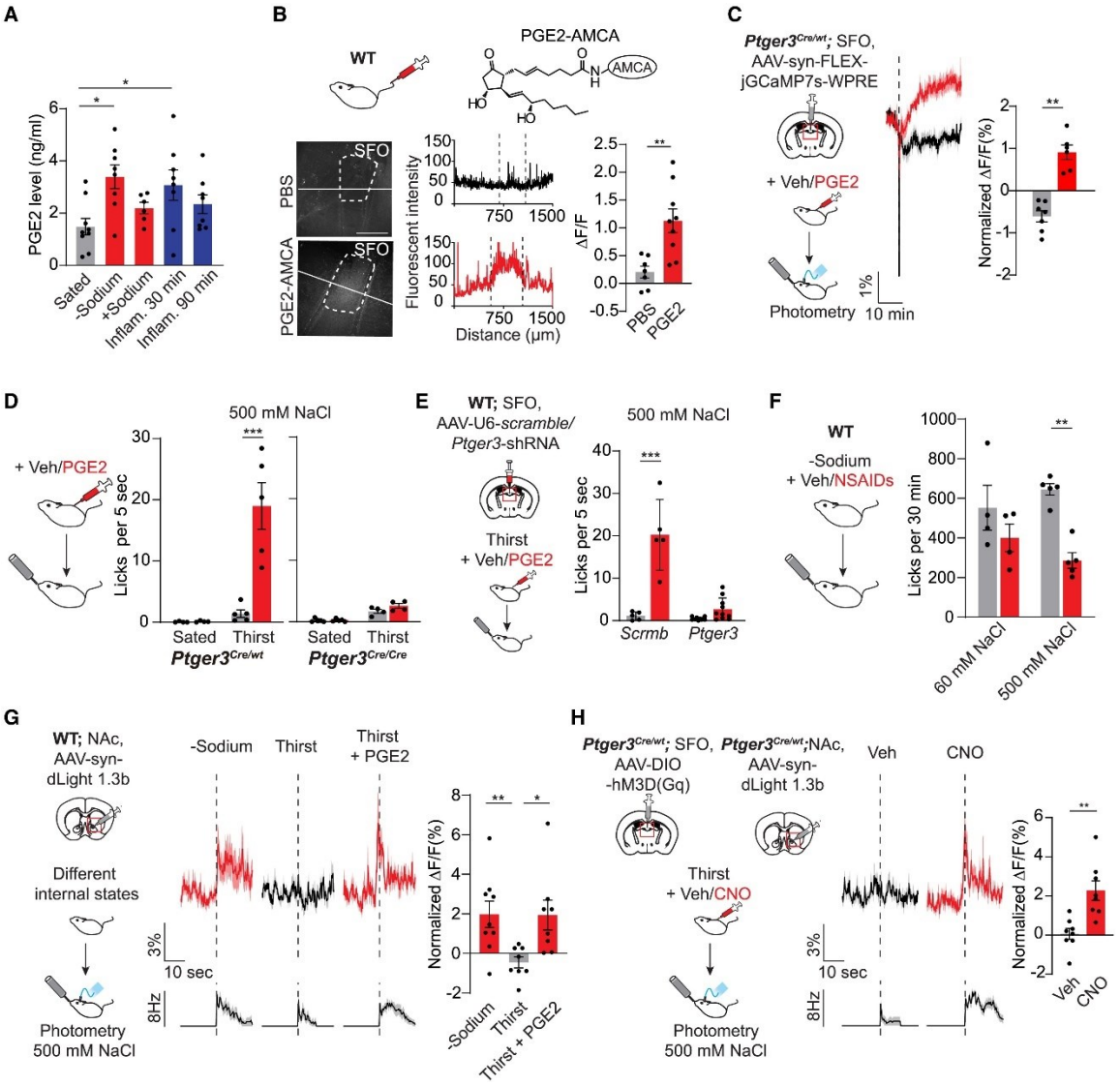
A
PGE2 level (ng/ml)
Sated
-Sodium
+Sodium
Inflam. 30 min
Inflam. 90 min
B
WT
PGE2-AMCA
AMCA
PBS
PGE2-AMCA
SFO
Fluorescent intensity
Distance (μm)
ΔF/F
PBS
PGE2
C
Ptger3Cre/wt; SFO, AAV-syn-FLEX-jGCaMP7s-WPRE
+ Veh/PGE2
Photometry
1%
10 min
Normalized ΔF/F(%)
D
+ Veh/PGE2
500 mM NaCl
Licks per 5 sec
Sated
Thirst
Ptger3Cre/wt
Ptger3Cre/Cre
E
WT; SFO, AAV-U6-scramble/Ptger3-shRNA
Thirst
+ Veh/PGE2
500 mM NaCl
Licks per 5 sec
Scrmb
Ptger3
F
WT
-Sodium
+ Veh/NSAIDs
Licks per 30 min
60 mM NaCl
500 mM NaCl
G
WT; NAc, AAV-syn-dLight 1.3b
Different internal states
Photometry
500 mM NaCl
-Sodium
Thirst
Thirst + PGE2
3%
10 sec
8Hz
Normalized ΔF/F(%)
H
Ptger3Cre/wt; SFO, AAV-DIO -hM3D(Gq)
Ptger3Cre/wt;NAc, AAV-syn-dLight 1.3b
Thirst
+ Veh/CNO
Photometry
500 mM NaCl
Veh
CNO
3%
10 sec
8Hz
Normalized ΔF/F(%)

Figure 2. Functional roles of PGE2-Ptger3 signaling for salt taste modulation

(A) ELISA measurement of the circulating PGE2 level. PGE2 was measured from sated (grey), and sodium depleted/repleted (red), and formalin-injected (blue) animals (n = 6-9 mice).

(B) Rapid PGE2 access to the SFO. *Ex vivo* imaging of the SFO was performed after intravenous injection of PGE2-AMCA. Top, experimental diagram and the chemical structure of a synthesized PGE2-AMCA. Bottle left, representative images showing fluorescence of PGE2-AMCA in acutely dissected SFO. Fluorescence levels were quantified across indicated white lines. Bottom middle, representative traces of relative fluorescence levels in vehicle- or PGE2-AMCA-injected animals. Bottom right, quantification of the relative fluorescence level (n = 7 mice for PBS, and 9 mice for PEG2-AMCA).

(C) Photometry recording from SFO^{Ptger3} neurons. Shown are calcium dynamics and quantified responses (normalized ΔF/F) from SFO^{Ptger3} neurons after subcutaneous injection of vehicle (grey) and PGE2 (red, n = 6 recordings from 5 mice for PGE2, and 7 recordings from 5 mice for vehicle).

(D) Peripheral injection of PGE2 induces salt tolerance in a Ptger3-dependent manner. High-salt consumption after subcutaneous vehicle (grey) or PGE2 (red) injection in $Ptger3^{Cre/wt}$ and $Ptger3^{Cre/Cre}$ animals was analyzed (n = 4-5 mice). PGE2 did not induce a drive to consume salt under sated conditions. Under thirst condition, $Ptger3^{Cre/wt}$, but not $Ptger3^{Cre/Cre}$, animals showed enhanced salt tolerance with PGE2 injection.

(E) *Ptger3* KD mice did not tolerate high salt upon PGE2 administration. *Scramble*- (grey) and *Ptger3*- (red) shRNA- injected mice were tested in high salt consumption assay (n = 5-10 mice).

(F) Anti-inflammatory drugs (NSAIDs) partially decreased salt tolerance in sodium depletion. Sodium-depleted mice supplemented with ibuprofen (drinking water) and aspirin (i.p. injection) showed decreased tolerance toward high salt (n = 4-5 mice).

(G) Enhanced dopamine signals toward high salt with PGE2 injection. Left, dopamine release in the NAc was monitored with dLight1.3b during high-salt consumption was measured. Middle and right, averaged dLight1.3b dynamics and quantified data are shown under sodium depletion, thirst, and thirst with PGE2 subcutaneous injection. Lick frequency is shown under dLight traces (n = 8-9 mice).

(H) Activation of SFO^{Ptger3} neurons induced dopamine release during high-salt consumption. Left, an experimental diagram for virus injection and salt consumption assay. Middle and right, averaged dLight1.3b dynamics and quantified data are shown after i.p. vehicle (grey) or CNO (red) injection (n = 8 mice).

Data are expressed as mean ± SEM, $*p < 0.05$, $**p < 0.01$, $***p < 0.001$. Scale bar, 100 μm.

See also Figure S2 and Table S1.

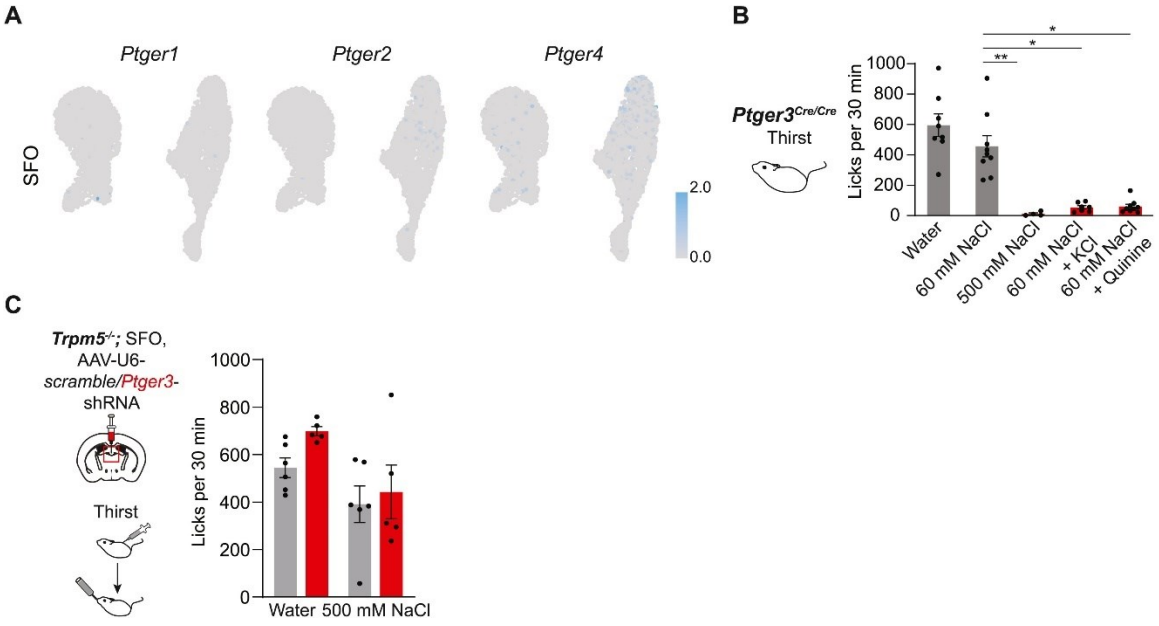
A
Ptger1
Ptger2
Ptger4
SFO
2.0
0.0
B
Ptger3Cre/Cre
Thirst
Licks per 30 min
1000
800
600
400
200
0
*
*
**
Water
60 mM NaCl
500 mM NaCl
60 mM NaCl + KCl
60 mM NaCl + Quinine
C
Trpm5-/-; SFO, AAV-U6-scramble/Ptger3-shRNA
Thirst
Licks per 30 min
1000
800
600
400
200
0
Water
500 mM NaCl

Figure S1. Ptger3 in the SFO plays a major function for aversive taste tolerance, related to Figure 1.

(A) UMAP embedding of *Ptger1*, *Ptger2* and *Ptger4* log-normalized expression in the SFO demonstrating minimal expression of these three prostaglandin receptors.

(B) *Ptger3*$^{Cre/Cre}$ mice did not show tolerance toward aversive taste under osmotic thirst (n = 4-9 mice).

(C) Knocking down of *Ptger3* in the SFO in the background of *Trpm5*$^{-/-}$ animals did not reduce tolerance toward aversive salt under osmotic thirst. The lick number of water and 500 mM NaCl in *scramble*- (grey) and *Ptger3*- (red) shRNA- injected *Trpm5*$^{-/-}$ animals were shown (n = 5-6 mice).

Data are expressed as mean ± SEM, $*p < 0.05$, $**p < 0.01$. See also Table S1.

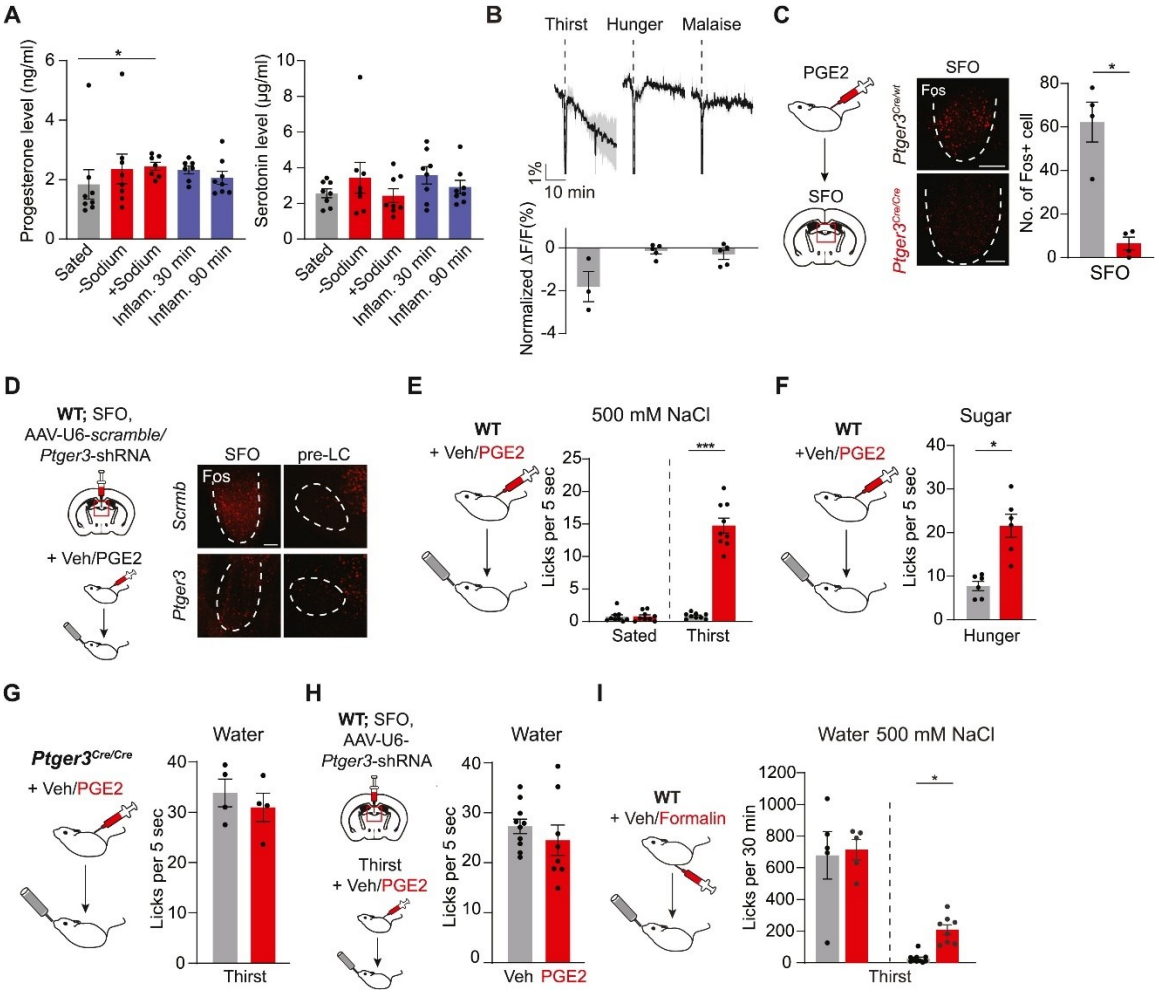
A
Progesterone level (ng/ml)
Serotonin level (μg/ml)
Sated
-Sodium
+Sodium
Inflam. 30 min
Inflam. 90 min
B
Thirst
Hunger
Malaise
1%
10 min
Normalized ΔF/F(%)
C
PGE2
SFO
Fos
Ptger3Cre/wt
Ptger3Cre/Cre
No. of Fos+ cell
D
WT; SFO,
AAV-U6-scramble/
Ptger3-shRNA
+ Veh/PGE2
SFO
pre-LC
Scrmb
Ptger3
E
WT
+ Veh/PGE2
500 mM NaCl
Licks per 5 sec
Sated
Thirst
F
WT
+Veh/PGE2
Sugar
Hunger
G
Ptger3Cre/Cre
+ Veh/PGE2
Water
Thirst
H
WT; SFO,
AAV-U6-
Ptger3-shRNA
Thirst
+ Veh/PGE2
Water
Veh
PGE2
I
WT
+ Veh/Formalin
Water 500 mM NaCl
Licks per 30 min
Thirst

Figure S2. Functional characterization of the PGE2/Ptger3 axis for aversive taste tolerance, related to Figure 2.

(A) Measurement of inflammation-related factors in the circulation by ELISA. Progesterone and serotonin (5-HT) levels were measured from sated (grey), formalin-injected (blue), and sodium depleted (red) animals (n = 7-8 mice).

(B) Control stimuli for fiber photometry recording from SFO^{Ptger3} neurons. These neurons showed no activation toward i.p. mannitol injection (2 M, 10 ml per kg BW; osmotic thirst), ghrelin (10 μg; hunger), or LiCl (0.15 M, 15 ml per kg BW; visceral malaise). Calcium dynamics and response amplitude (normalized ΔF/F) of SFO^{Ptger3} neurons are shown (n = 5 mice).

(C) PGE2 activated the SFO in a Ptger3-dependent pattern. Representative images and quantification of Fos immunofluorescence signals after subcutaneous injection of PGE2 in *Ptger3*$^{Cre/wt}$ (grey, n = 4 mice) and *Ptger3*$^{Cre/Cre}$ mice (red, n = 4 mice).

(D) Ptger3 in the SFO is required for PGE2 responses. Representative images after subcutaneous injection of PGE2 in *scramble*- (top) and *Ptger3*- (bottom) shRNA-injected mice were shown. No Fos signal was found in the pre-LC.

(E) PGE2 induced tolerance in wild-type animals. Consumption of 500 mM NaCl was measured under sated and osmotic thirst after subcutaneous injection of vehicle (grey) or PGE2 (red, n =9 mice).

(F) PGE2-induced aversive taste tolerance in food-deprived, wild-type animals. Left, a diagram of the behavioral paradigm. Right, the number of licks toward 0.25 mM quinine

with 500 mM glucose in food-deprived mice after vehicle (grey) or PGE2 injection (red, n = 6).

(G) Thirsty *Ptger3*$^{Cre/Cre}$ mice consumed pure water after vehicle (grey) or PGE2 (red) subcutaneous injection (n = 4 mice).

(H) Thirsty *Ptger3* KD mice consumed pure water after vehicle (grey) or PGE2 (red) subcutaneous injection (n = 8-10 mice).

(I) Formalin-induced inflammation increased tolerance towards 500 mM NaCl during thirst (n = 5-10). Water intake was unaffected by the same treatment.

Data are expressed as mean ± SEM, $*p < 0.05$, $**p < 0.01$, $***p < 0.001$. Scale bar, 100 μm. See also Table S1.

Chapter 4

FLUID HOMEOSTASIS AND SALT IMBALANCE

Maintaining the fluid balance requires complex crosstalk within the neural circuits and endocrine systems through the brain-body axis. Previous research focused upon the thirst-driving pathways in the brain. Recent studies have shed more light on the role of post-ingestive feed-forward modulation mediated by peripheral signals. Advances in technology have unveiled the genetic profiles of the underlying circuits, enabling more precise interventions in future translational research. Despite the prevalence of fluid balance dysregulation in modern life, its health relevance remains underappreciated. Importantly, the crisis of salt overconsumption has been overlooked. The close linkage between salt consumption and inflammation shed a new light on the potential strategy of salt reduction.

4.1 Fluid homeostasis

The stability of the *milieu interieur* is vital for survival.[154] In particular, fluid *homeostasis* ensures the body fluids are stabilized within a precise range. Fluids, a combination of water and minerals, are constantly exchanged between the external environment and the body, as well as between internal compartments (intracellular fluid [ICF] and extracellular fluid [ECF]). In healthy individuals, the total body fluid constitutes approximately 60% of body weight, with an average of 3–4 liters consumed and metabolized daily. Throughout this process, osmolality is constantly preserved at 275-295 mOsmol/kg. Acute deviation from this equilibrium causes thirst or osmotic shock, while the long-term failure to maintain the

proper balance leads to pathological states, such as diabetes, cardiovascular diseases and kidney failure.

4.1.1 Thirst regulation

The sensation of thirst arises with a rapid 1–2% reduction in body mass.[155] Homeostatic thirst is a sensation arising from a disturbance in homeostasis driven by osmolality and volemic stimuli. Thus, the thirst drive can be categorized as osmotic thirst and volemic thirst (Figure 1). Interestingly, thirst can be triggered by a change in plasma volume (about 10%), whereas only 1% acute change in osmolality is sufficient to induce water intake. These perturbations of equilibrium are directly detected by the central and peripheral nervous systems. In addition, non-homeostatic thirst can be triggered independently of osmotic and volemic signals. For instance, in prandial thirst and circadian-induced thirst, water intake occurs before any physiological challenges.[156–158]

4.1.2 Central nervous system

Thirst has been extensively studied from the physiological and behavioral standpoints. The induction of thirst involves integrative inputs from multiple organs which detect and modulate osmolality, blood pressure, and fluid volume.[155] Advances in neuroscience techniques have provided researchers with powerful tools to identify specific brain loci and link distinct physiological responses to distinct neural circuits. In Drosophila, the Janu interneurons are newly proposed as selective drivers for water seeking behaviors.[159] Outside the brain, the downstream of the interoceptive subesophageal zone neurons (ISNs) respond to hunger and thirst oppositely as well, forming distinct pathways for sucrose and water

ingestion.[160] Recent studies identified the hygrosensory neurons expressing ionotropic receptor 8a (IR8a) in Drosophila melanogaster are activated by high humidities, and attenuated during thirst, facilitating the behavioral transition from humidity aversion to water seeking.[161] In mammals, including humans, the major brain regions involved in thirst regulation are the circumventricular organs (CVOs), which lack the blood brain barrier (BBB).[162–164] Subfornical organ (SFO) and organum vasculosum of the lamina terminalis (OVLT) compose the lamina terminalis (LT) along with the median preoptic nucleus (MnPO). Extensive studies have demonstrated the necessity and sufficiency of LT neurons in thirst.[162,163] Genetically defined neural populations that drive thirst have been identified in the LT, where MnPO neurons serve as a integration center of interoceptive signals.[158,165] A study with single-cell transcriptomics further demonstrated that LT thirst neurons comprise diverse neuron types that mediate hypovolemic and osmotic thirst.[166] Despite differences in brain organization, both invertebrates and mammals exhibit functionally specialized neural pathways that govern thirst and fluid-seeking behaviors. A common theme across species appears to be the role of interoceptive neurons in balancing competing physiological needs. The input to CVOs functions as the primary sensory signal to induce thirst. At the molecular level, several sensors and channels have been proposed. The Na_X (SCN7A) channels in glial cells and Transmembrane Protein 63B (TMEM63B) channels in excitatory neurons ae identified to detect osmolality changes in blood.[167,168] Other studies proposed the osmosensing role of epithelial sodium channel (ENaC),[169] transient receptor potential vanilloid-1 (Trpv1), and vanilloid-4 (Trpv4) channels.[170] However, genetic deletion of Trp channels did not fully abolish the hypernatremia or hyperosmolality-induced water intake,[171] suggesting that multiple mechanisms may be involved in osmosensation.

The lateral hypothalamic area (LHA) has been known to modulate ingestive behaviors in general. A recent study reported that neurotensin (Nts)-expressing LHA neurons selectively encode for thirst drive instead of hunger.[172] Since the LHA is a downstream area of the LT, it would be interesting to examine if Nts neurons integrate thirst signals from interoceptive brain areas. Additionally, the crosstalk between the suprachiasmatic nucleus (SCN) and OVLT through vasopressin (VP)- expressing neurons mediates anticipatory thirst prior to sleep,[173] which is further validated by the blood flow between these two regions.[174] Interestingly, the well-known hunger neurons, namely, agouti-related protein (Agrp) neurons, were found with a subset related to thirst regulation. The knockout of carnitinea palmitoyltransferase 1A (Cpt1a) in the Agrp neurons resulted in polydipsia and polyuria.[175] Apart from these well-studied areas, emerging studies indicated brain-wide regulation of thirst and drinking behavior. For example, the Purkinje neurons in the cerebellum were shown to modulate water intake under thirst conditions.[176] Beyond specific brain areas, thirst regulation engages the whole brain network that collectively drive water consumption and modulate satiety feedback. Multiunit electrophysiological recording from 24,000 neurons across brain demonstrated unique neural population dynamics under thirst and satiety state[177] Additionally, recent findings showed that brain employs a energy landscape to balance internal needs such as hunger vs. thirst.[178] This innovative landscape framework helps explain how organisms resolve conflicting physiological needs over time, with neural activity shifting probabilistically towards the behavior that best addresses the current internal state.

4.1.3 Endocrine system

There are several endocrine signals critically involved in thirst and fluid balance regulation.[179] For hypovolemia, physiological signals such as angiotensin II (Ang II) are the critical regulators driving the thirst. The intracerebroventricular injection of Ang II is sufficient to drive immediate thirst, and the blockage of central Ang II receptor largely attenuates thirst.[179] Interestingly, a recent study showed the same individual neuron in the OVLT responds to both Ang II and high sodium concentrations.[180] A significant impact of Ang II is the stimulation of aldosterone production, a mineralocorticoid hormone that increases in response to elevated Ang II levels during hypovolemia. In addition, adrenocorticotropin and potassium play key roles in regulating the aldosterone level. Interestingly, one recent study proposed the deletion of the angiotensinogen gene (Agt) in brain and liver, which encodes the precursor of angiotensin peptides, did not eliminate thirst or sodium appetite.[181]Vasopressin or arginine vasopressin (AVP) is another well-studied hormone in the regulation of thirst, more specifically, in the osmotic thirst. Instead of driving thirst and water intake, AVP acts on the kidney and promotes water reabsorption. In diabetes insipidus, AVP deficiency and resistance resulted in excessive urine output.[182]

4.1.4 Satiation and feed-forward sensory modulations from body-brain axis

Recent studies have provided deeper insights into the central and peripheral pathways that regulate the termination of water consumption, ensuring adequate replenishment while preventing overconsumption.[183] As other appetite, the satiation from water retention is generated through the dopaminergic neurons in the brain areas encoding rewards. The recent research showed D1 and D2 neurons in the nucleus accumbens (NAc) are responsive to both

hunger and thirst cues, suggesting a shared neural circuit for processing these nutrient needs.[184]

Inhibitory neurons expressing glucagon-like peptide 1 receptor (Glp1r) in the LT quickly respond to drinking behavior and directly inhibit the SFO thirst-driving neurons by hypo-osmotic signals in the gut.[185] In addition to local inhibition within thirst-driving regions, the hindbrain plays a critical role in modulating satiation. A recent study suggested the nucleus solitarius tract (NTS) to paraventricular hypothalamic nucleus (PVH) pathway quenches water intake through endogenous Glp1 effect.[186] Parabrachial nucleus is another critical region in the feedback regulation of fluid consumption. One study proposed the potential role of the oxytocin-receptor (Oxtr) expressing neurons in PBN during fluid satiation.[187,188] Another recent study showed the PBN Pdyn neurons project to PVH and suppress fluid intake in response to the vagal signals triggered by stomach distension.[189] Meanwhile, the heterogeneous cholecystokinin (Cck) neurons in the lateral PBN project to GABAergic neurons in the MnPO and vBNST respectively, and each projection suppresses thirst and salt appetite accordingly.[190] Furthermore, peri-locus coeruleus (peri-LC) was identified as a converged hub for food and water ingestion, where neurons construct a double-negative feedback system.[191]

These thirst-quenching signals seem to arise from the peripheral sensory signals. Early studies in dogs suggested the oropharyngeal motor activities, for example swallowing, reduce the secretion of vasopressin drastically through the glossopharyngeal and vagus nerves.[192] Recent studies further demonstrated that ascending sensory pathways play an important role in transmitting thirst-quenching signals from the periphery to the brain.[185,193]

The hepatic portal vein functions as an osmosensory site in satiation, through its connection to the spleen and gastrointestinal tract.[194,195] Vagal and spinal afferents innervate to the hepatic portal vein and delivers the signal to the lateral hypothalamus.[196] The hepatic vagotomy impairs regulation of urine compositions against acute osmotic stimuli. A recent study showed the vagal afferents innervating the hepatic portal area mediate the osmolality through vasoactive intestinal peptide (VIP).[197] With more advanced technological approach, it has become possible to establish the genetic profile of the vagal afferent and understand the mechanism underlying how the feedback information is delivered to the brain. How the spinal pathway is involved in thirst regulation is still not well-understood, and exploring its role is a future research area.

In addition, the baroreceptors contribute to the body-brain axis by regulating blood pressure. Baroreceptors are expressed on the afferent of the glossopharyngeal (carotid) and vagus (aortic arch) nerves, and the cell bodies are located at the petrosal and nodose ganglia. The double knockout of Piezo1 and Piezo 2 channels blocks the detection from the afferents, destabilizes the blood pressure and impairs baroreflex.[198] On the other hand, the activation of the Piezo2-expressing neurons in the baroreceptor afferents rapidly reduces blood pressure and heart rate (see summary Figure 2).[198]

4.2 Excessive salt and dehydration

Long-term disruption in fluid balance has been identified as one of the key risk factors of developing hypertension. Guyton's cardiovascular model emphasized the role of kidney in long-term blood pressure control.[199] Another perspective proposed the significance of the interstitial hypertonic sodium dynamics and the role of mononuclear phagocyte system

(MPS) cells.[200] From the perspective of immune factors and vasculature, the lymphangiogenesis increases pro-inflammatory biomarkers and decreases endothelial nitric oxide synthase expression and nitric oxide level, leading to reduced vasodilation and elevated blood pressure.[201] The degree of hypertension is known to vary in the population due to the different level of sodium sensitivity from genetic background.[202] A combination of direct and indirect effects by high sodium diet contributes to cardiovascular disorders and hypertension, though the specific neural mechanisms remain to be explored.

Disrupt in fluid homeostasis prevails in the elderly population.[203] Dehydration has been widely found in hospitalized or home-stayed elderly groups. Total body water level peaks at 80% at birth, and declines to about 50% in the aged state.[204] Multiple cross-sectional studies revealed insufficient fluid intake for elderly groups at home or hospitalized. For instance, one study from 822 care residents reported 1104.1 ml/day water intake for the older population, which is below a recommended level of 1500 ml/day.[205] Interestingly, there are mixed results regarding the osmolality in the elderly population. Though there are studies characterizing a higher baseline osmolality in the elderly,[206] multiple studies in humans and rodents fail to capture the significant osmolality increase compared to adults in the sated state.[207–210] Various factors complexed the issue of fluid imbalance in the elderly population, including dysphagia, cognitive impairment, heart failure, diabetes, cirrhosis, nephrotic syndrome, emesis, and gastroentritis. The resulted hyperosmotic dehydration state exacerbates the inflammatory internal state and accelerates the decline of biological functions.

Decline of renal functions has been recognized as the major factor of dehydration. Increased nephrosclerosis in the geriatric population decreases the number of functional nephrons. The

number of functioning glomeruli (NFG) of in the older group was approximately 20% lower compared to in the younger group.[211] Renal plasma flow in the older group was depressed in proportion to the decreased glomerular filtration rate (GFR).[211] These morphological changes in kidney contribute to the inability to concentrate sodium in the urine. The older population dehydrates chronically and become more susceptible to developing cardiovascular diseases, including hypertension.

One common phenomenon observed in the older population (both humans and rodents) is a decreased sensation of thirst under dehydration.[210,212] The specific mechanism underlying the change in brain remains unknown. One of the popular hypotheses proposed that the osmotic thirst has been preserved in the older population while the volemic thirst was impaired.[207] The different response to osmotic and volemic thirst implies distinct neural populations might be compromised during ageing. However, one study showed the osmotic thirst induced intake in older population is significantly lower than the adult group.[212] The renin-angiotensin system is reported to be inhibited in the aged population; however, there are studies demonstrating increased renin and Ang II levels in the serum.[213] Increased AVP secretion has been identified in the elderly population as well.[214] According to several studies, the baseline level of circulatory AVP is higher but there is one study showing a decrease of AVP level in the elderly group.[214] There are also mixed results on whether the aged group elevates the osmoreceptor sensitivities, and it remains unclear whether the aged group has a greater AVP release by a unit change in osmolality.[214] Indeed, there are obstacles dissecting out the specific pathways attenuating the thirst drive in the elderly population due to the complex nature of this problem. Nevertheless, another approach to tackle the dehydration is through the satiation and quenching mechanism. The older population might

demonstrate over-sensitized reward feedback, leading to suboptimal rehydration. One PET study showed that in aged population, the regional cerebral blood flow (rCBF) is reduced to a greater level in anterior midcingulate cortex (aMCC) during rehydration, implying a possible change in the satiation threshold during ageing.[210] In general, significant potential remains for future research to elucidate the changes in thirst neural circuits throughout the lifespan.[215]

4.3 Salt overconsumption

Sodium is the most abundant electrolyte in the body for maintaining overall osmotic balance and cell functions. Though we retrieve a significant amount of sodium through daily food intake, sodium balance is precisely regulated by multiple organs and hormones. Daily fluctuations in serum sodium are minimal, often within 1-2 mmol/L. Various studies have investigated peripheral and central mechanisms that modulate sodium balance during depletion and consumption.[216] In addition to the known neural substrates for appetite in the hindbrain, a recent study revealed a parallel pathway in the forebrain regulating the taste valence of sodium. This novel model distinguishes regulation of fluid balance from energy balance.[217]

Maintaining an optimal sodium level is crucial for the regulation of fluid balance. However, modern dietary patterns pose significant obstacles to maintaining optimal sodium levels in the body. Excess sodium consumption is a critical and persistent public health challenge. According to the Centers for Disease Control and Prevention (CDC) and U.S. Food and Drug Administration (FDA), over 90% of Americans exceed the recommended daily sodium intake of 2,300 mg, with the average intake reaching approximately 3,400 mg per day.[218,219]

The overconsumption problem is even more prevalent in China with 43,00 mg daily intake.[220] This dietary excess not just causes systematic sub-healthy states, but also contributes to millions of deaths annually worldwide from high-blood-pressure-related cardiovascular events.[221–226] Despite decades of public education campaigns, front-of-package labeling, and reformulation efforts by the food industry, population-level sodium intake has remained largely unchanged over the past 20 years.[227,228]

This stagnant trend is not due to lack of awareness; rather, it reflects the strong physiological and neurobehavioral drive for salt, which is insufficiently addressed by external interventions. Current public health efforts (e.g., food labeling and education) rely heavily on individual behavioral change and have limited success in modifying innate salt appetite.[229,230] Individuals attempting to reduce sodium often struggle with cravings and report dissatisfaction with low-salt foods.

Established research have revealed the high correlation between high sodium intake and cardiovascular and renal disorders. These disorders were underestimated at their early stages, often perceived as transient fluid imbalances that could be resolved through increased water intake. However, emerging evidence reveals intricate pathological alterations in the body associated with sodium dysregulation. Acute high sodium intake has been known for the induction of thirst. Nevertheless, in a recent human study, high sodium diet over consecutive days already shifted the body to an insufficient hydration state.[231] From the perspective of the gut microbiome, several studies demonstrated how a high sodium diet chronically shifts the gastrointestinal microbiota: the abundances of bacteria producing short-chain fatty acid (SCFA) have been reduced, while Clostridia, Alistipes, and Akkermansia have been more enriched.[232] Consequently, the pathogenic T helper 17 (Th17) lymphocytes in the gut

increase the circulating pro-inflammatory cytokine levels, leading to autoimmune disfunction and even cognitive impairment.[233,234]

The long-term high salt consumption model has not been fully established in rodent studies. Commonly used high sodium diets in mice contain sodium levels approximately 5–10 times higher than standard chow, which may not accurately recapture human patterns of overconsumption. In addition, most rodent studies focus on exposure durations ranging from two weeks to three months, whereas high sodium intake in humans often persists across the lifespan. Thus, it is reasonable to consider adopting diets with physiologically relevant sodium levels and extending exposure periods in future experimental designs.

Our preliminary data indicate that mice maintained on a high-sodium diet demonstrated an augmented sodium craving which is consistent with the previous results that prolonged high salt intake shifts preference toward higher sodium concentrations in humans.[235,236] Interestingly, this craving of sodium was attenuated by local Ptger3 knockdown in the SFO of rodent brain. This result echo back to the important role of Ptger3 in the taste valence and implied the PGE2–Ptger3 brain–body axis may recalibrate sodium taste sensitivity under conditions of chronic overconsumption.

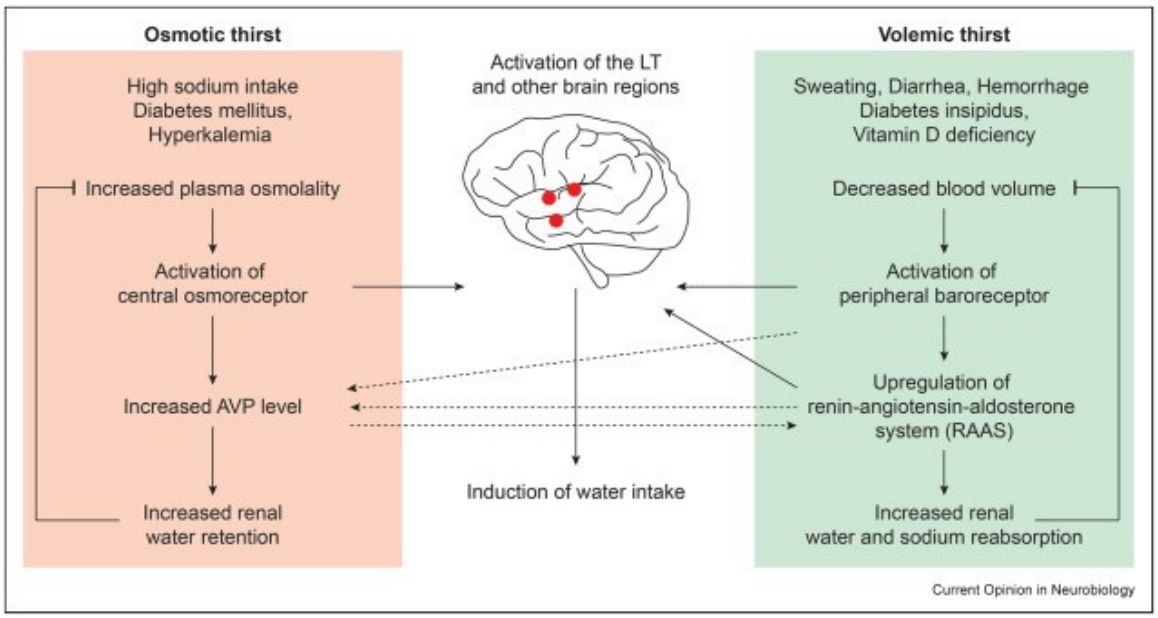
Osmotic thirst
High sodium intake
Diabetes mellitus,
Hyperkalemia
Increased plasma osmolality
Activation of
central osmoreceptor
Increased AVP level
Increased renal
water retention
Activation of the LT
and other brain regions
Induction of water intake
Volemic thirst
Sweating, Diarrhea, Hemorrhage
Diabetes insipidus,
Vitamin D deficiency
Decreased blood volume
Activation of
peripheral baroreceptor
Upregulation of
renin-angiotensin-aldosterone
system (RAAS)
Increased renal
water and sodium reabsorption
Current Opinion in Neurobiology

Figure 1. Different types of thirst and adaptive responses in the body.
Osmotic and volemic thirst triggers distinct but interactive circuits in the body-brain axis to induce ingestion.[155]

Physiological elements for thirst regulation

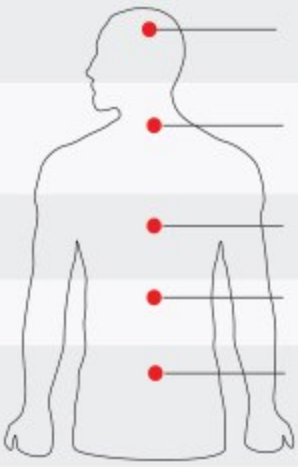

Brain
Osmoreceptors outside BBB (SCN7A and TMEM63B channels)
Initiation of thirst drive (SFO, OVLT and MnPO)
Downstream consumption cascade (LH, PVH, and SON)
Satiation and reward feedback (NTS, PBN and peripheral input)

Glossopharyngeal and Vagus nerves
Arterial baroreceptors in the aortic arch and carotid bodies (Piezos)
Rapid quenching of thirst
Transmission of peripheral satiation signal

Heart and Cardiovascular system
Cardiovascular baroreceptors in the heart (Piezos)
Circulatory hormonal change (renin, Ang II, aldosterone, and AVP)

Gastrointestinal tract
Ingestion feedback (gastric distention and osmotic signal)

Kidney
Detection of salt, metabolic and volemic change (juxtaglomerular apparatus)
Activation of renin-angiotensin-aldosterone system
Absorption or retention of electrolytes and water

Current Opinion in Neurobiology

Figure 2. Central and peripheral regulation in dehydration and rehydration.
Specific elements are summarized in the graph to introduce the key concepts in fluid homeostasis.

Reference

1. Cabanac, M. (1971). Physiological Role of Pleasure. Science *173*, 1103–1107. https://doi.org/10.1126/science.173.4002.1103.

2. Cabanac, M., and Duclaux, R. (1970). Specificity of internal signals in producing satiety for taste stimuli. Nature *227*, 966–967. https://doi.org/10.1038/227966a0.

3. Cabanac, M., Brondel, L., and Cabanac, A. (2020). Alliesthesia. Up-date of the Word and Concept. AJBSR *8*, 313.

4. Cabanac, M. (1979). Sensory pleasure. Q Rev Biol *54*, 1–29. https://doi.org/10.1086/410981.

5. Cabanac, M., Guillaume, J., Balasko, M., and Fleury, A. (2002). Pleasure in decision-making situations. BMC Psychiatry *2*, 7. https://doi.org/10.1186/1471-244X-2-7.

6. Keramati, M., and Gutkin, B. Homeostatic reinforcement learning for integrating reward collection and physiological stability. eLife *3*, e04811. https://doi.org/10.7554/eLife.04811.

7. Rangel, A., Camerer, C., and Montague, P.R. (2008). A framework for studying the neurobiology of value-based decision making. Nat Rev Neurosci *9*, 545–556. https://doi.org/10.1038/nrn2357.

8. Posner, J., Russell, J.A., and Peterson, B.S. (2005). The circumplex model of affect: An integrative approach to affective neuroscience, cognitive development, and psychopathology. Dev Psychopathol *17*, 715–734. https://doi.org/10.1017/S0954579405050340.

9. Berridge, K.C., and Robinson, T.E. (2016). Liking, wanting, and the incentive-sensitization theory of addiction. Am Psychol *71*, 670–679. https://doi.org/10.1037/amp0000059.

10. Berridge, K.C., Robinson, T.E., and Aldridge, J.W. (2009). Dissecting components of reward: 'liking', 'wanting', and learning. Curr Opin Pharmacol *9*, 65–73. https://doi.org/10.1016/j.coph.2008.12.014.

11. Finlayson, G., and Dalton, M. (2012). Current progress in the assessment of "liking" vs. "wanting" food in human appetite. Comment on " 'You say it's liking, i say it's wanting...'. On the difficulty of disentangling food reward in man." Appetite *58*, 373–378; discussion 252-5. https://doi.org/10.1016/j.appet.2011.10.011.

12. Barrett, L.F. (2017). The theory of constructed emotion: an active inference account of interoception and categorization. Soc Cogn Affect Neurosci *12*, 1–23. https://doi.org/10.1093/scan/nsw154.

13. Hanci, D., and Altun, H. (2016). Hunger state affects both olfactory abilities and gustatory sensitivity. Eur Arch Otorhinolaryngol *273*, 1637–1641. https://doi.org/10.1007/s00405-015-3589-6.

14. Ramaekers, M.G., Verhoef, A., Gort, G., Luning, P.A., and Boesveldt, S. (2016). Metabolic and Sensory Influences on Odor Sensitivity in Humans. Chem Senses *41*, 163–168. https://doi.org/10.1093/chemse/bjv068.

15. Atlas, L.Y., and Wager, T.D. (2014). A Meta-analysis of Brain Mechanisms of Placebo Analgesia: Consistent Findings and Unanswered Questions. Handb Exp Pharmacol *225*, 37–69. https://doi.org/10.1007/978-3-662-44519-8_3.

16. Wager, T.D., Rilling, J.K., Smith, E.E., Sokolik, A., Casey, K.L., Davidson, R.J., Kosslyn, S.M., Rose, R.M., and Cohen, J.D. (2004). Placebo-Induced Changes in fMRI in the Anticipation and Experience of Pain. Science. https://doi.org/10.1126/science.1093065.

17. Deschênes, A., Duncan, J., Daudelin-Peltier, C., Dion Marcoux, Y., Blais, C., Fiset, D., and Forget, H. (2014). The impact of psychological stress on the contrast sensitivity function. Journal of Vision *14*, 1407. https://doi.org/10.1167/14.10.1407.

18. Zhang, X., Zuo, B., Erskine, K., and Hu, T. (2016). Feeling light or dark? Emotions affect perception of brightness. Journal of Environmental Psychology *47*, 107–111. https://doi.org/10.1016/j.jenvp.2016.05.007.

19. Lang, P.J., Bradley, M.M., and Cuthbert, B.N. (1990). Emotion, attention, and the startle reflex. Psychol Rev *97*, 377–395.

20. Bradley, M.M., Cuthbert, B.N., and Lang, P.J. (1990). Startle reflex modification: emotion or attention? Psychophysiology *27*, 513–522. https://doi.org/10.1111/j.1469-8986.1990.tb01966.x.

21. Fu, O., Minokoshi, Y., and Nakajima, K. (2021). Recent Advances in Neural Circuits for Taste Perception in Hunger. Front. Neural Circuits *15*. https://doi.org/10.3389/fncir.2021.609824.

22. Berridge, K.C. (1991). Modulation of taste affect by hunger, caloric satiety, and sensory-specific satiety in the rat. Appetite *16*, 103–120. https://doi.org/10.1016/0195-6663(91)90036-r.

23. Rolls, E.T., Rolls, B.J., and Rowe, E.A. (1983). Sensory-specific and motivation-specific satiety for the sight and taste of food and water in man. Physiol Behav *30*, 185–192. https://doi.org/10.1016/0031-9384(83)90003-3.

24. Berridge, K.C. (1991). Modulation of taste affect by hunger, caloric satiety, and sensory-specific satiety in the rat. Appetite *16*, 103–120. https://doi.org/10.1016/0195-6663(91)90036-r.

25. Hanci, D., and Altun, H. (2016). Hunger state affects both olfactory abilities and gustatory sensitivity. Eur Arch Otorhinolaryngol *273*, 1637–1641. https://doi.org/10.1007/s00405-015-3589-6.

26. Fu, O., Iwai, Y., Narukawa, M., Ishikawa, A.W., Ishii, K.K., Murata, K., Yoshimura, Y., Touhara, K., Misaka, T., Minokoshi, Y., et al. (2019). Hypothalamic neuronal circuits regulating hunger-induced taste modification. Nat Commun *10*, 4560. https://doi.org/10.1038/s41467-019-12478-x.

27. Zverev, Y.P. (2004). Effects of caloric deprivation and satiety on sensitivity of the gustatory system. BMC Neurosci *5*, 5. https://doi.org/10.1186/1471-2202-5-5.

28. Fu, O., Iwai, Y., Narukawa, M., Ishikawa, A.W., Ishii, K.K., Murata, K., Yoshimura, Y., Touhara, K., Misaka, T., Minokoshi, Y., et al. (2019). Hypothalamic neuronal circuits regulating hunger-induced taste modification. Nature communications *10*, 4560. https://doi.org/10.1038/s41467-019-12478-x.

29. Kawai, K., Sugimoto, K., Nakashima, K., Miura, H., and Ninomiya, Y. (2000). Leptin as a modulator of sweet taste sensitivities in mice. Proc Natl Acad Sci U S A *97*, 11044–11049. https://doi.org/10.1073/pnas.190066697.

30. Pasquet, P., Monneuse, M.-O., Simmen, B., Marez, A., and Hladik, C.-M. (2006). Relationship between taste thresholds and hunger under debate. Appetite *46*, 63–66. https://doi.org/10.1016/j.appet.2005.09.004.

31. Nakano, Y., Oomura, Y., Nishino, H., Aou, S., Yamamoto, T., and Nemoto, S. (1984). Neuronal activity in the medial orbitofrontal cortex of the behaving monkey: modulation by glucose and satiety. Brain Res Bull *12*, 381–385. https://doi.org/10.1016/0361-9230(84)90109-6.

32. Burton, M.J., Rolls, E.T., and Mora, F. (1976). Effects of hunger on the responses of neurons in the lateral hypothalamus to the sight and taste of food. Exp Neurol *51*, 668–677. https://doi.org/10.1016/0014-4886(76)90189-8.

33. Nakano, Y., Oomura, Y., Lénárd, L., Nishino, H., Aou, S., Yamamoto, T., and Aoyagi, K. (1986). Feeding-related activity of glucose- and morphine-sensitive neurons in the monkey amygdala. Brain Res *399*, 167–172. https://doi.org/10.1016/0006-8993(86)90613-x.

34. Rolls, E.T., Sienkiewicz, Z.J., and Yaxley, S. (1989). Hunger Modulates the Responses to Gustatory Stimuli of Single Neurons in the Caudolateral Orbitofrontal Cortex of the Macaque Monkey. Eur J Neurosci *1*, 53–60. https://doi.org/10.1111/j.1460-9568.1989.tb00774.x.

35. Kringelbach, M.L., O'Doherty, J., Rolls, E.T., and Andrews, C. (2003). Activation of the human orbitofrontal cortex to a liquid food stimulus is correlated with its subjective pleasantness. Cereb Cortex *13*, 1064–1071. https://doi.org/10.1093/cercor/13.10.1064.

36. Siep, N., Roefs, A., Roebroeck, A., Havermans, R., Bonte, M.L., and Jansen, A. (2009). Hunger is the best spice: an fMRI study of the effects of attention, hunger and calorie content on food reward processing in the amygdala and orbitofrontal cortex. Behav Brain Res *198*, 149–158. https://doi.org/10.1016/j.bbr.2008.10.035.

37. Wright, H., Li, X., Fallon, N.B., Crookall, R., Giesbrecht, T., Thomas, A., Halford, J.C.G., Harrold, J., and Stancak, A. (2016). Differential effects of hunger and satiety on insular cortex and hypothalamic functional connectivity. Eur J Neurosci *43*, 1181–1189. https://doi.org/10.1111/ejn.13182.

38. Chen, Y., Lin, Y.-C., Kuo, T.-W., and Knight, Z.A. (2015). Sensory detection of food rapidly modulates arcuate feeding circuits. Cell *160*, 829–841. https://doi.org/10.1016/j.cell.2015.01.033.

39. Deem, J.D., Faber, C.L., and Morton, G.J. (2022). AgRP neurons: Regulators of feeding, energy expenditure, and behavior. FEBS J *289*, 2362–2381. https://doi.org/10.1111/febs.16176.

40. Betley, J.N., Cao, Z.F.H., Ritola, K.D., and Sternson, S.M. (2013). Parallel, Redundant Circuit Organization for Homeostatic Control of Feeding Behavior. Cell *155*, 1337–1350. https://doi.org/10.1016/j.cell.2013.11.002.

41. Sternson, S.M., and Atasoy, D. (2014). Agouti-Related Protein Neuron Circuits That Regulate Appetite. Neuroendocrinology *100*, 95–102. https://doi.org/10.1159/000369072.

42. Sternson, S.M., Nicholas Betley, J., and Cao, Z.F. (2013). Neural circuits and motivational processes for hunger. Current opinion in neurobiology *23*, 353–360. https://doi.org/10.1016/j.conb.2013.04.006.

43. Aponte, Y., Atasoy, D., and Sternson, S.M. (2011). AGRP neurons are sufficient to orchestrate feeding behavior rapidly and without training. Nature neuroscience *14*, 351–355. https://doi.org/10.1038/nn.2739.

44. Atasoy, D., Betley, J.N., Su, H.H., and Sternson, S.M. (2012). Deconstruction of a neural circuit for hunger. Nature *488*, 172–177. https://doi.org/10.1038/nature11270.

45. Betley, J.N., Xu, S., Cao, Z.F., Gong, R., Magnus, C.J., Yu, Y., and Sternson, S.M. (2015). Neurons for hunger and thirst transmit a negative-valence teaching signal. Nature *521*, 180–185. https://doi.org/10.1038/nature14416.

46. Burgess, C.R., Ramesh, R.N., Sugden, A.U., Levandowski, K.M., Minnig, M.A., Fenselau, H., Lowell, B.B., and Andermann, M.L. (2016). Hunger-Dependent Enhancement of Food Cue Responses in Mouse Postrhinal Cortex and Lateral Amygdala. Neuron *91*, 1154–1169. https://doi.org/10.1016/j.neuron.2016.07.032.

47. Livneh, Y., Ramesh, R.N., Burgess, C.R., Levandowski, K.M., Madara, J.C., Fenselau, H., Goldey, G.J., Diaz, V.E., Jikomes, N., Resch, J.M., et al. (2017). Homeostatic circuits selectively gate food cue responses in insular cortex. Nature *546*, 611–616. https://doi.org/10.1038/nature22375.

48. Livneh, Y., Sugden, A.U., Madara, J.C., Essner, R.A., Flores, V.I., Sugden, L.A., Resch, J.M., Lowell, B.B., and Andermann, M.L. (2020). Estimation of Current and Future Physiological States in Insular Cortex. Neuron *105*, 1094-1111 e10. https://doi.org/10.1016/j.neuron.2019.12.027.

49. Wang, L., Gillis-Smith, S., Peng, Y., Zhang, J., Chen, X., Salzman, C.D., Ryba, N.J.P., and Zuker, C.S. (2018). The coding of valence and identity in the mammalian taste system. Nature *558*, 127–131. https://doi.org/10.1038/s41586-018-0165-4.

50. Inagaki, H.K., Panse, K., and Anderson, D.J. (2014). Independent, reciprocal neuromodulatory control of sweet and bitter taste sensitivity during starvation in Drosophila. Neuron *84*, 806–820. https://doi.org/10.1016/j.neuron.2014.09.032.

51. Shin, Y.-K., Martin, B., Kim, W., White, C.M., Ji, S., Sun, Y., Smith, R.G., Sévigny, J., Tschöp, M.H., Maudsley, S., et al. (2010). Ghrelin Is Produced in Taste Cells and Ghrelin Receptor Null Mice Show Reduced Taste Responsivity to Salty (NaCl) and Sour (Citric Acid) Tastants. PLoS One *5*, e12729. https://doi.org/10.1371/journal.pone.0012729.

52. Yoshida, R. (2012). Hormones and bioactive substances that affect peripheral taste sensitivity. Journal of Oral Biosciences *54*, 67–72. https://doi.org/10.1016/j.job.2012.02.002.

53. Kawai, K., Sugimoto, K., Nakashima, K., Miura, H., and Ninomiya, Y. (2000). Leptin as a modulator of sweet taste sensitivities in mice. Proceedings of the National Academy of Sciences *97*, 11044–11049. https://doi.org/10.1073/pnas.190066697.

54. Shigemura, N., Ohta, R., Kusakabe, Y., Miura, H., Hino, A., Koyano, K., Nakashima, K., and Ninomiya, Y. (2004). Leptin modulates behavioral responses to sweet substances by influencing peripheral taste structures. Endocrinology *145*, 839–847. https://doi.org/10.1210/en.2003-0602.

55. Martin, B., Dotson, C.D., Shin, Y.-K., Ji, S., Drucker, D.J., Maudsley, S., and Munger, S.D. (2009). Modulation of taste sensitivity by GLP-1 signaling in taste buds. Ann N Y Acad Sci *1170*, 98–101. https://doi.org/10.1111/j.1749-6632.2009.03920.x.

56. Gillard, B.T., Amor, N., Iraizoz, F.A., Pauža, A.G., Campbell, C., Greenwood, M.P., Alagaili, A.N., and Murphy, D. (2023). Mobilisation of jerboa kidney gene networks during dehydration and opportunistic rehydration. iScience *26*, 107574. https://doi.org/10.1016/j.isci.2023.107574.

57. Elson, A.E.T., Dotson, C.D., Egan, J.M., and Munger, S.D. (2010). Glucagon signaling modulates sweet taste responsiveness. FASEB J *24*, 3960–3969. https://doi.org/10.1096/fj.10-158105.

58. Baquero, A.F., and Gilbertson, T.A. (2011). Insulin activates epithelial sodium channel (ENaC) via phosphoinositide 3-kinase in mammalian taste receptor cells. Am J Physiol-Cell Ph *300*, C860–C871. https://doi.org/10.1152/ajpcell.00318.2010.

59. Rodriguez-Raecke, R., Yang, H., Bruenner, Y.F., and Freiherr, J. (2017). Intranasal Insulin Boosts Gustatory Sensitivity. J Neuroendocrinol *29*. https://doi.org/10.1111/jne.12449.

60. Herness, S., Zhao, F., Lu, S., Kaya, N., and Shen, T. (2002). Expression and Physiological Actions of Cholecystokinin in Rat Taste Receptor Cells. J. Neurosci. *22*, 10018–10029. https://doi.org/10.1523/JNEUROSCI.22-22-10018.2002.

61. Yoshida, R., Shin, M., Yasumatsu, K., Takai, S., Inoue, M., Shigemura, N., Takiguchi, S., Nakamura, S., and Ninomiya, Y. (2017). The Role of Cholecystokinin in Peripheral Taste Signaling in Mice. Front Physiol *8*, 866. https://doi.org/10.3389/fphys.2017.00866.

62. Shigemura, N., Iwata, S., Yasumatsu, K., Ohkuri, T., Horio, N., Sanematsu, K., Yoshida, R., Margolskee, R.F., and Ninomiya, Y. (2013). Angiotensin II Modulates Salty and Sweet Taste Sensitivities. J Neurosci *33*, 6267–6277. https://doi.org/10.1523/JNEUROSCI.5599-12.2013.

63. Al'Absi, M., Nakajima, M., Hooker, S., Wittmers, L., and Cragin, T. (2012). Exposure to acute stress is associated with attenuated sweet taste. Psychophysiology *49*, 96–103. https://doi.org/10.1111/j.1469-8986.2011.01289.x.

64. Dahir, N.S., Calder, A.N., McKinley, B.J., Liu, Y., and Gilbertson, T.A. (2021). Sex differences in fat taste responsiveness are modulated by estradiol. Am J Physiol Endocrinol Metab *320*, E566–E580. https://doi.org/10.1152/ajpendo.00331.2020.

65. Sinclair, M.S., Perea-Martinez, I., Abouyared, M., St. John, S.J., and Chaudhari, N. (2015). Oxytocin decreases sweet taste sensitivity in mice. Physiol Behav *141*, 103–110. https://doi.org/10.1016/j.physbeh.2014.12.048.

66. Cabanac, M. (1971). Physiological Role of Pleasure. Science *173*, 1103–1107. https://doi.org/10.1126/science.173.4002.1103.

67. Berridge, K.C., and Schulkin, J. (1989). Palatability shift of a salt-associated incentive during sodium depletion. Q J Exp Psychol B *41*, 121–138.

68. Berridge, K.C., Flynn, F.W., Schulkin, J., and Grill, H.J. (1984). Sodium depletion enhances salt palatability in rats. Behav Neurosci *98*, 652–660. https://doi.org/10.1037//0735-7044.98.4.652.

69. Horio, N., and Liberles, S.D. (2021). Hunger enhances food-odour attraction through a neuropeptide Y spotlight. Nature *592*, 262–266. https://doi.org/10.1038/s41586-021-03299-4.

70. Fu, O., Iwai, Y., Narukawa, M., Ishikawa, A.W., Ishii, K.K., Murata, K., Yoshimura, Y., Touhara, K., Misaka, T., Minokoshi, Y., et al. (2019). Hypothalamic neuronal circuits regulating hunger-induced taste modification. Nature communications *10*, 4560. https://doi.org/10.1038/s41467-019-12478-x.

71. Fitzsimons, J.T. (1978). Angiotensin, thirst, and sodium appetite: retrospect and prospect. Fed Proc *37*, 2669–2675.

72. McKinley, M.J., and Johnson, A.K. (2004). The physiological regulation of thirst and fluid intake. News Physiol Sci *19*, 1–6.

73. Farquhar, W.B., Edwards, D.G., Jurkovitz, C.T., and Weintraub, W.S. (2015). Dietary Sodium and Health: More Than Just Blood Pressure. J Am Coll Cardiol *65*, 1042–1050. https://doi.org/10.1016/j.jacc.2014.12.039.

74. Jobin, K., Stumpf, N.E., Schwab, S., Eichler, M., Neubert, P., Rauh, M., Adamowski, M., Babyak, O., Hinze, D., Sivalingam, S., et al. (2020). A high-salt diet compromises antibacterial neutrophil responses through hormonal perturbation. Science Translational Medicine *12*, eaay3850. https://doi.org/10.1126/scitranslmed.aay3850.

75. Wilck, N., Matus, M.G., Kearney, S.M., Olesen, S.W., Forslund, K., Bartolomaeus, H., Haase, S., Mähler, A., Balogh, A., Markó, L., et al. (2017). Salt-responsive gut commensal modulates TH17 axis and disease. Nature *551*, 585–589. https://doi.org/10.1038/nature24628.

76. Beauchamp, G.K., Bertino, M., Burke, D., and Engelman, K. (1990). Experimental sodium depletion and salt taste in normal human volunteers. The American journal of clinical nutrition *51*, 881–889.

77. Roper, S.D., and Chaudhari, N. (2017). Taste buds: cells, signals and synapses. Nat Rev Neurosci *18*, 485–497. https://doi.org/10.1038/nrn.2017.68.

78. Oka, Y., Butnaru, M., von Buchholtz, L., Ryba, N.J., and Zuker, C.S. (2013). High salt recruits aversive taste pathways. Nature *494*, 472–475. https://doi.org/10.1038/nature11905.

79. Chandrashekar, J., Hoon, M.A., Ryba, N.J., and Zuker, C.S. (2006). The receptors and cells for mammalian taste. Nature *444*, 288–294. https://doi.org/10.1038/nature05401.

80. Duriez, A., Bergerot, C., Cone, J.J., Roitman, M.F., and Gutkin, B. (2023). Homeostatic Reinforcement Theory Accounts for Sodium Appetitive State- and Taste-Dependent Dopamine Responding. Nutrients *15*, 1015. https://doi.org/10.3390/nu15041015.

81. Geerling, J.C., and Loewy, A.D. (2008). Central regulation of sodium appetite. Experimental physiology *93*, 177–209. https://doi.org/10.1113/expphysiol.2007.039891.

82. Heck, G.L., Mierson, S., and DeSimone, J.A. (1984). Salt taste transduction occurs through an amiloride-sensitive sodium transport pathway. Science *223*, 403–405.

83. Chandrashekar, J., Kuhn, C., Oka, Y., Yarmolinsky, D.A., Hummler, E., Ryba, N.J., and Zuker, C.S. (2010). The cells and peripheral representation of sodium taste in mice. Nature *464*, 297–301. https://doi.org/10.1038/nature08783.

84. Ninomiya, Y. (1996). Salt taste responses of mouse chorda tympani neurons: evidence for existence of two different amiloride-sensitive receptor components for NaCl with different temperature dependencies. J Neurophysiol *76*, 3550–3554. https://doi.org/10.1152/jn.1996.76.5.3550.

85. Lewandowski, B.C., Sukumaran, S.K., Margolskee, R.F., and Bachmanov, A.A. (2016). Amiloride-Insensitive Salt Taste Is Mediated by Two Populations of Type III Taste Cells with Distinct Transduction Mechanisms. The Journal of neuroscience : the official journal of the Society for Neuroscience *36*, 1942–1953. https://doi.org/10.1523/JNEUROSCI.2947-15.2016.

86. Jarvie, B.C., and Palmiter, R.D. (2017). HSD2 neurons in the hindbrain drive sodium appetite. Nature neuroscience *20*, 167–169. https://doi.org/10.1038/nn.4451.

87. Augustine, V., Lee, S., and Oka, Y. (2020). Neural Control and Modulation of Thirst, Sodium Appetite, and Hunger. Cell *180*, 25–32. https://doi.org/10.1016/j.cell.2019.11.040.

88. Resch, J.M., Fenselau, H., Madara, J.C., Wu, C., Campbell, J.N., Lyubetskaya, A., Dawes, B.A., Tsai, L.T., Li, M.M., Livneh, Y., et al. (2017). Aldosterone-Sensing Neurons in the NTS Exhibit State-Dependent Pacemaker Activity and Drive Sodium Appetite via Synergy with Angiotensin II Signaling. Neuron *96*, 190-206 e7. https://doi.org/10.1016/j.neuron.2017.09.014.

89. Geerling, J.C., and Loewy, A.D. (2006). Aldosterone-sensitive neurons in the nucleus of the solitary tract: efferent projections. The Journal of comparative neurology *497*, 223–250. https://doi.org/10.1002/cne.20993.

90. Lee, S., Augustine, V., Zhao, Y., Ebisu, H., Ho, B., Kong, D., and Oka, Y. (2019). Chemosensory modulation of neural circuits for sodium appetite. Nature *568*, 93–97. https://doi.org/10.1038/s41586-019-1053-2.

91. Geerling, J.C., and Loewy, A.D. (2007). Sodium deprivation and salt intake activate separate neuronal subpopulations in the nucleus of the solitary tract and the parabrachial complex. The Journal of comparative neurology *504*, 379–403. https://doi.org/10.1002/cne.21452.

92. Fitts, D.A., Freece, J.A., Van Bebber, J.E., Zierath, D.K., and Bassett, J.E. (2004). Effects of forebrain circumventricular organ ablation on drinking or salt appetite after sodium depletion or hypernatremia. American journal of physiology. Regulatory, integrative and comparative physiology *287*, R1325-34. https://doi.org/10.1152/ajpregu.00391.2004.

93. Hiyama, T.Y., Watanabe, E., Okado, H., and Noda, M. (2004). The subfornical organ is the primary locus of sodium-level sensing by Na(x) sodium channels for the control of salt-intake behavior. The Journal of neuroscience : the official journal of the Society for Neuroscience *24*, 9276–9281.

94. Ch'ng, S.S., and Lawrence, A.J. (2019). The subfornical organ in sodium appetite: Recent insights. Neuropharmacology *154*, 107–113. https://doi.org/10.1016/j.neuropharm.2018.08.012.

95. Pool, A.-H., Wang, T., Stafford, D.A., Chance, R.K., Lee, S., Ngai, J., and Oka, Y. (2020). The cellular basis of distinct thirst modalities. Nature *588*, 112–117. https://doi.org/10.1038/s41586-020-2821-8.

96. Matsuda, T., Hiyama, T.Y., Niimura, F., Matsusaka, T., Fukamizu, A., Kobayashi, K., Kobayashi, K., and Noda, M. (2017). Distinct neural mechanisms for the control of thirst and salt appetite in the subfornical organ. Nature neuroscience *20*, 230–241. https://doi.org/10.1038/nn.4463.

97. Wright, J., and Colling, A. (1995). CHAPTER 6 - THE SEAWATER SOLUTION. In Seawater: its Composition, Properties and Behaviour (Second Edition), J. Wright and A. Colling, eds. (Pergamon), pp. 85–127. https://doi.org/10.1016/B978-0-08-042518-4.50011-6.

98. Stein, M.K., and Loewy, A.D. (2010). Area postrema projects to FoxP2 neurons of the pre-locus coeruleus and parabrachial nuclei: brainstem sites implicated in sodium appetite regulation. Brain Res *1359*, 116–127. https://doi.org/10.1016/j.brainres.2010.08.085.

99. Vivas, L., Pastuskovas, C.V., and Tonelli, L. (1995). Sodium depletion induces Fos immunoreactivity in circumventricular organs of the lamina terminalis. Brain Res *679*, 34–41. https://doi.org/10.1016/0006-8993(95)00208-8.

100. Wu, Y.E., Pan, L., Zuo, Y.N., Li, X.M., and Hong, W.Z. (2017). Detecting Activated Cell Populations Using Single-Cell RNA-Seq. Neuron *96*, 313-+. https://doi.org/10.1016/j.neuron.2017.09.026.

101. Eng, C.L., Lawson, M., Zhu, Q., Dries, R., Koulena, N., Takei, Y., Yun, J., Cronin, C., Karp, C., Yuan, G.C., et al. (2019). Transcriptome-scale super-resolved imaging in tissues by RNA seqFISH. Nature *568*, 235–239. https://doi.org/10.1038/s41586-019-1049-y.

102. Lohoff, T., Ghazanfar, S., Missarova, A., Koulena, N., Pierson, N., Griffiths, J.A., Bardot, E.S., Eng, C.-H.L., Tyser, R.C.V., Argelaguet, R., et al. (2022). Integration of spatial and

single-cell transcriptomic data elucidates mouse organogenesis. Nat Biotechnol *40*, 74–85. https://doi.org/10.1038/s41587-021-01006-2.

103. Zhang, Y., Hoon, M.A., Chandrashekar, J., Mueller, K.L., Cook, B., Wu, D., Zuker, C.S., and Ryba, N.J. (2003). Coding of sweet, bitter, and umami tastes: different receptor cells sharing similar signaling pathways. Cell *112*, 293–301.

104. Pérez, C.A., Huang, L., Rong, M., Kozak, J.A., Preuss, A.K., Zhang, H., Max, M., and Margolskee, R.F. (2002). A transient receptor potential channel expressed in taste receptor cells. Nat Neurosci *5*, 1169–1176. https://doi.org/10.1038/nn952.

105. Leffler, A., Mönter, B., and Koltzenburg, M. (2006). The role of the capsaicin receptor TRPV1 and acid-sensing ion channels (ASICS) in proton sensitivity of subpopulations of primary nociceptive neurons in rats and mice. Neuroscience *139*, 699–709. https://doi.org/10.1016/j.neuroscience.2005.12.020.

106. Teng, B., Wilson, C.E., Tu, Y.-H., Joshi, N.R., Kinnamon, S.C., and Liman, E.R. (2019). Cellular and Neural Responses to Sour Stimuli Require the Proton Channel Otop1. Curr Biol *29*, 3647-3656.e5. https://doi.org/10.1016/j.cub.2019.08.077.

107. Zhang, J., Jin, H., Zhang, W., Ding, C., O'Keeffe, S., Ye, M., and Zuker, C.S. (2019). Sour Sensing from the Tongue to the Brain. Cell *179*, 392-402 e15. https://doi.org/10.1016/j.cell.2019.08.031.

108. Caterina, M.J., Schumacher, M.A., Tominaga, M., Rosen, T.A., Levine, J.D., and Julius, D. (1997). The capsaicin receptor: a heat-activated ion channel in the pain pathway. Nature *389*, 816–824. https://doi.org/10.1038/39807.

109. Nelson, G., Hoon, M.A., Chandrashekar, J., Zhang, Y., Ryba, N.J., and Zuker, C.S. (2001). Mammalian sweet taste receptors. Cell *106*, 381–390.

110. Jin, H., Fishman, Z.H., Ye, M., Wang, L., and Zuker, C.S. (2021). Top-Down Control of Sweet and Bitter Taste in the Mammalian Brain. Cell *184*, 257-271 e16. https://doi.org/10.1016/j.cell.2020.12.014.

111. Inagaki, H.K., Panse, K., and Anderson, D.J. (2014). Independent, reciprocal neuromodulatory control of sweet and bitter taste sensitivity during starvation in Drosophila. Neuron *84*, 806–820. https://doi.org/10.1016/j.neuron.2014.09.032.

112. Devineni, A.V., Sun, B., Zhukovskaya, A., and Axel, R. (2019). Acetic acid activates distinct taste pathways in Drosophila to elicit opposing, state-dependent feeding responses. Elife *8*, e47677. https://doi.org/10.7554/eLife.47677.

113. Shigemura, N., Iwata, S., Yasumatsu, K., Ohkuri, T., Horio, N., Sanematsu, K., Yoshida, R., Margolskee, R.F., and Ninomiya, Y. (2013). Angiotensin II Modulates Salty and Sweet Taste Sensitivities. J. Neurosci. *33*, 6267–6277. https://doi.org/10.1523/JNEUROSCI.5599-12.2013.

114. Inoue, M., McCaughey, S.A., Bachmanov, A.A., and Beauchamp, G.K. (2001). Whole-nerve chorda tympani responses to sweeteners in C57BL/6ByJ and 129P3/J mice. Chem Senses *26*, 915–923.

115. Danilova, V., and Hellekant, G. (2003). Comparison of the responses of the chorda tympani and glossopharyngeal nerves to taste stimuli in C57BL/6J mice. BMC Neurosci *4*, 5. https://doi.org/10.1186/1471-2202-4-5.

116. Oka, Y., Ye, M., and Zuker, C.S. (2015). Thirst driving and suppressing signals encoded by distinct neural populations in the brain. Nature *520*, 349–352. https://doi.org/10.1038/nature14108.

117. Verma, D., Wood, J., Lach, G., Herzog, H., Sperk, G., and Tasan, R. (2016). Hunger Promotes Fear Extinction by Activation of an Amygdala Microcircuit. Neuropsychopharmacol *41*, 431–439. https://doi.org/10.1038/npp.2015.163.

118. Alhadeff, A.L., Su, Z.W., Hernandez, E., Klima, M.L., Phillips, S.Z., Holland, R.A., Guo, C.Y., Hantman, A.W., De Jonghe, B.C., and Betley, J.N. (2018). A Neural Circuit for the Suppression of Pain by a Competing Need State. Cell *173*, 140-+. https://doi.org/10.1016/j.cell.2018.02.057.

119. Neal, B., Wu, Y., Feng, X., Zhang, R., Zhang, Y., Shi, J., Zhang, J., Tian, M., Huang, L., Li, Z., et al. (2021). Effect of Salt Substitution on Cardiovascular Events and Death. New England Journal of Medicine *385*, 1067–1077. https://doi.org/10.1056/NEJMoa2105675.

120. Park, S., and Sohn, J.-W. (2021). Protocol for sodium depletion and measurement of sodium appetite in mice. STAR Protocols *2*, 101026. https://doi.org/10.1016/j.xpro.2021.101026.

121. Bachmanov, A.A., Beauchamp, G.K., and Tordoff, M.G. (2002). Voluntary consumption of NaCl, KCl, CaCl2, and NH4Cl solutions by 28 mouse strains. Behav Genet *32*, 445–457. https://doi.org/10.1023/a:1020832327983.

122. Eylam, S., and Spector, A.C. (2005). Taste discrimination between NaCl and KCl is disrupted by amiloride in inbred mice with amiloride-insensitive chorda tympani nerves. American journal of physiology. Regulatory, integrative and comparative physiology *288*, R1361-8. https://doi.org/10.1152/ajpregu.00796.2004.

123. Simons, C.T., Dessirier, J.-M., Jinks, S.L., and Carstens, E. (2001). An Animal Model to Assess Aversion to Intra-oral Capsaicin: Increased Threshold in Mice Lacking Substance P. Chemical Senses *26*, 491–497. https://doi.org/10.1093/chemse/26.5.491.

124. Augustine, V., Gokce, S.K., Lee, S., Wang, B., Davidson, T.J., Reimann, F., Gribble, F., Deisseroth, K., Lois, C., and Oka, Y. (2018). Hierarchical neural architecture underlying thirst regulation. Nature *555*, 204–209. https://doi.org/10.1038/nature25488.

125. Zocchi, D., Wennemuth, G., and Oka, Y. (2017). The cellular mechanism for water detection in the mammalian taste system. Nature neuroscience *20*, 927–933. https://doi.org/10.1038/nn.4575.

126. Butler, A., Hoffman, P., Smibert, P., Papalexi, E., and Satija, R. (2018). Integrating single-cell transcriptomic data across different conditions, technologies, and species. Nature biotechnology *36*, 411–420. https://doi.org/10.1038/nbt.4096.

127. Stuart, T., Butler, A., Hoffman, P., Hafemeister, C., Papalexi, E., Mauck, W.M., Hao, Y., Stoeckius, M., Smibert, P., and Satija, R. (2019). Comprehensive Integration of Single-Cell Data. Cell *177*, 1888-1902 e21. https://doi.org/10.1016/j.cell.2019.05.031.

128. Ricciotti, E., and FitzGerald, G.A. (2011). Prostaglandins and Inflammation. Arterioscler Thromb Vasc Biol *31*, 986–1000. https://doi.org/10.1161/ATVBAHA.110.207449.

129. Kawahara, K., Hohjoh, H., Inazumi, T., Tsuchiya, S., and Sugimoto, Y. (2015). Prostaglandin E2-induced inflammation: Relevance of prostaglandin E receptors. Biochimica et Biophysica Acta (BBA) - Molecular and Cell Biology of Lipids *1851*, 414–421. https://doi.org/10.1016/j.bbalip.2014.07.008.

130. Machado, N.L.S., Bandaru, S.S., Abbott, S.B.G., and Saper, C.B. (2020). EP3R-Expressing Glutamatergic Preoptic Neurons Mediate Inflammatory Fever. J Neurosci *40*, 2573–2588. https://doi.org/10.1523/JNEUROSCI.2887-19.2020.

131. Lazarus, M., Yoshida, K., Coppari, R., Bass, C.E., Mochizuki, T., Lowell, B.B., and Saper, C.B. (2007). EP3 prostaglandin receptors in the median preoptic nucleus are critical for fever responses. Nat Neurosci *10*, 1131–1133. https://doi.org/10.1038/nn1949.

132. Vane, J.R. (1971). Inhibition of Prostaglandin Synthesis as a Mechanism of Action for Aspirin-like Drugs. Nature New Biology *231*, 232–235. https://doi.org/10.1038/newbio231232a0.

133. Bacchi, S., Palumbo, P., Sponta, A., and Coppolino, M.F. (2012). Clinical pharmacology of non-steroidal anti-inflammatory drugs: a review. Antiinflamm Antiallergy Agents Med Chem *11*, 52–64. https://doi.org/10.2174/187152312803476255.

134. Vane, J.R., Bakhle, Y.S., and Botting, R.M. (1998). Cyclooxygenases 1 and 2. Annu Rev Pharmacol Toxicol *38*, 97–120. https://doi.org/10.1146/annurev.pharmtox.38.1.97.

135. Yamamoto, T., Habuchi, Y., Tanaka, H., Suto, F., Morikawa, J., Kashima, K., and Yoshimura, M. (1999). EP receptor-mediated inhibition by prostaglandin E(1) of cardiac L-type Ca(2+) current of rabbits. Am J Physiol *277*, H1369-1374. https://doi.org/10.1152/ajpheart.1999.277.4.H1369.

136. Verharen, J.P.H., Roelofs, T.J.M., Menting-Henry, S., Luijendijk, M.C.M., Vanderschuren, L.J.M.J., and Adan, R.A.H. (2019). Limbic control over the homeostatic need for sodium. Sci Rep *9*, 1050. https://doi.org/10.1038/s41598-018-37405-w.

137. Roitman, M.F., Schafe, G.E., Thiele, T.E., and Bernstein, I.L. (1997). Dopamine and sodium appetite: Antagonists suppress sham drinking of NaC1 solutions in the rat. Behavioral Neuroscience *111*, 606–611. https://doi.org/10.1037/0735-7044.111.3.606.

138. Hsu, T.M., Bazzino, P., Hurh, S.J., Konanur, V.R., Roitman, J.D., and Roitman, M.F. (2020). Thirst recruits phasic dopamine signaling through subfornical organ neurons. Proceedings of the National Academy of Sciences *117*, 30744–30754. https://doi.org/10.1073/pnas.2009233117.

139. Augustine, V., Ebisu, H., Zhao, Y., Lee, S., Ho, B., Mizuno, G.O., Tian, L., and Oka, Y. (2019). Temporally and Spatially Distinct Thirst Satiation Signals. Neuron *103*, 242-249 e4. https://doi.org/10.1016/j.neuron.2019.04.039.

140. Patriarchi, T., Cho, J.R., Merten, K., Howe, M.W., Marley, A., Xiong, W.H., Folk, R.W., Broussard, G.J., Liang, R., Jang, M.J., et al. (2018). Ultrafast neuronal imaging of dopamine dynamics with designed genetically encoded sensors. Science *360*. https://doi.org/10.1126/science.aat4422.

141. Patriarchi, T., Cho, J.R., Merten, K., Marley, A., Broussard, G.J., Liang, R., Williams, J., Nimmerjahn, A., von Zastrow, M., Gradinaru, V., et al. (2019). Imaging neuromodulators with high spatiotemporal resolution using genetically encoded indicators. Nat Protoc *14*, 3471–3505. https://doi.org/10.1038/s41596-019-0239-2.

142. Biringer, R.G. (2021). A Review of Prostanoid Receptors: Expression, Characterization, Regulation, and Mechanism of Action. J Cell Commun Signal *15*, 155–184. https://doi.org/10.1007/s12079-020-00585-0.

143. Scammell, T.E., Elmquist, J.K., Griffin, J.D., and Saper, C.B. (1996). Ventromedial Preoptic Prostaglandin E2 Activates Fever-Producing Autonomic Pathways. J Neurosci *16*, 6246–6254. https://doi.org/10.1523/JNEUROSCI.16-19-06246.1996.

144. Saper, C.B., and Breder, C.D. (1994). The neurologic basis of fever. N Engl J Med *330*, 1880–1886. https://doi.org/10.1056/NEJM199406303302609.

145. Lipopolysaccharide-Induced Fever Depends on Prostaglandin E2 Production Specifically in Brain Endothelial Cells | Endocrinology | Oxford Academic https://academic.oup.com/endo/article/153/10/4849/2424441.

146. Jang, Y., Kim, M., and Hwang, S.W. (2020). Molecular mechanisms underlying the actions of arachidonic acid-derived prostaglandins on peripheral nociception. Journal of Neuroinflammation *17*, 30. https://doi.org/10.1186/s12974-020-1703-1.

147. Chen, H., Hu, B., Lv, X., Zhu, S., Zhen, G., Wan, M., Jain, A., Gao, B., Chai, Y., Yang, M., et al. (2019). Prostaglandin E2 mediates sensory nerve regulation of bone homeostasis. Nat Commun *10*, 181. https://doi.org/10.1038/s41467-018-08097-7.

148. Cochran, B. (1999). Dehydration, Heat Stroke, or Hyponatremia? The Recognition, Treatment, and Prevention of Hyponatremia Caused by High Exercise Outdoor Activities.

149. Oliver, J.A., Pinto, J., Sciacca, R.R., and Cannon, P.J. (1980). Increased renal secretion of norepinephrine and prostaglandin E2 during sodium depletion in the dog. J Clin Invest *66*, 748–756. https://doi.org/10.1172/JCI109912.

150. Stahl, R.A., Jonassen, A.J., Paravicini, M., and Schollmeyer, P. (1982). Sodium chloride as regulator of renal prostaglandin E2 production in patients with essential hypertension. Klin Wochenschr *60*, 579–581. https://doi.org/10.1007/BF01724215.

151. Zapf, A.M., Grimm, P.R., Al-Qusairi, L., Delpire, E., and Welling, P.A. (2022). Low Salt Delivery Triggers Autocrine Release of Prostaglandin E2 From the Aldosterone-Sensitive Distal Nephron in Familial Hyperkalemic Hypertension Mice. Frontiers in Physiology *12*.

152. Frommel, T.O., Dyavanapalli, M., Oldham, T., Kazi, N., Lietz, H., Liao, Y., and Mobarhan, S. (1997). Effect of aspirin on prostaglandin E2 and leukotriene B4 production in human colonic mucosa from cancer patients. Clin Cancer Res *3*, 209–213.

153. Bin, N.-R., Prescott, S.L., Horio, N., Wang, Y., Chiu, I.M., and Liberles, S.D. (2023). An airway-to-brain sensory pathway mediates influenza-induced sickness. Nature *615*, 660–667. https://doi.org/10.1038/s41586-023-05796-0.

154. Cannon, W.B. (1918). Croonian Lecture: the physiological basis of thirst. Proceedings of the Royal Society of London. Series B, Containing Papers of a Biological Character *90*, 283–301.

155. Armstrong, L.E., and Kavouras, S.A. (2019). Thirst and Drinking Paradigms: Evolution from Single Factor Effects to Brainwide Dynamic Networks. Nutrients *11*, 2864. https://doi.org/10.3390/nu11122864.

156. Dunning, J.L., Lopez, C., Krull, C., Kreifeldt, M., Angelo, M., Shu, L., Ramakrishnan, C., Deisseroth, K., and Contet, C. (2024). The parasubthalamic nucleus refeeding ensemble delays feeding initiation and hastens water drinking. Mol Psychiatry. https://doi.org/10.1038/s41380-024-02653-y.

157. Gizowski, C., and Bourque, C.W. (2018). The neural basis of homeostatic and anticipatory thirst. Nat Rev Nephrol *14*, 11–25. https://doi.org/10.1038/nrneph.2017.149.

158. Zimmerman, C.A., Leib, D.E., and Knight, Z.A. (2017). Neural circuits underlying thirst and fluid homeostasis. Nature reviews. Neuroscience *18*, 459–469. https://doi.org/10.1038/nrn.2017.71.

159. Landayan, D., Wang, B.P., Zhou, J., and Wolf, F.W. Thirst interneurons that promote water seeking and limit feeding behavior in Drosophila. eLife *10*, e66286. https://doi.org/10.7554/eLife.66286.

160. González Segarra, A.J., Pontes, G., Jourjine, N., Del Toro, A., and Scott, K. (2023). Hunger- and thirst-sensing neurons modulate a neuroendocrine network to coordinate sugar and water ingestion. eLife *12*, RP88143. https://doi.org/10.7554/eLife.88143.

161. Chu, L.-A., Tai, C.-Y., and Chiang, A.-S. (2024). Thirst-driven hygrosensory suppression promotes water seeking in Drosophila. Proc Natl Acad Sci U S A *121*, e2404454121. https://doi.org/10.1073/pnas.2404454121.

162. Wang, J., Lv, F., Yin, W., Gao, Z., Liu, H., Wang, Z., and Sun, J. (2023). The organum vasculosum of the lamina terminalis and subfornical organ: regulation of thirst. Front Neurosci *17*, 1223836. https://doi.org/10.3389/fnins.2023.1223836.

163. McKinley, M.J., and Johnson, A.K. (2004). The physiological regulation of thirst and fluid intake. News Physiol Sci *19*, 1–6.

164. Farrell, M.J., Bowala, T.K., Gavrilescu, M., Phillips, P.A., McKinley, M.J., McAllen, R.M., Denton, D.A., and Egan, G.F. (2011). Cortical activation and lamina terminalis functional connectivity during thirst and drinking in humans. American Journal of Physiology-Regulatory, Integrative and Comparative Physiology *301*, R623–R631. https://doi.org/10.1152/ajpregu.00817.2010.

165. Augustine, V., Gokce, S.K., Lee, S., Wang, B., Davidson, T.J., Reimann, F., Gribble, F., Deisseroth, K., Lois, C., and Oka, Y. (2018). Hierarchical neural architecture underlying thirst regulation. Nature *555*, 204–209. https://doi.org/10.1038/nature25488.

166. Pool, A.H., Wang, T., Stafford, D.A., Chance, R.K., Lee, S., Ngai, J., and Oka, Y. (2020). The cellular basis of distinct thirst modalities. Nature. https://doi.org/10.1038/s41586-020-2821-8.

167. Yang, G., Jia, M., Li, G., Zang, Y.-Y., Chen, Y.-Y., Wang, Y.-Y., Zhan, S.-Y., Peng, S.-X., Wan, G., Li, W., et al. (2024). TMEM63B channel is the osmosensor required for thirst drive of interoceptive neurons. Cell Discov *10*, 1. https://doi.org/10.1038/s41421-023-00628-x.

168. Hiyama, T.Y., Watanabe, E., Okado, H., and Noda, M. (2004). The subfornical organ is the primary locus of sodium-level sensing by Na(x) sodium channels for the control of salt-intake behavior. The Journal of neuroscience : the official journal of the Society for Neuroscience *24*, 9276–9281.

169. Miller, R.L., Wang, M.H., Gray, P.A., Salkoff, L.B., and Loewy, A.D. (2013). ENaC-expressing neurons in the sensory circumventricular organs become c-Fos activated following systemic sodium changes. American journal of physiology. Regulatory, integrative and comparative physiology *305*, R1141-52. https://doi.org/10.1152/ajpregu.00242.2013.

170. Bourque, C.W. (2008). Central mechanisms of osmosensation and systemic osmoregulation. Nat Rev Neurosci *9*, 519–531. https://doi.org/10.1038/nrn2400.

171. Kinsman, B., Cowles, J., Lay, J., Simmonds, S.S., Browning, K.N., and Stocker, S.D. (2014). Osmoregulatory thirst in mice lacking the transient receptor potential vanilloid type 1 (TRPV1) and/or type 4 (TRPV4) receptor. American journal of physiology. Regulatory, integrative and comparative physiology *307*, R1092-100. https://doi.org/10.1152/ajpregu.00102.2014.

172. Kurt, G., Woodworth, H.L., Fowler, S., Bugescu, R., and Leinninger, G.M. (2019). Activation of Lateral Hypothalamic Area Neurotensin-Expressing Neurons Promotes Drinking. Neuropharmacology *154*, 13–21. https://doi.org/10.1016/j.neuropharm.2018.09.038.

173. Gizowski, C., Zaelzer, C., and Bourque, C.W. (2016). Clock-driven vasopressin neurotransmission mediates anticipatory thirst prior to sleep. Nature *537*, 685–688. https://doi.org/10.1038/nature19756.

174. Roy, R.K., Yao, Y., Green, I.K., Aitken, A.V., Biancardi, V.C., Silver, R., and Stern, J.E. (2024). Blood flows from the SCN toward the OVLT within a new brain vascular portal pathway. Science Advances *10*, eadn8350. https://doi.org/10.1126/sciadv.adn8350.

175. Zagmutt, S., Mera, P., González-García, I., Ibeas, K., Romero, M.D.M., Obri, A., Martin, B., Esteve-Codina, A., Soler-Vázquez, M.C., Bastias-Pérez, M., et al. (2023). CPT1A in AgRP neurons is required for sex-dependent regulation of feeding and thirst. Biol Sex Differ *14*, 14. https://doi.org/10.1186/s13293-023-00498-8.

176. Mishra, I., Feng, B., Basu, B., Brown, A.M., Kim, L.H., Lin, T., Raza, M.A., Moore, A., Hahn, A., Bailey, S., et al. (2024). The cerebellum modulates thirst. Nat Neurosci *27*, 1745–1757. https://doi.org/10.1038/s41593-024-01700-9.

177. Allen, W.E., Chen, M.Z., Pichamoorthy, N., Tien, R.H., Pachitariu, M., Luo, L., and Deisseroth, K. (2019). Thirst regulates motivated behavior through modulation of brainwide neural population dynamics. Science *364*, eaav3932. https://doi.org/10.1126/science.aav3932.

178. Richman, E.B., Ticea, N., Allen, W.E., Deisseroth, K., and Luo, L. (2023). Neural landscape diffusion resolves conflicts between needs across time. Nature *623*, 571–579. https://doi.org/10.1038/s41586-023-06715-z.

179. Todini, L., and Fantuz, F. (2023). Thirst: neuroendocrine regulation in mammals. Vet Res Commun *47*, 1085–1101. https://doi.org/10.1007/s11259-023-10104-2.

180. Kinsman, B.J., Simmonds, S.S., Browning, K.N., Wenner, M.M., Farquhar, W.B., and Stocker, S.D. (2020). Integration of Hypernatremia and Angiotensin II by the Organum Vasculosum of the Lamina Terminalis Regulates Thirst. J. Neurosci. *40*, 2069–2079. https://doi.org/10.1523/JNEUROSCI.2208-19.2020.

181. Peltekian, L., Gasparini, S., Fazan, F.S., Karthik, S., Iverson, G., Resch, J.M., and Geerling, J.C. (2023). Sodium appetite and thirst do not require angiotensinogen production in astrocytes or hepatocytes. J Physiol *601*, 3499–3532. https://doi.org/10.1113/JP283169.

182. Chasseloup, F., Tabarin, A., and Chanson, P. (2024). Diabetes insipidus: Vasopressin deficiency…. Annales d'Endocrinologie *85*, 294–299. https://doi.org/10.1016/j.ando.2023.11.006.

183. Augustine, V., Lee, S., and Oka, Y. (2020). Neural Control and Modulation of Thirst, Sodium Appetite, and Hunger. Cell *180*, 25–32. https://doi.org/10.1016/j.cell.2019.11.040.

184. Tan, B., Nöbauer, T., Browne, C.J., Nestler, E.J., Vaziri, A., and Friedman, J.M. (2022). Dynamic processing of hunger and thirst by common mesolimbic neural ensembles. Proceedings of the National Academy of Sciences *119*, e2211688119. https://doi.org/10.1073/pnas.2211688119.

185. Augustine, V., Ebisu, H., Zhao, Y., Lee, S., Ho, B., Mizuno, G.O., Tian, L., and Oka, Y. (2019). Temporally and Spatially Distinct Thirst Satiation Signals. Neuron *103*, 242-249 e4. https://doi.org/10.1016/j.neuron.2019.04.039.

186. Volcko, K.L., Brakey, D.J., McNamara, T.E., Meyer, M.J., McKay, N.J., Santollo, J., and Daniels, D. (2022). Control of water intake by a pathway from the nucleus of the solitary tract to the paraventricular hypothalamic nucleus. Appetite *172*, 105943. https://doi.org/10.1016/j.appet.2022.105943.

187. Jaramillo, J.C.M., Aitken, C.M., Lawrence, A.J., and Ryan, P.J. (2024). Oxytocin-receptor-expressing neurons in the lateral parabrachial nucleus activate widespread brain regions predominantly involved in fluid satiation. Journal of Chemical Neuroanatomy *137*, 102403. https://doi.org/10.1016/j.jchemneu.2024.102403.

188. Ryan, P.J., Ross, S.I., Campos, C.A., Derkach, V.A., and Palmiter, R.D. (2017). Oxytocin-receptor-expressing neurons in the parabrachial nucleus regulate fluid intake. Nat Neurosci *20*, 1722–1733. https://doi.org/10.1038/s41593-017-0014-z.

189. Kim, D.Y., Heo, G., Kim, M., Kim, H., Jin, J.A., Kim, H.K., Jung, S., An, M., Ahn, B.H., Park, J.H., et al. (2020). A neural circuit mechanism for mechanosensory feedback control of ingestion. Nature *580*, 376–380. https://doi.org/10.1038/s41586-020-2167-2.

190. Matsuda, T., Kobayashi, K., Kobayashi, K., and Noda, M. (2024). Two parabrachial Cck neurons involved in the feedback control of thirst or salt appetite. Cell Rep *43*, 113619. https://doi.org/10.1016/j.celrep.2023.113619.

191. Gong, R., Xu, S., Hermundstad, A., Yu, Y., and Sternson, S.M. (2020). Hindbrain Double-Negative Feedback Mediates Palatability-Guided Food and Water Consumption. Cell *182*, 1589-1605.e22. https://doi.org/10.1016/j.cell.2020.07.031.

192. Thrasher, T.N., Keil, L.C., and Ramsay, D.J. (1987). Drinking, oropharyngeal signals, and inhibition of vasopressin secretion in dogs. American Journal of Physiology-Regulatory, Integrative and Comparative Physiology *253*, R509–R515.

193. Zimmerman, C.A., Lin, Y.-C., Leib, D.E., Guo, L., Huey, E.L., Daly, G.E., Chen, Y., and Knight, Z.A. (2016). Thirst neurons anticipate the homeostatic consequences of eating and drinking. Nature *537*, 680–684. https://doi.org/10.1038/nature18950.

194. Lechner, S.G., Markworth, S., Poole, K., Smith, E.S., Lapatsina, L., Frahm, S., May, M., Pischke, S., Suzuki, M., Ibanez-Tallon, I., et al. (2011). The molecular and cellular identity of peripheral osmoreceptors. Neuron *69*, 332–344. https://doi.org/10.1016/j.neuron.2010.12.028.

195. Baertschi, A.J., and Vallet, P.G. (1981). Osmosensitivity of the hepatic portal vein area and vasopressin release in rats. The Journal of physiology *315*, 217–230. https://doi.org/10.1113/jphysiol.1981.sp013743.

196. Zhang, Y.-P., Zhu, J.-N., Chen, K., Li, H.-Z., and Wang, J.-J. (2005). Neurons in the rat lateral hypothalamic area integrate information from the gastric vagal nerves and the cerebellar interpositus nucleus. Neurosignals *14*, 234–243. https://doi.org/10.1159/000088639.

197. Ichiki, T., Wang, T., Kennedy, A., Pool, A.H., Ebisu, H., Anderson, D.J., and Oka, Y. (2022). Sensory representation and detection mechanisms of gut osmolality change. Nature *602*, 468–474. https://doi.org/10.1038/s41586-021-04359-5.

198. Zeng, W.-Z., Marshall, K.L., Min, S., Daou, I., Chapleau, M.W., Abboud, F.M., Liberles, S.D., and Patapoutian, A. (2018). PIEZOs mediate neuronal sensing of blood pressure and the baroreceptor reflex. Science *362*, 464–467. https://doi.org/10.1126/science.aau6324.

199. Montani, J.-P., and Van Vliet, B.N. (2009). Understanding the contribution of Guyton's large circulatory model to long-term control of arterial pressure. Exp Physiol *94*, 382–388. https://doi.org/10.1113/expphysiol.2008.043299.

200. Machnik, A., Dahlmann, A., Kopp, C., Goss, J., Wagner, H., van Rooijen, N., Eckardt, K.-U., Müller, D.N., Park, J.-K., Luft, F.C., et al. (2010). Mononuclear phagocyte system depletion blocks interstitial tonicity-responsive enhancer binding protein/vascular endothelial growth factor C expression and induces salt-sensitive hypertension in rats. Hypertension *55*, 755–761. https://doi.org/10.1161/HYPERTENSIONAHA.109.143339.

201. Kanbay, M., Chen, Y., Solak, Y., and Sanders, P.W. (2011). Mechanisms and Consequences of Salt Sensitivity and Dietary Salt Intake. Curr Opin Nephrol Hypertens *20*, 37–43. https://doi.org/10.1097/MNH.0b013e32834122f1.

202. Maaliki, D., Itani, M.M., and Itani, H.A. (2022). Pathophysiology and genetics of salt-sensitive hypertension. Front Physiol *13*, 1001434. https://doi.org/10.3389/fphys.2022.1001434.

203. Li, S., Xiao, X., and Zhang, X. (2023). Hydration Status in Older Adults: Current Knowledge and Future Challenges. Nutrients *15*, 2609. https://doi.org/10.3390/nu15112609.

204. Lu, H., Ayers, E., Patel, P., and Mattoo, T.K. (2023). Body water percentage from childhood to old age. Kidney Res Clin Pract *42*, 340–348. https://doi.org/10.23876/j.krcp.22.062.

205. Masot, O., Miranda, J., Santamaría, A.L., Paraiso Pueyo, E., Pascual, A., and Botigué, T. (2020). Fluid Intake Recommendation Considering the Physiological Adaptations of Adults Over 65 Years: A Critical Review. Nutrients *12*, 3383. https://doi.org/10.3390/nu12113383.

206. McLean, K.A., O'Neill, P.A., Davies, I., and Morris, J. (1992). Influence of age on plasma osmolality: a community study. Age Ageing *21*, 56–60. https://doi.org/10.1093/ageing/21.1.56.

207. Cowen, L.E., Hodak, S.P., and Verbalis, J.G. (2013). Age-Associated Abnormalities of Water Homeostasis. Endocrinol Metab Clin North Am *42*, 349–370. https://doi.org/10.1016/j.ecl.2013.02.005.

208. O'Neill, P.A., Faragher, E.B., Davies, I., Wears, R., McLean, K.A., and Fairweather, D.S. (1990). Reduced survival with increasing plasma osmolality in elderly continuing-care patients. Age Ageing *19*, 68–71. https://doi.org/10.1093/ageing/19.1.68.

209. Terwel, D., and Jolles, J. (1994). The relationship between plasma osmolality and plasma vasopressin concentration is altered in old male Lewis rats. Eur J Endocrinol *131*, 86–90. https://doi.org/10.1530/eje.0.1310086.

210. Farrell, M.J., Zamarripa, F., Shade, R., Phillips, P.A., McKinley, M., Fox, P.T., Blair-West, J., Denton, D.A., and Egan, G.F. (2008). Effect of aging on regional cerebral blood flow responses associated with osmotic thirst and its satiation by water drinking: A PET study. Proceedings of the National Academy of Sciences *105*, 382–387. https://doi.org/10.1073/pnas.0710572105.

211. Weinstein, J.R., and Anderson, S. (2010). THE AGING KIDNEY: PHYSIOLOGICAL CHANGES. Adv Chronic Kidney Dis *17*, 302–307. https://doi.org/10.1053/j.ackd.2010.05.002.

212. Begg, D.P. (2017). Disturbances of thirst and fluid balance associated with aging. Physiology & Behavior *178*, 28–34. https://doi.org/10.1016/j.physbeh.2017.03.003.

213. Yoon, H.E., Kim, E.N., Kim, M.Y., Lim, J.H., Jang, I.-A., Ban, T.H., Shin, S.J., Park, C.W., Chang, Y.S., and Choi, B.S. (2016). Age-Associated Changes in the Vascular Renin-Angiotensin System in Mice. Oxid Med Cell Longev *2016*, 6731093. https://doi.org/10.1155/2016/6731093.

214. Cowen, L.E., Hodak, S.P., and Verbalis, J.G. (2013). Age-Associated Abnormalities of Water Homeostasis. Endocrinol Metab Clin North Am *42*, 349–370. https://doi.org/10.1016/j.ecl.2013.02.005.

215. Elsamad, G., Mecawi, A.S., Pauža, A.G., Gillard, B., Paterson, A., Duque, V.J., Šarenac, O., Žigon, N.J., Greenwood, M., Greenwood, M.P., et al. (2023). Ageing restructures the transcriptome of the hypothalamic supraoptic nucleus and alters the response to dehydration. npj Aging *9*, 1–15. https://doi.org/10.1038/s41514-023-00108-2.

216. Geerling, J.C., and Loewy, A.D. (2008). Central regulation of sodium appetite. Experimental physiology *93*, 177–209. https://doi.org/10.1113/expphysiol.2007.039891.

217. Zhang, Y., Pool, A.-H., Wang, T., Liu, L., Kang, E., Zhang, B., Ding, L., Frieda, K., Palmiter, R., and Oka, Y. (2023). Parallel neural pathways control sodium consumption and taste valence. Cell. https://doi.org/10.1016/j.cell.2023.10.020.

218. Vega-Vega, O., Fonseca-Correa, J.I., Mendoza-De la Garza, A., Rincón-Pedrero, R., Espinosa-Cuevas, A., Baeza-Arias, Y., Dary, O., Herrero-Bervera, B., Nieves-Anaya, I., and Correa-Rotter, R. (2018). Contemporary Dietary Intake: Too Much Sodium, Not Enough Potassium, yet Sufficient Iodine: The SALMEX Cohort Results. Nutrients *10*, 816. https://doi.org/10.3390/nu10070816.

219. Committee on the Consequences of Sodium Reduction in Populations, Food and Nutrition Board, Board on Population Health and Public Health Practice, and Institute of Medicine (2013). Sodium Intake in Populations: Assessment of Evidence B. L. Strom, A. L. Yaktine, and M. Oria, eds. (National Academies Press (US)).

220. Tan, M., He, F., Morris, J.K., and MacGregor, G. (2022). Reducing daily salt intake in China by 1 g could prevent almost 9 million cardiovascular events by 2030: a modelling study. BMJ Nutr Prev Health *5*, 164–170. https://doi.org/10.1136/bmjnph-2021-000408.

221. Mozaffarian, D., Fahimi, S., Singh, G.M., Micha, R., Khatibzadeh, S., Engell, R.E., Lim, S., Danaei, G., Ezzati, M., Powles, J., et al. (2014). Global sodium consumption and death from cardiovascular causes. N Engl J Med *371*, 624–634. https://doi.org/10.1056/NEJMoa1304127.

222. Wang, K., Jin, Y., Wang, M., Liu, J., Bu, X., Mu, J., and Lu, J. (2023). Global cardiovascular diseases burden attributable to high sodium intake from 1990 to 2019. J Clin Hypertens (Greenwich) *25*, 868–879. https://doi.org/10.1111/jch.14717.

223. Balan, Y., Packirisamy, R.M., and Mohanraj, P.S. (2020). High dietary salt intake activates inflammatory cascades via Th17 immune cells: impact on health and diseases. Arch Med Sci *18*, 459–465. https://doi.org/10.5114/aoms.2020.96344.

224. Bier, A., Braun, T., Khasbab, R., Di Segni, A., Grossman, E., Haberman, Y., and Leibowitz, A. (2018). A High Salt Diet Modulates the Gut Microbiota and Short Chain Fatty Acids Production in a Salt-Sensitive Hypertension Rat Model. Nutrients *10*, 1154. https://doi.org/10.3390/nu10091154.

225. Drenjančević-Perić, I., Jelaković, B., Lombard, J.H., Kunert, M.P., Kibel, A., and Gros, M. (2011). High-Salt Diet and Hypertension: Focus on the Renin-Angiotensin System. Kidney Blood Press Res *34*, 1–11. https://doi.org/10.1159/000320387.

226. Brown, I.J., Tzoulaki, I., Candeias, V., and Elliott, P. (2009). Salt intakes around the world: implications for public health. Int J Epidemiol *38*, 791–813. https://doi.org/10.1093/ije/dyp139.

227. Santos, J.A., Tekle, D., Rosewarne, E., Flexner, N., Cobb, L., Al-Jawaldeh, A., Kim, W.J., Breda, J., Whiting, S., Campbell, N., et al. (2021). A Systematic Review of Salt Reduction Initiatives Around the World: A Midterm Evaluation of Progress Towards the 2025 Global Non-Communicable Diseases Salt Reduction Target. Adv Nutr *12*, 1768–1780. https://doi.org/10.1093/advances/nmab008.

228. Campbell, N., Legowski, B., Legetic, B., Ferrante, D., Nilson, E., Campbell, C., and L'Abbé, M. (2014). Targets and Timelines for Reducing Salt in Processed Food in the Americas. J Clin Hypertens (Greenwich) *16*, 619–623. https://doi.org/10.1111/jch.12379.

229. Mente, A., O'Donnell, M., and Yusuf, S. (2021). Sodium Intake and Health: What Should We Recommend Based on the Current Evidence? Nutrients *13*, 3232. https://doi.org/10.3390/nu13093232.

230. Jachimowicz-Rogowska, K., and Winiarska-Mieczan, A. (2023). Initiatives to Reduce the Content of Sodium in Food Products and Meals and Improve the Population's Health. Nutrients *15*, 2393. https://doi.org/10.3390/nu15102393.

231. Zhang, J., Zhang, N., Liu, S., Du, S., and Ma, G. (2022). Young Adults with Higher Salt Intake Have Inferior Hydration Status: A Cross-Sectional Study. Nutrients *14*, 287. https://doi.org/10.3390/nu14020287.

232. Hamad, I., Cardilli, A., Côrte-Real, B.F., Dyczko, A., Vangronsveld, J., and Kleinewietfeld, M. (2022). High-Salt Diet Induces Depletion of Lactic Acid-Producing Bacteria in Murine Gut. Nutrients *14*, 1171. https://doi.org/10.3390/nu14061171.

233. Faraco, G., Hochrainer, K., Segarra, S.G., Schaeffer, S., Santisteban, M.M., Menon, A., Jiang, H., Holtzman, D.M., Anrather, J., and Iadecola, C. (2019). Dietary salt promotes cognitive impairment through tau phosphorylation. Nature *574*, 686–690. https://doi.org/10.1038/s41586-019-1688-z.

234. Kleinewietfeld, M., Manzel, A., Titze, J., Kvakan, H., Yosef, N., Linker, R.A., Muller, D.N., and Hafler, D.A. (2013). Sodium chloride drives autoimmune disease by the induction of pathogenic TH17 cells. Nature *496*, 518–522. https://doi.org/10.1038/nature11868.

235. Teow, B.H., Di Nicolantonio, R., and Morgan, T.O. (1985). Sodium chloride preference and recognition threshold in normotensive subjects on high and low salt diet. Clin Exp Hypertens A *7*, 1681–1695. https://doi.org/10.3109/10641968509073618.

236. Bertino, M., Beauchamp, G.K., and Engelman, K. (1986). Increasing dietary salt alters salt taste preference. Physiol Behav *38*, 203–213. https://doi.org/10.1016/0031-9384(86)90155-1.